Study on the Solderability and Different Aspects of Performance Evaluation for Lead-Free Sn-Ag-Based Solder Alloys

Noboru HIDAKA

March 2010

首都大学東京　博士（工学）学位論文（課程博士）

論 文 名　Sn－Ag 系鉛フリーはんだの接合性と各種特性評価に関する研究（英文）

著　者　　日高昇

審査担当者

主　査　　吉葉正行

委　員　　真鍋健一

委　員　　清水敏久

委　員　　楊　明

上記の論文を合格と判定する

平成22 年 3 月25 日

首都大学東京大学院理工学研究科教授会

研究科長　　岡部　豊

DISSERTATION FOR A DEGREE OF DOCTOR OF PHILOSOPHY IN ENGINEERING TOKYO METROPOLITAN UNIVERSITY

TITLE : Study on the Solderability and Different Aspects of Performance Evaluation for Lead-Free Sn-Ag-Based Solder Alloys

AUTHOR : Noboru HIDAKA

EXAMINED BY

Examiner in chief Masayuki Yoshida

Examiner Ken-ichi Manabe

Examiner Toshihisa Shimizu

Examiner Ming YANG

QUALIFIED BY THE GRADUATE SCHOOL OF SCIENCE AND ENGINEERING TOKYO METROPOLITAN UNIVERSITY

Dean Yutaka Okabe

Date March 25, 2010

CONTNETS

Chapter 1. INTRODUCTION

1.1. Background

1.1.1. Function of Solder Alloys

Solder interconnects have to perform successfully three major functions: electrical, mechanical, and thermal. They provide the electrical connection path from the silicon chip to the circuitry on the substrate within a package, between the different packages (as in packaging stacking) [1-1], and between the elements and the copper (Cu) traces on the printed wiring board.

At the same time, they also serve as the mechanical support for the various elements, which are interconnected. As the power of the chips rises, heat dissipation is becoming an increasingly critical issue that can affect the performance of the electronic system; solder interconnects, along with other thermal management tools, also serve the function of heat dissipation. The successful functioning of electronic products depends on the reliable interconnections provided by these tiny and numerous solder joints, over the life of the product, under vastly different use conditions. Here, as an example, the products of Fuji electric, which used solder, are shown in Fig.1-1 and Fig.1-2.

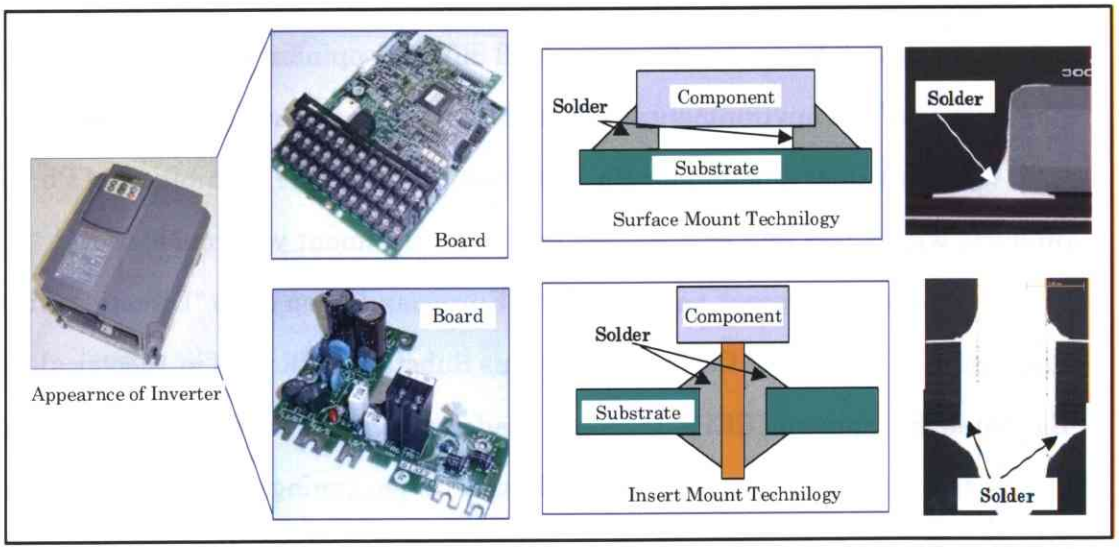

Fig.1-1 Solder be used in inverter products

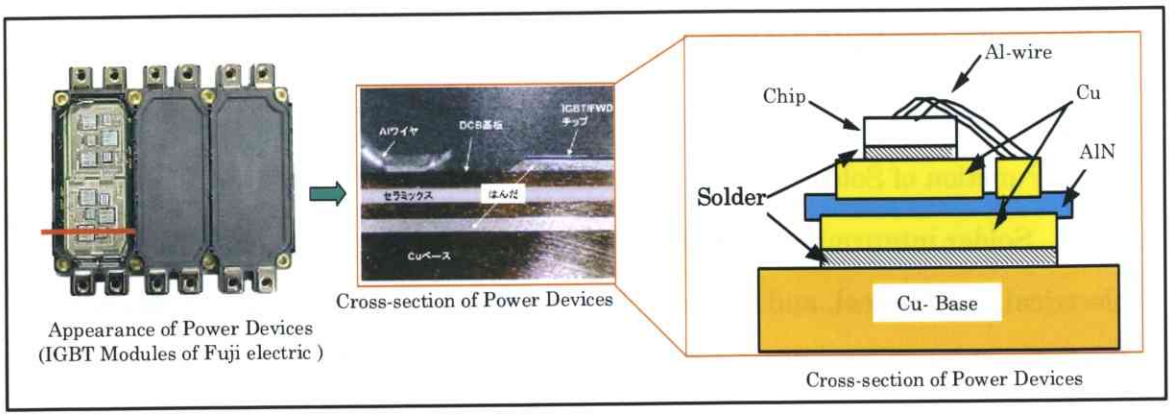

Fig.1-2 Solder be used in power devices products.

From the last century beginning of the electronics industry, solder joints have been made primarily of alloys of tin (Sn) and lead (Pb). There are many good reasons for this, including the high ductility and mechanical robustness of this material. In particular, the eutectic tin-lead alloy (63%Sn and 37%Pb by weight, eutectic temperature l83℃) has been used almost exclusively in electronics, due to its unique characteristics(cost, availability, ease of use, and electrical/ mechanical/ chemical characteristics)[1-2].

1.1.2. Environment Issues

The ever-increasing amount of electronic waste (e-waste), most of which end up in land-fi1ls, has become a serious worldwide concern. The harmful effect of lead to humans is well known[1-3]. There are still differing opinions, however, on the significance of the environmental impact of lead from electronics.

As consumer demand for Pb-free products grew, the prohibition of Pb in products with a less immediate effect on the environment was considered.

Notably, the recent passage of the European Union (EU) "Directive on the Restriction of the Use of Certain Hazardous Substances (RoHS) in Electrical and Electronic Equipment (EEE)" [1-4,1-5] has made the drive towards worldwide adoption of lead-free soldering unstoppable for electronics packaging, board assembly, and manufacturing of electronics products, along with the elimination of mercury (Hg), cadmium (Cd), hexavalent chromium (Cr^{+6}), polybrominated biphenyls (PBB), and

polybrominated diphenyl ethers (PBDE) after June 2006. Although some products are initially exempted from the legislation, they will likely be subject to similar restrictions within a few years.

Over the last decade, the industry has studied a wide range of alloys to replace the tin-lead alloy[1-6-1-8]. The alloy selection has been based on the following considerations: toxicity, physical properties (melting temperature, wettability and thermal and electrical conductivity), mechanical properties, microstructural characteristics, electrochemical properties (corrosion, oxidation and dross formation, and compatibility with no-clean fluxes), manufacturability, cost, and availability.

Yet another important consideration for selecting the lead-free solder alloy for commercial use is whether or not any patents may cover the alloy. Lead-free alloy selection, as well as associated patent issues, has been described in detail in the literature[6].

As a result, the industry is converging on the Sn-Ag base solder alloy. Particularly, ternary eutectic Sn-Ag-Cu(SAC) alloy (eutectic temperature approximately 217℃) are currently among the most popular Pb-free solder materials[6-8]. It is generally believed that the different variations of the Sn-Ag-Cu alloy, with silver content from 3.0% to 4.0%, are all acceptable compositions.

1.2. Demand for Lead-free Solder Alloys

The commonly used eutectic mixture of the Sn-Ag-Cu alloy involves an Sn-3.5Ag composition (eutectic temperature: 221°C).

On the other hand, as shown in Fig.1-3, electronic devices, especially used in vehicles and industrial products, are much more frequently loaded into more severe environments, such as condition of higher temperature and fluctuating stresses and temperatures, which induces higher temperature creep and thermal fatigue in the joining materials of solder.

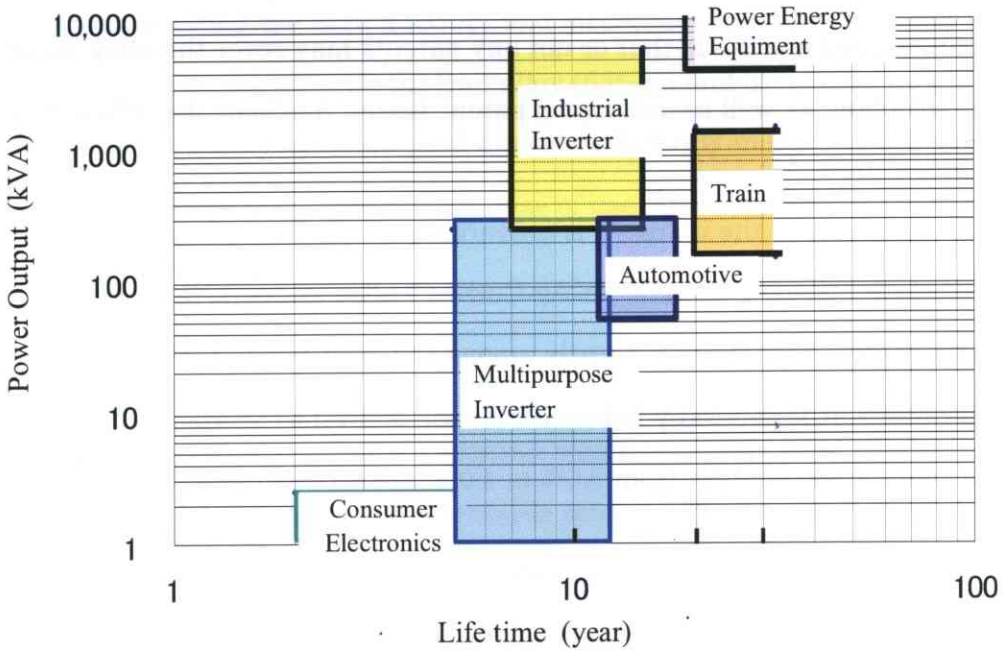

Fig.1-3 The life time and power output for various industrial products.

In order to answer those demands, a small amount of Ni, and Ge was added into the Sn-Ag-Cu solder and an advanced solder alloy, Sn-Ag-Cu-Ni-Ge solder, was developed (Table 1-1).

Table 1-1 Typical characteristics between Sn-Ag-based solders and SnPb solder

Solder Alloy	Melting point		Tensile strength	Modulus of elasticity	Coefficient of expansion	Density g/cm^3	Thermal conduction λ $W\,m^{-1}K^{-1}$
	Solidus	Liquidus	MPa	GPa	$10^{-6}/℃$	25℃	25℃
Sn3.5Ag0.5Cu+NiGe	217	219	42	53.3	22.3	7.41	62.4
Sn3.0Ag0.5Cu	217	220	43	54	21.7	7.4	64.2
Sn-37Pb	182	184	37	27.3	23.5	7.4	54.1

However, recently because the base metal market has been volatile, high cost of Ag has created a certain demand, particularly in flow soldering applications for alloys with lower Ag content. As described, a single board includes hundreds, sometime even thousands of solder joints. The failure of even a single solder joints is usually enough to compromise the functionality of an electronic device or system. Turning a device on often causes differential thermal expansions that can only be accommodated through significant plastic deformation of the solder joints and thus eventually leads to thermal fatigue. Joints must be able to survive mechanical loading caused by vibration, bending, of dropping. Predicting and controlling the reliability of the billions of solder joints formed in the automated manufacturing of a typical, high-volume product requires a through understanding of solder joint mechanical properties[1-9-1-11]. In particular, the variability of the properties of solder must be understood and controlled. Extreme cost pressures, increasing reliability demand and the cost of field failures will need a maker to make a balance[1-12].

1.3. Purpose of this Study

The purpose of this study was to evaluate the behavior of Sn-Ag based solder alloys to provide a lineup solder alloys (cost, reliability, etc) to correspond the products (Fig.1-4).

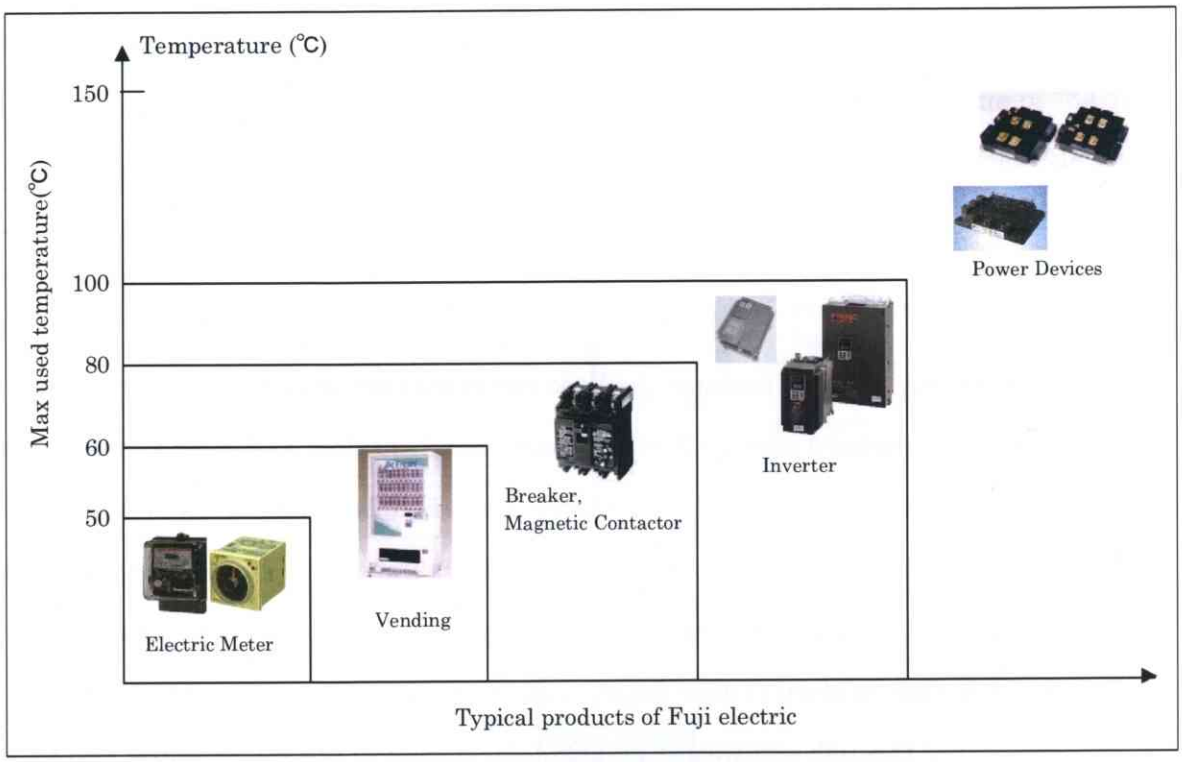

Fig.1-4 Typical products of Fuji and max used temperature

Especially, Ag compositions varying within the range of 0% to 3.5%, with or without the addition of Ni and Ge was investigated. The effects of adding Ag, Cu, Ni, and Ge elements into the Sn-based solder were shown in Fig.1-4 and considered as the following.

Adding Ag into the Sn-base alloy was to form a eutectic mixture with Sn, Ag precipitates the microscopic structures of Ag-Sn compounds at the crystal grain boundary, enhancing the strength and thermal fatigue properties of the solder alloy.

For this reason, low-Ag composition alloys must be carefully developed to ensure optimal performance and to retain as much of Ag's benefits as possible.

Adding Cu into the Sn-base alloy was to form a solid solution in Sn and improve heat resistance and alloy strength without degrading the wettability.

Addition of Ni, since which is high in melting point (1450℃) , provides thermal stability of the alloy, formation of fine crystal texture, improvement of the thermal fatigue characteristic by formation of a Ni-Sn compound, and suppresses formation of intermetallic compound (Cu_3Sn) which degrades the soldering strength.

Adding a small mount of Ge into the solder alloy was to form a very thin oxidation layer of Ge on the surface of Sn-Ag-Cu-Ni-Ge solder to suppress formation of the dross (Sn-oxide).

Table 1-2 The effects of adding Ag, Cu, Ni, and Ge on solderability

Items \ Elements	Ag	Cu	Ni	Ge
Wettability	↑	→	→	↑
Spreadability	↑	→	→	↑
Cu Erosion	→	↑	↑	→
Oxidation Resistant	→	→	→	↑

↑ : Good; →: No effect; ↓ : Bad

1.4. Evaluation Item for the Sn-Ag Base Lead-free Solder Alloys

A systematic and holistic approach, as illustrated in Fig.1-5, encompassing design, materials, processes, quality, reliability, and operations and business considerations, is critical to successful implementation of lead-free solders.

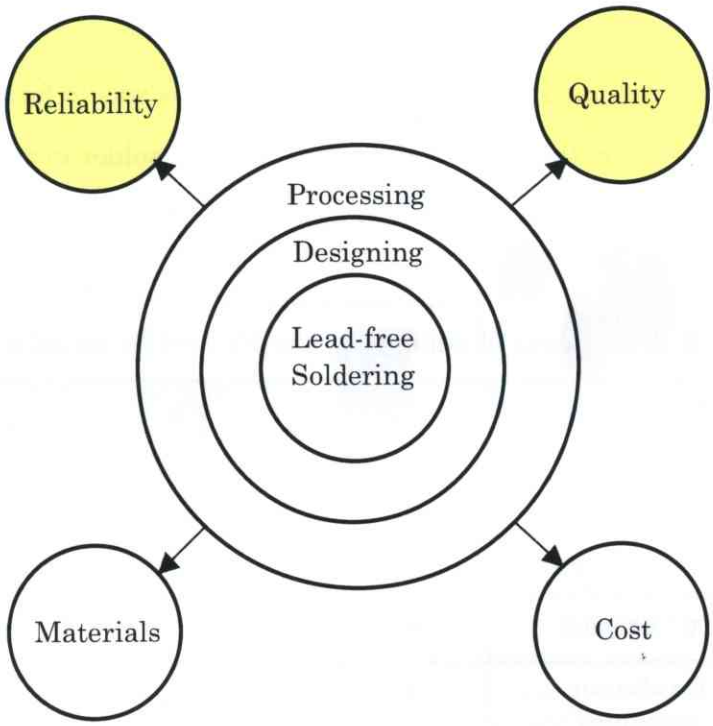

Fig.1-5 A holistic approach to lead-free soldering

In generaly, the damage factors of soldering joint can be is classified as shown in the Fig.1-6. In order to keep the quality and reliability, this study was focused on solderability (which includes wettability, spreadability, and dissolution), and reliability (which includes tensile strength, low-cycle fatigue, creep properties, and Interface reaction).

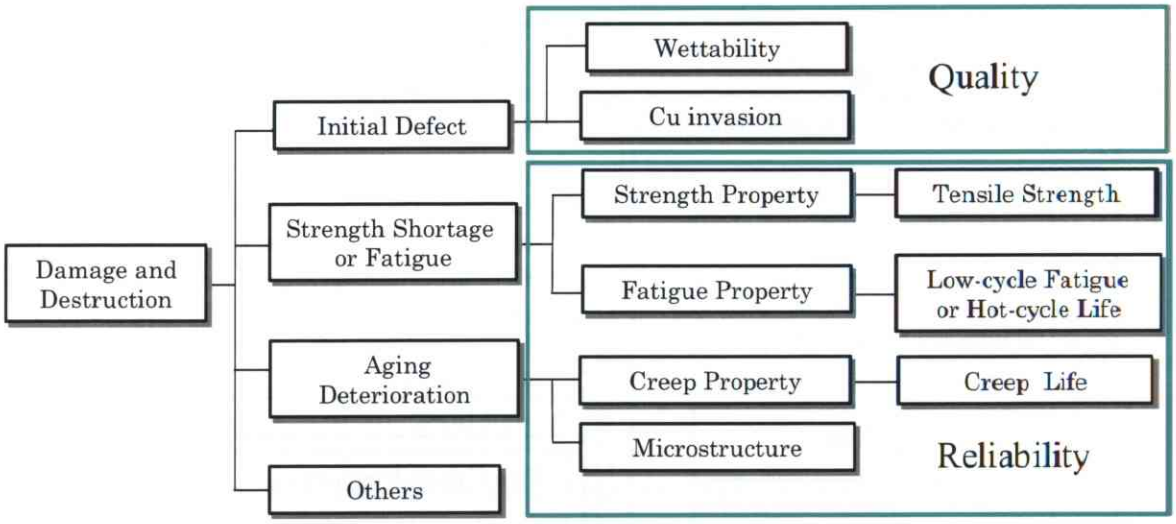

Fig.1-6 The damage factors in soldering (assembly)

1.5. Composition and Flow Chart in this Study

The study is composed with Chapter 1 to Chapter 6, and the main contents are as follows. Figure 1-7 shows the flow chart.

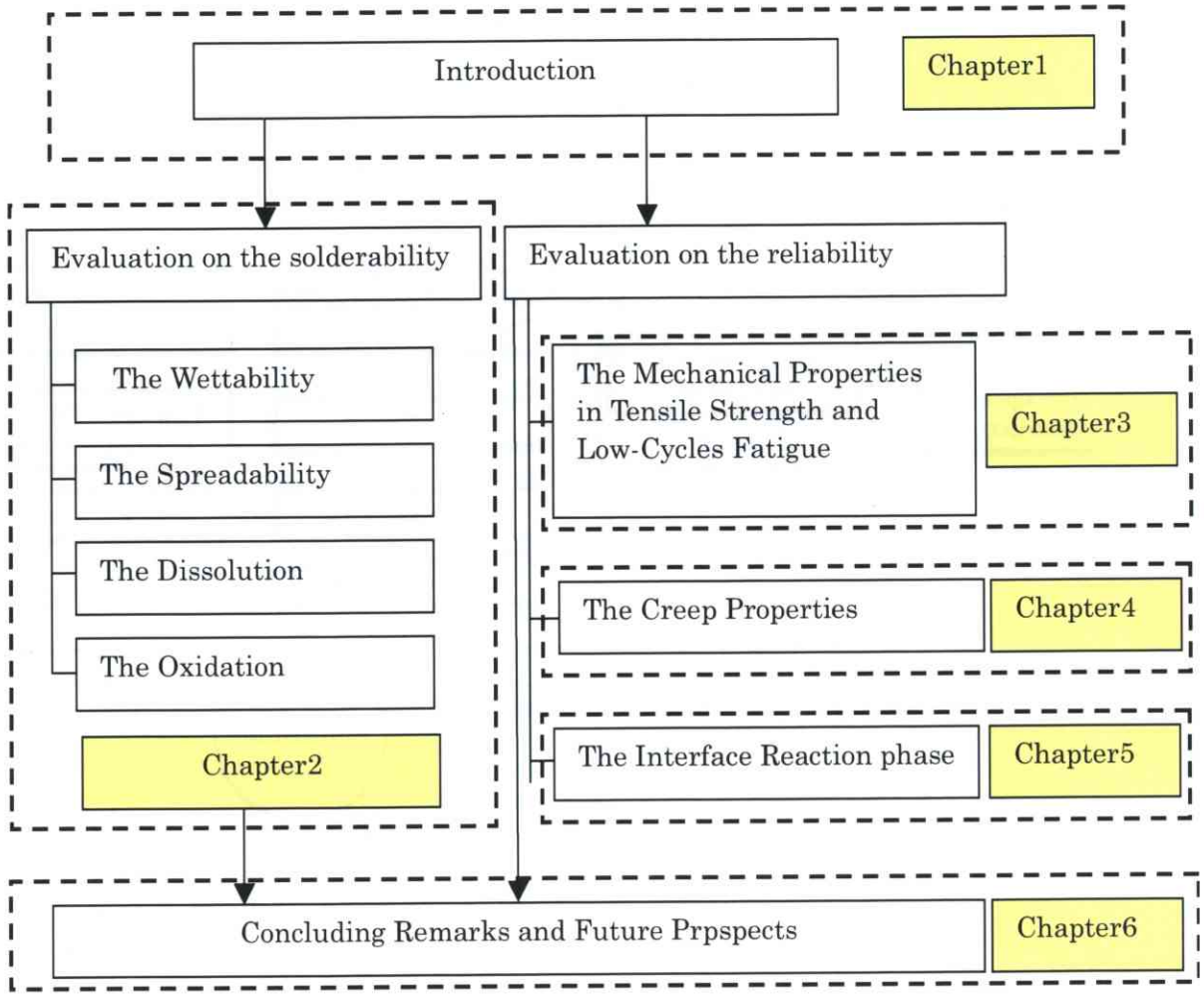

Fig.1-7 The flow chart in this study.

1.6. References

1-1. D.Shangguan: "Packaging & Board Assembly Technology Trend and Impact on the Supply Chain", (Keynote) Proceedings of the 6th IEEE CPMT Conference on High Density Microsystem Design and Packaging and Component Failure Analysis (HDP'04), June 2004,pp.14-17.

1-2. W.Hofmann: "Lead and Lead Alloys", Springer-Verlag Berlin·Heidelberg·New York 1970.

1-3. U.S. Department of Health and Human Services: "Toxicology Profile for Lead", Clement International Corporation, April 1993.

1-4. Directive 2002/95/EC of the European Parliament and of the Council of 27 January 2003 on the Restriction of the Use of Certain Hazardous Substances in Electrical and Electronic Equipment, Off. J.Eur.Union, 13,2,2003.

1-5. Japan Machiery Center for Trade and Inverstment: "WEEE Handbook V", JMC environment Update, 2003-3.

1-6. National Center for Manufacturing Sciences (NCMS): "Lead-Free Solder Project -Final report", Aug 1997.

1-7. Improved Design Life and Environmentally Aware Manufacturing of Electronics Assemblies by Lead-Free Soldering "IDEALS", BE95-1994 'IDEALS' Synthesis Report, 1999-6.

1-8. JEITA Lead-free Roadmap, 2002 ver.1.0 (2002). JEITA.

1-9. P.Borgesen, T.Bieler, L.P.Lehman, and E.J.Cotts: "Pb-free solder: New Materials Consideration for Microelectronics Processing" Mrs Bulletin, Vol.32, 2007, pp.360-364.

1-10. D.Shangguan,G.Gao:"Lead-Free & No-Clean Soldering for Automotive Electronics", Solder. Surf. Mt. Technol., 26,1997,pp.5-8.

1-11. R.W.Johnson, J.L.Evans, P.Jacobsen, J.R.Thompson, and M.Christopher: "The Changing Automotive Environment: High-Temperature Electronics", IEEE Transactions on electronics Packaging Manufacturing, Vol.27, No.3, 2004, pp.164-175.

1-12. M.Okamoto, K.Serizawa, H.Satoh, M.Chiba, K.Omae, E.Hirao, N.Itsubo, A.Inaba, T.Takemoto, H.Nishikawa: "The Overview of IMS Project EFSOT Japan 2003", Proc. The Sixth International Conference on EcoBalance, 2004, pp.1-4.

Chapter 2 SOLDERABILITY OF LEAD-FREE SN-AG-BASED SOLDER ALLOYS

2.1. Introduction

The purpose of Chapter 2 is to evaluate solderability of the Sn-Ag-based solder alloys and to keep the high quality between the elements and the copper traces on the Printed Wiring Board (PWB) in manufacturing processes[2-1-2-2].

A single board includes hundreds, sometime even thousands of solder joints. The failure of even a single solder joints is usually enough to compromise the functionality of an electronic device or system. Controlling the solderability is very important to reliability of the billions of solder joints formed in the automated manufacturing processes[2-3-2-4].

In this chapter, all of the behaviors which includes wettability and spread-ability , dissolution of Cu, and dross(Sn oxidation) are investigated. Moreover, the effects of adding Ag, Ni, Ge elements on solderability will be confirmed (table 2-1).

The Sn-Ag -Cu solder alloys as base material with compositions varying from 0% to 3% Ag by weight with or without addition of 0.07 wt% Ni and 0.01 wt.% Ge are used and listed at table 2-2.

Table 2-1 The effects of adding Ag, Cu, Ni, and Ge on solderability

Items \ Elements	Ag	Cu	Ni	Ge
Wettability	↑	→	→	↑
Spreadability	↑	→	→	↑
Cu Erosion	→	↑	↑	→
Oxidation Resistant	→	→	→	↑

↑ : Good; →: No effect; ↓ : Bad

Table 2-2. Composition of the Solder Alloys

No.	Element					Alloy codes
	Sn	Ag	Cu	Ni	Ge	
1-1	Bal	0	0.5	0.07	0.01	SCNG
1-2	Bal	0	0.5	0.07	–	SCN
1-3	Bal	0	0.5	–	–	SC
2-1	Bal	0.05	0.5	0.07	0.01	S005ACNG
2-2	Bal	0.05	0.5	0.07	–	S005ACN
2-3	Bal	0.05	0.5	–	–	S005AC
3-1	Bal	0.1	0.5	0.07	0.01	S01ACNG
3-2	Bal	0.1	0.5	0.07	–	S01ACN
3-3	Bal	0.1	0.5	–	–	S01AC
4-1	Bal	0.3	0.5	0.07	0.01	S03ACNG
4-2	Bal	0.3	0.5	0.07	–	S03ACN
4-3	Bal	0.3	0.5	–	–	S03AC
5-1	Bal	0.5	0.5	0.07	0.01	S05ACNG
5-2	Bal	0.5	0.5	0.07	—	S05ACN
5-3	Bal	0.5	0.5	–	–	S05AC
6-1	Bal	1	0.5	0.07	0.01	S1ACNG
6-2	Bal	1	0.5	0.07	–	S1ACN
6-3	Bal	1	0.5	–	–	S1AC
7-1	Bal	3	0.5	0.07	0.01	S3ACNG
7-2	Bal	3	0.5	0.07	–	S3ACN
7-3	Bal	3	0.5	–	–	S3AC

2.2. Wettability and Spreadability

2.2.1. Experimental Procedures

Wettability evaluation was performed by the menisco-graph method[2-5]. The device is shown in Fig.2-1. The mechanism of measurement is shown in Fig.2-2. After melting the specified 500 g of the sample at 320°C, we transferred 150 g of the melt to the crucible of the tester (Tarutin Kester SWET-2100), maintaining a temperature of 255°C while performing measurements. The test piece was a 10 mm × 30 mm × 0.3 mm phosphorus-deoxidized Cu plate. After a wash with 5% HCl solution and a water rinse, the plate was acetone-dried. The flux was RMA. The immersion rate and time were 2 mm/sec and 10 sec, respectively. Five tests (t = 5) were performed for each composition, and then calculated an average based on the results of this test.

The spread test[2-6] was performed as follows: The specified 500 g alloy sample was melted at 320°C in an electric furnace. A portion was then cast into a quartz tube to create a solid cylindrical test piece, which was then cut into 0.3 g pieces.

The phosphorus deoxidized Cu plate (50 mm × 50 mm × 0.3 mmt) was prepared for the spread test by rough polishing, rinsing with IPA, then oxidization (150°C × 1hour), in accordance with JIS Z3284. The used flux was RMA.

The solder sample was placed on the test plate and 0.05 ml of flux dropped onto the plate. The sample was then heated to 250°C above a solder bath (110 mm × 60 mm × 60 mm). The heating time was 30 seconds after the melting of the solder.

The test piece was then lifted from the bath and cooled before measuring the height of the spread solder. The spread factor was calculated from the measured height. Spread factor (%) = (H − D)/D × 100

where, H: height of the spread solder (mm),D: diameter of the solder used in the test, assuming a spherical form (mm), D =1.24V/3(V: Volume of solder used in the test). The test was repeated five times for each composition (n = 5), based on which an average value was calculated.

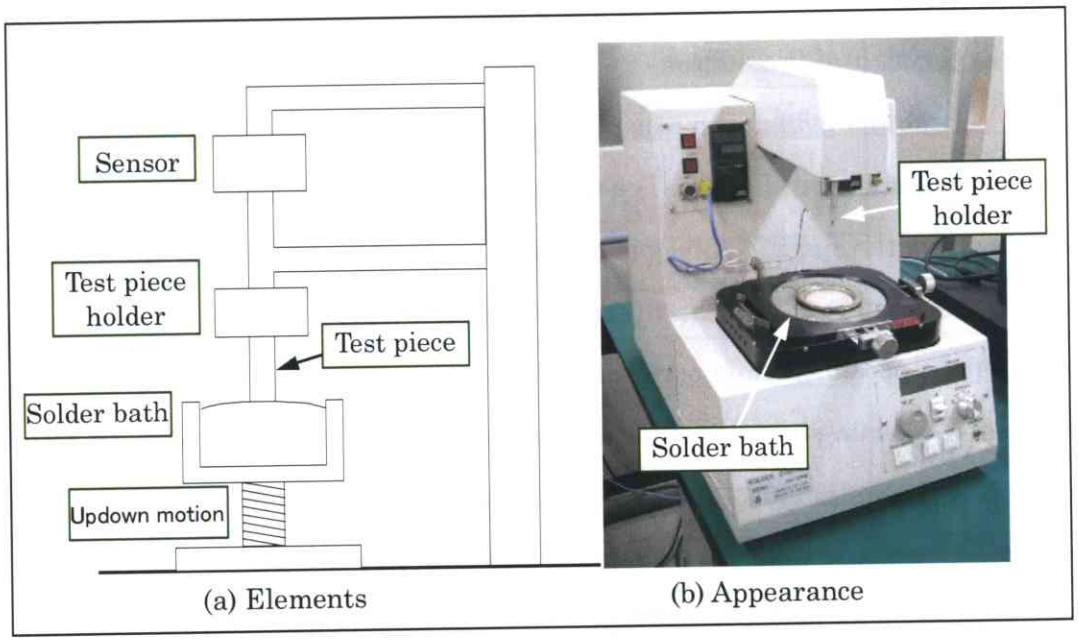

Fig.2-1 Wetting balance test device

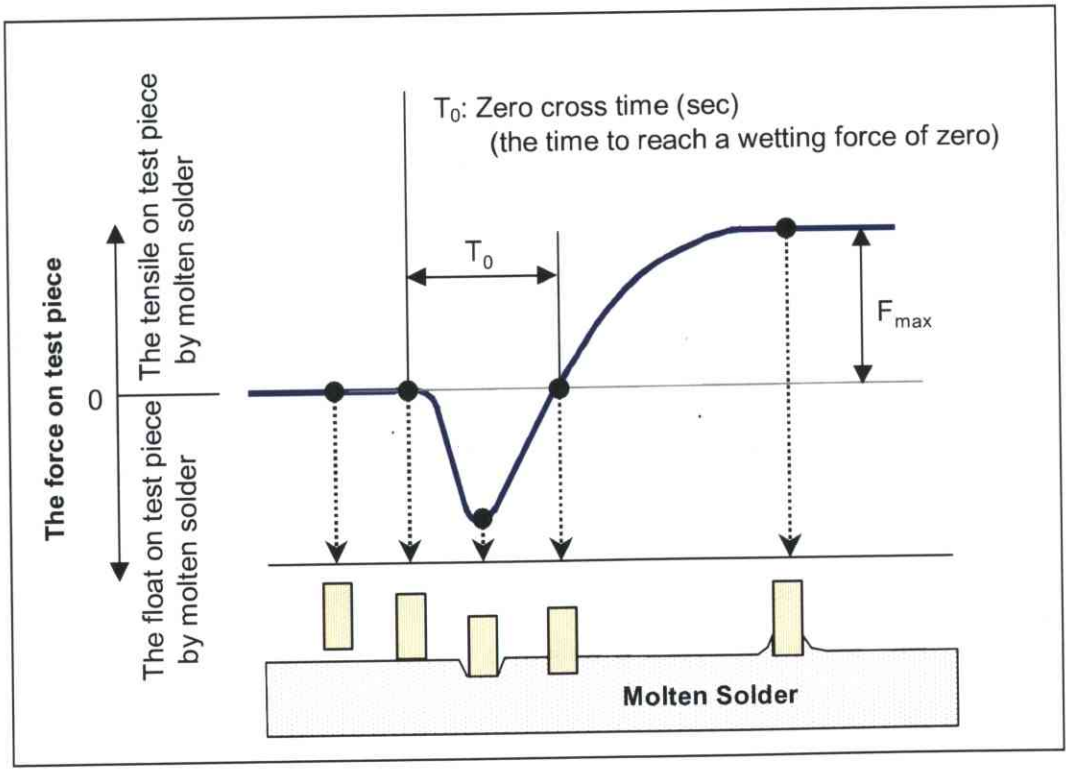

Fig.2-2 Wetting balance testing method

2.2.2. Results

Figure 2-3 shows measured wetting time for the various compositions. Adding Ni and Ge resulted in less variation than that of adding different Ag content, with no clear resulting differences or trends. Wetting time clearly drops as Ag content increases from 0% to 3%.

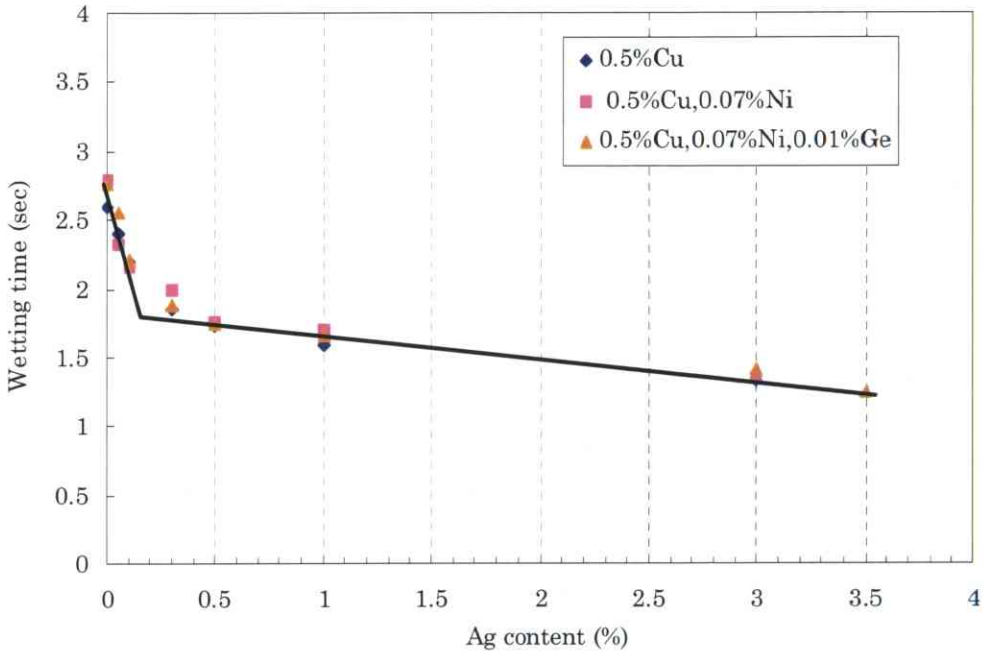

Effect of Ag on wetting time of Sn-Ag-based solder alloys

Fig.2-3. Measured wetting time results for the various compositions

Figure 2-4 presents the results of spread factor measurements (average values), comparing the relationship found between Ag content and spread factor for various cases: without adding Ni or Ge, adding Ni, or adding both Ni and Ge. In general, the spread factor varies between 76–81%. In the 0–3% range of Ag content examined in the present study, the solder alloys to which Ni or Ni and Ge have been added tend to exhibit higher spreadability than those containing neither Ni or Ge. This trend was clearest for Ag 1% and Ag 3% solder.

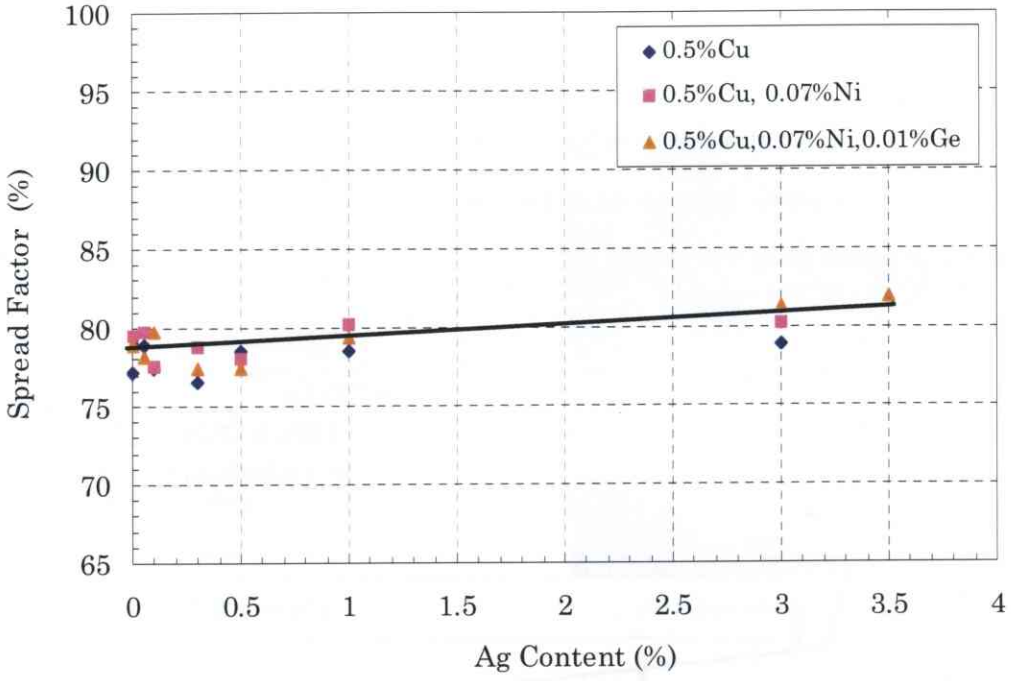

Effect of Ag on spreadability of Sn-Ag-based solder alloys

Fig. 2-4. Spread test results for various compositions

2.2.3. Discussion

Wetting times tend to be shorter with higher Ag content. In this study, wetting times dropped from 2.94 sec. to 1.18 sec. as Ag content rose from 0% to 3%. The factors controlling zero cross time are generally regarded to be solder viscosity, solderability to the base, solder surface tension, compound formation with Cu, and Cu surface conditions. The following factors are for the wetting times as Ag content rises from 0% to 3%: (1) suppression of the liquidus line associated with increased Ag content; (2) increase in viscosity associated with increased Ag content; and (3) influence of increasing Ag content on solderability to Cu plate. In this case, factors (1) and (3) are believed to predominate.

To confirm the effects of increased Ag content, I evaluated wetting times under the condition of uniform difference between the liquidus line and tested temperatures. The test was performed at 255°C. Since the liquidus line corresponding to Sn-3%Ag-0.5%Cu is at approximately 219°C, the temperature

difference is 36°C. Since the melting temperature for Sn-0.5%Cu is 232°C, the temperature difference is 23°C. Thus, for Sn-3%Ag-0.5%Cu, the wetting time was measured at 242°C to adjust the difference to 23°C; for Sn-0.5%Cu, the wetting time was measured at 268°C to adjust the difference to 36°C.

Figure 2-5 shows the results. Wetting times were nearly equivalent with equal temperature differences above the liquidus line, implying that the changes in wetting time with Ag content shown in Fig.2-3 may be almost entirely attributable to changes in the liquidus line associated with varying Ag content. The soldering temperatures must be higher with lower Ag content than that of which the composition is near the eutectic point.

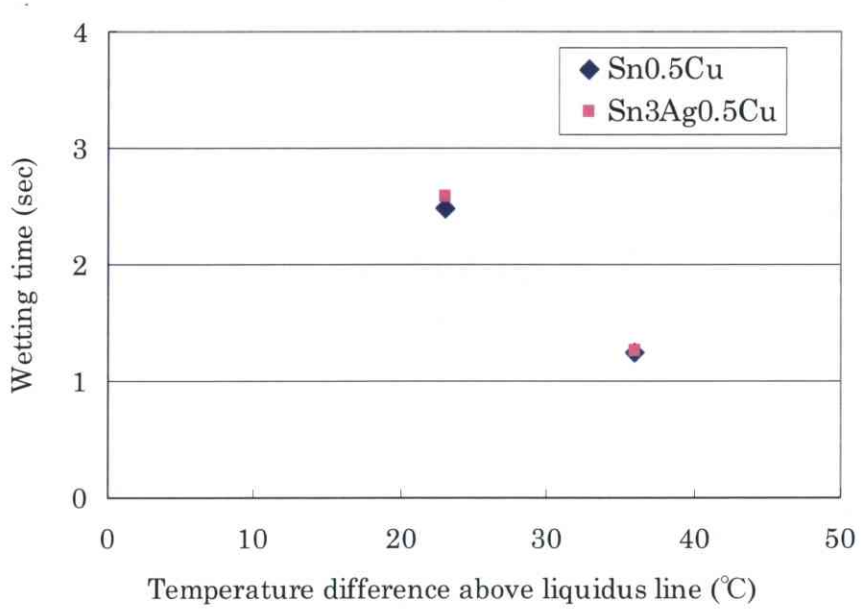

Fig.2-5. Relation between the wet time and the temperature difference above liquidus line

On the other hand, in spread tests, alloys of higher Ag content appear to have increased wetting spreadability in which add Ni and Ge. Apparently, this is because alloys with higher Ag content have a lower liquidus line and lower viscosity.

Additionally, the tendency for alloys to which Ni-Ge has been added to spread may be attributed to the suppression of Sn oxide formation by Ge and the high

solderability between the Ni and Cu test plate. As described above and in past reports, Ge exhibits higher oxidation activity than Sn and forms a thin oxide film that suppresses Sn oxidation[2-7-2-8]. Suppression of Sn oxidation increases the viscosity of the molten solder, resulting in higher wetting spreadability.

Furthermore, adding Ni-Ge appears to have clearer effects in the spread test than in the meniscograph test, due to the longer soldering times in the spread test, which allow the emergence of the effects of adding Ni-Ge described above.

2.3. Dissolution of Cu

2.3.1. Experimental Procedures

The specified sample alloy volume of 500 g was melted at 320°C in an electric furnace, after which 150 g of the melt was transferred to the SWET-2100 tester crucible, where it was retained at the specified temperature (250°C and 300°C) to perform the Cu erosion test.

The test specimen was an annealed Cu wire (0.4 mm × 60 mm) bent into a U-shape using a 1-mm rod. The specimen was cleaned with a 5% HCl solution, rinsed with water, and then dried with acetone. The flux was of the same RMA type used in the wetting and spread tests.

The specimen was immersed in molten solder and the time to rupture measured. The test was repeated five times for each composition and temperature (n = 5), after which average values were calculated. The cross-sections of the ruptured specimens near the rupture point were examined under an optical microscope, EPMA (JXA-8900RL), and transmission electron microscope (TEM, SMI-3050MS model) to determine solder composition distributions.

2.3.2. Results

Figure 2-6 shows the results of a Cu erosion rupture test performed at 255°C. In general, alloys to which Ni and Ge have been added appear to have rupture times 5-6 times that of those without. Under Ag-free conditions, we obtained data for cases with Ni and Ge added, Ni added, and neither Ni nor Ge added. No clear effects could be observed for adding Ge, indicating that Ni content is the dominant factor with respect to rupture time. At Ag compositions ranging from 0% to 3%, rupture times for the Sn-Ag-Cu specimens appear to be slightly in 1%Ag and 3%Ag solders, although remaining within the range of statistical variation (3,000 to 4,140 sec).

Figure 2-7 shows the results of a rupture test at 300°C. Compared to results obtained for tests at 255°C, rupture times are reduced by roughly half. I observed no clear differences in rupture times with varying Ag content. Moreover, I observed no differences in rupture times with between temperature conditions with varying Ag content. Adding Ni to the sample prepared for comparison had more significant effects, suggesting rupture time depends on Ni content.

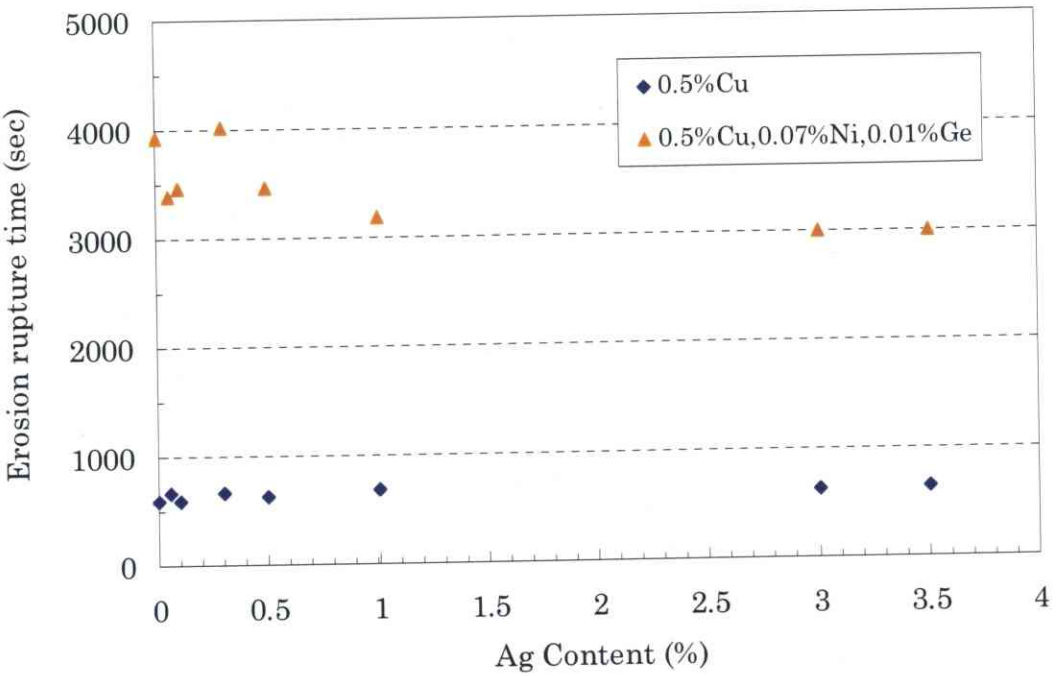

Effect of Ag on Cu erosion of Sn-Ag-based solder alloys at 255℃

Fig.2-6. Erosion test results at 255℃

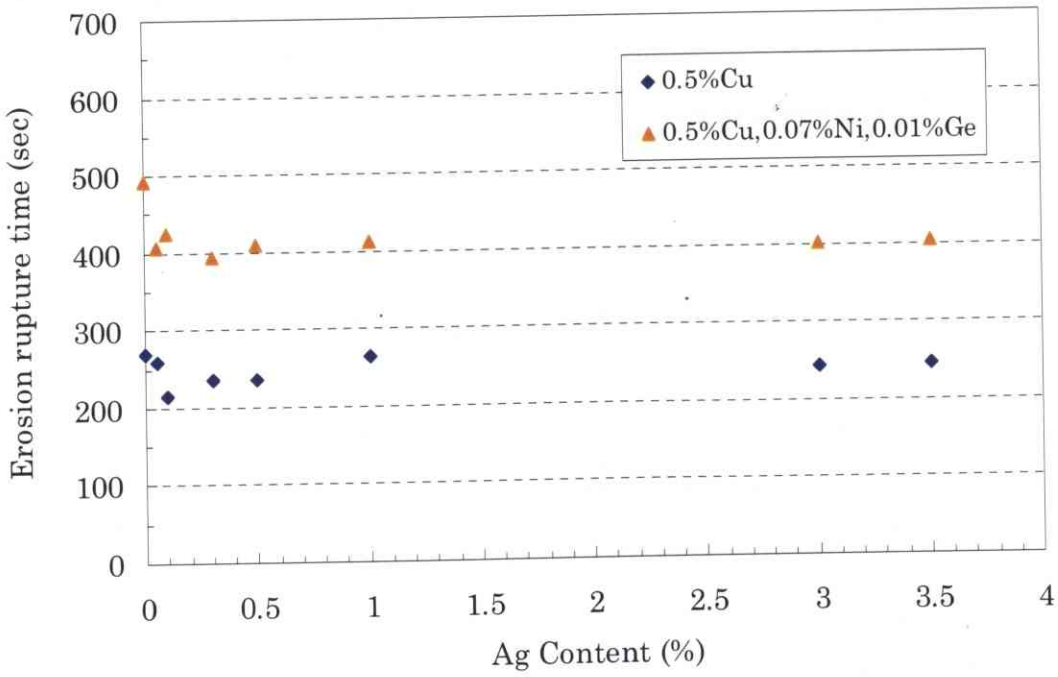

Effect of Ag on Cu erosion of Sn-Ag-based solder alloys at 300℃

Fig.2-7. Erosion test results at 300℃

2.3.3. Discussion

To identify factors contributing to the results of our Cu wire rupture test, we observed cross-sections of the specimens tested at 255°C with compositions of 0%, 0.5%, and 1% Ag.

Figure 2-8 shows the cross-sections of the (a) SCNG and (b) SC for Ag 0% composition. For the Ni-Ge added solder, we found that a thick layer of compound formed at the area of dissolution from the root to the tip of the Cu wire immersed in the molten solder. The layer thickness was nearly equivalent to the diameter of the wire. Solder adheres to the external surface of the thick compound layer. Since similar conditions were observed in cases in which only Ni was added, the presence of Ge apparently did not affect outcomes. In SC without Ni and Ge, no compound layer was observed to form with narrow Cu wire diameters, and solder was found to partially adhere to the surface.

(a) SCNG

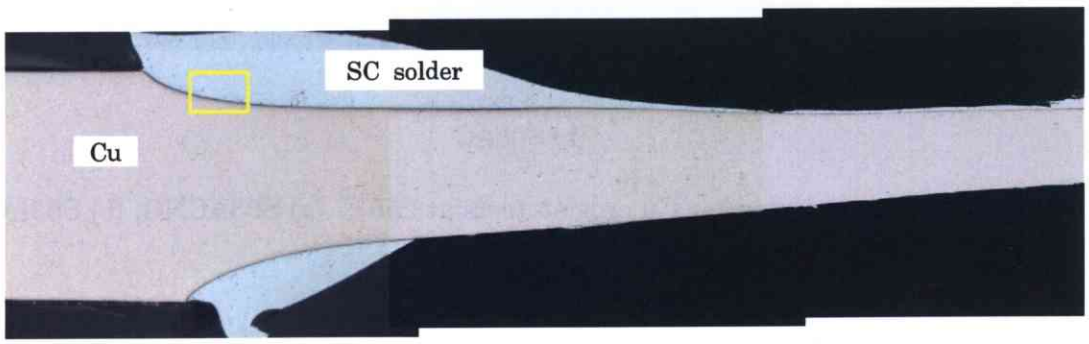

(b) SC

Fig.2-8. Cross section after Cu erosion tests at 255℃ (a) SCNG, (b) SC

Similar conditions were observed for the 0.3% and 1.0% Ag SACNG and SAC

Figure 2-9 (a) 0.3% Ag S03ACNG and (b) Ag 0.3% SAC.

Figure 2-10 (a) 1% Ag S1ACNG and (b) 1% Ag SAC).

The Cu wire cross sections in these figures were short because the positioning of the cross section was off-center in the sample preparation. The compositional distributions was investigated in these cross sections using EPMA.

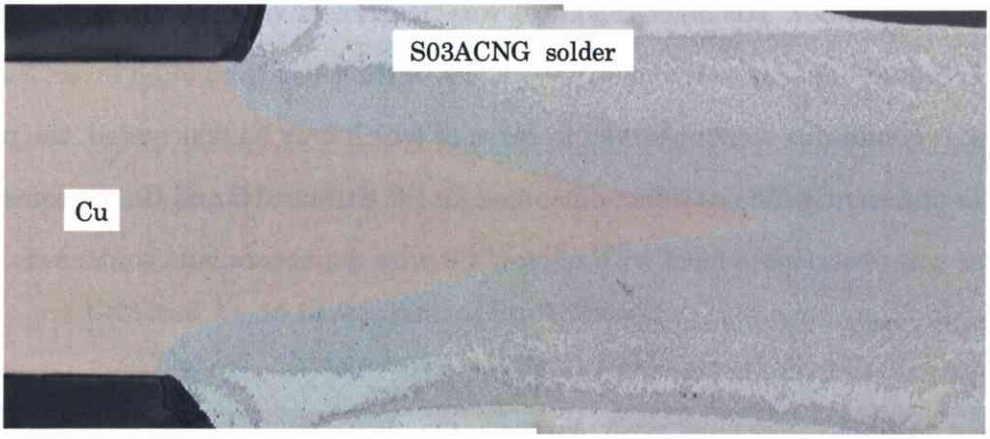

(a) S03ACNG

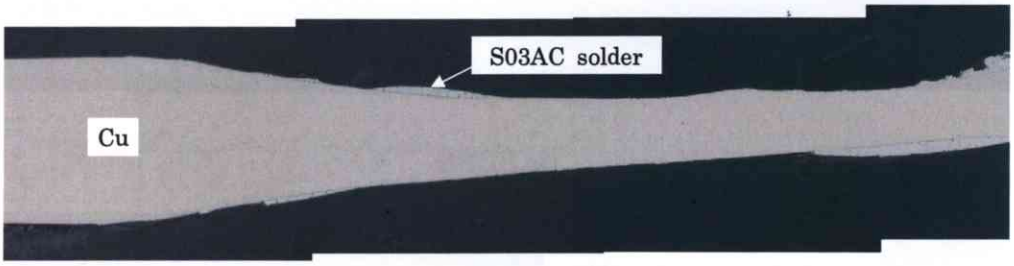

(b) S03AC

Fig.2-9. Cross section after Cu erosion tests at 255℃ (a) S03ACNG, (b) S03AC

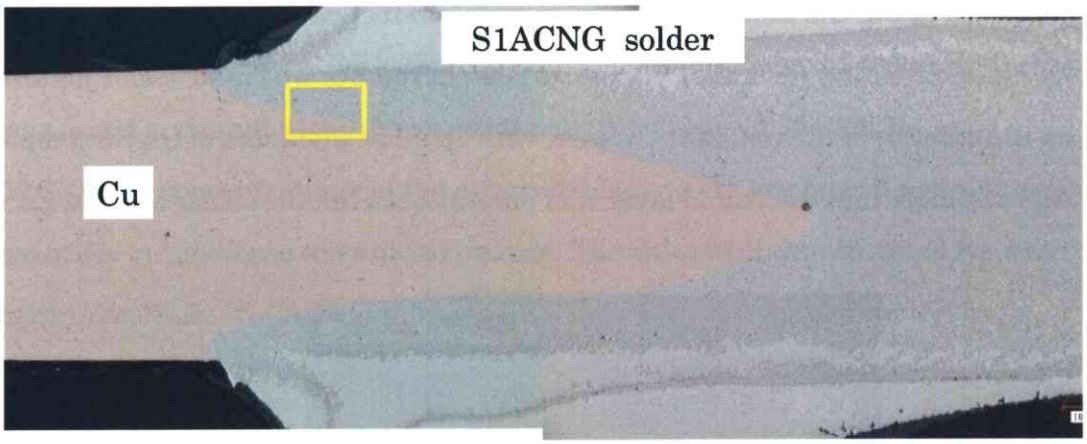

(a) S1ACNG

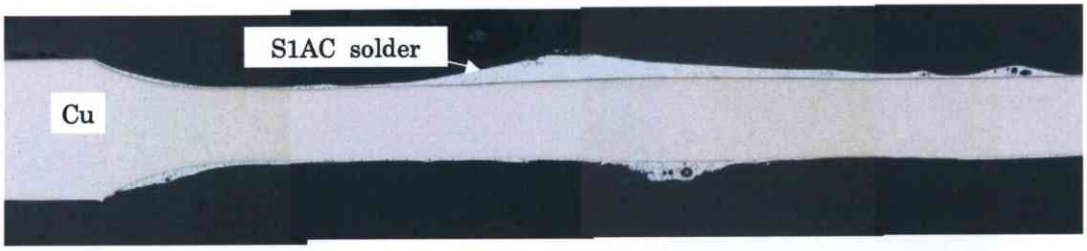

(b) S1AC

Fig.2-10. Cross section after Cu erosion tests at 255℃ (a) S1ACNG, (b) S1AC

Figure 2-11 shows the compositional distributions of SCNG and SC without Ag. In the SCNG compound layer, we understood that the compound ((Cu, Ni)-Sn) composed of Sn, Cu, and Ni and Ni concentration increased as the distance increased from the remnant Cu wire surface. In the SC, we found solder materials on the exterior of the remnant Cu wire, with sporadic instances of Cu-Sn compound. An extremely thin compound layer was present between the solder and the Cu wire.

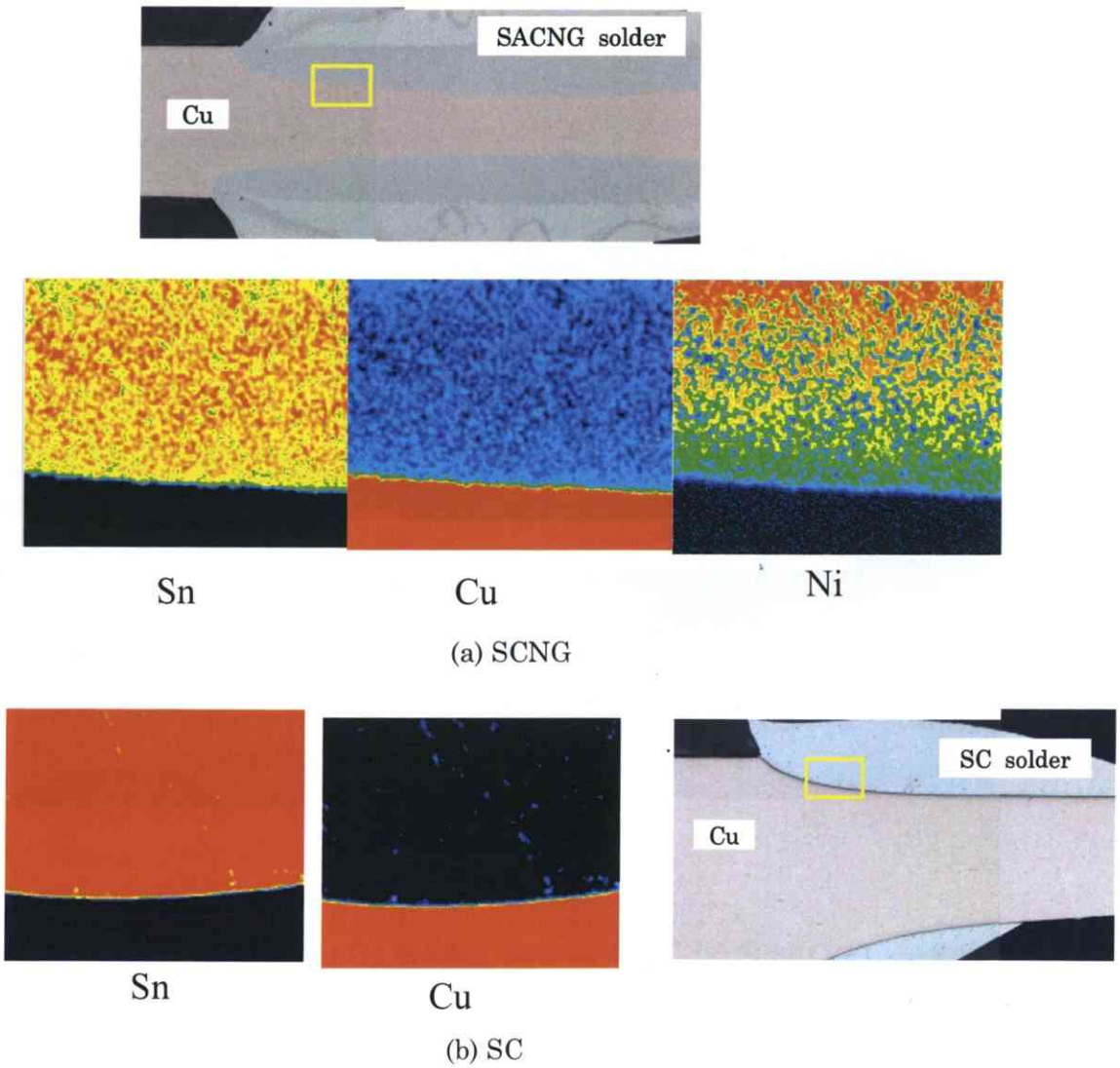

Fig.2-11. Distribution in cross section after Cu erosion tests at 255℃
(a) SCNG, (b) SC

Figure 2-12 shows the compositional distribution of S1.0ACNG with 1.0% Ag. As with 0% Ag, Ni concentrations increased in the direction away from the external surface of the Cu wire. Sn, Cu and Ni were detected by EDX. These were also observed for 0.3%Ag S0.3ACNG. The compound layer was believed to be (Ni, Cu)-Sn. Ag was found scattered within the compound layer in both 0.3% and 1%Ag S1.0ACNG. Ag concentrations in the compound layer were low near the remnant Cu wire surface but increase toward the outside. The volume of the scattered Ag was higher in the 1%Ag S1.0ACNG compared with 0.3%AgS0.3ACNG. The Ag-poor compound layer near the Cu wire was also deficient in Ni. The results of compositional analysis of a surface section of the Cu wire with adhering solder for 0.3% and 1%Ag SAC, which contains no Ni or Ge, show that solder layers are composed primarily of Sn without containing Cu, and that a thin compound layer forms at the interface between the solder layer and the Cu wire. Furthermore, in the cases of both 0.3% and 1%Ag SAC, Ag is scattered within the Sn-based solder layer.

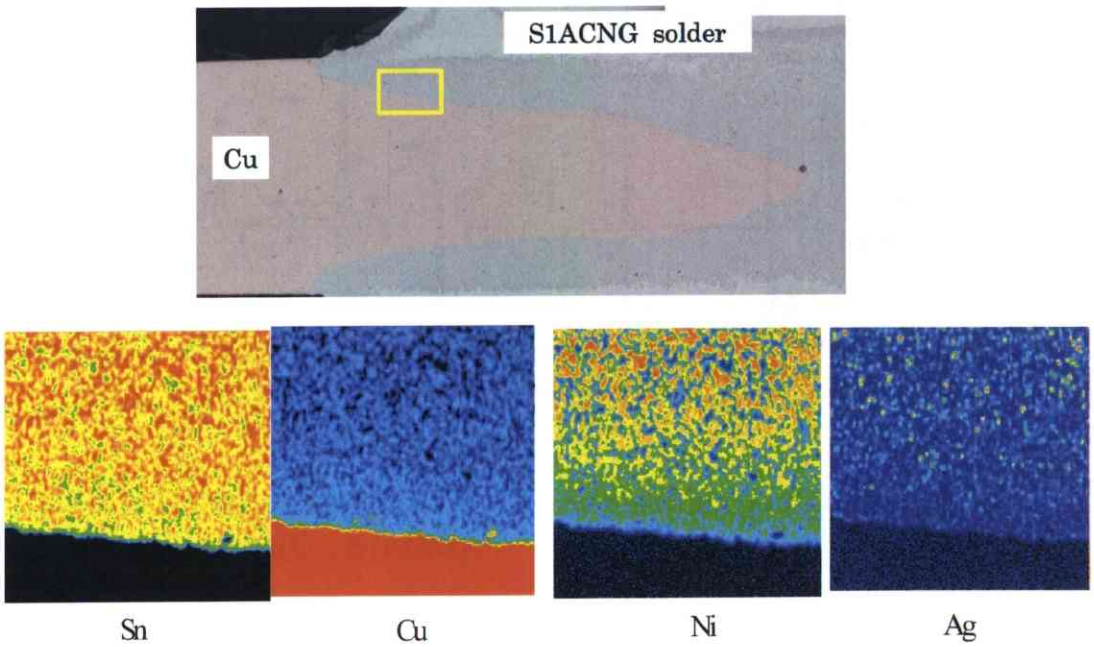

Fig.2-12. Distribution in cross section after Cu erosion tests at 255℃, S1ACNG

The compound layer and the scattered Ag were also investigated with TEM analysis for S03ACNG and S1ACNG.

Figure 2-13 shows TEM images of S03ACNG. The thick compound layer (a) was identified as $(Cu, Ni)_6Sn_5$ [2-7-2-8] ,while the thin compound layer between the thick compound layer and remnant Cu wire was observed to be Cu_3Sn, which containing no Ni(b). More scattered Ag was in S1ACNG.

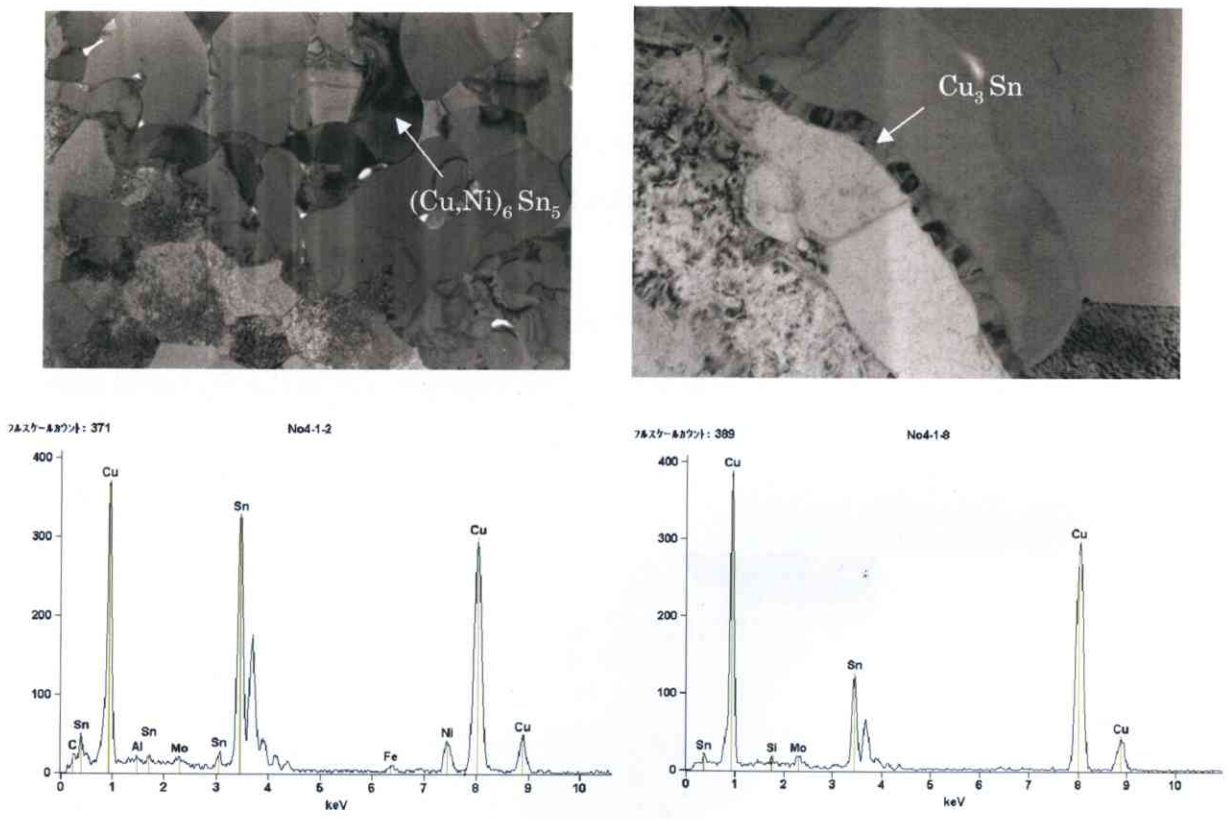

Fig.2-13. TEM and EDX analysis in cross section after Cu erosion tests at 255℃ , S03ACNG

Figure 2-14 shows TEM images of the S1.0ACNG. Figure 2-14 also shows a thin compound layer of Cu_3Sn, while the scattered Ag also observed at the grain boundaries was identified as Ag_3Sn. While Ag is not directly involved in Cu dissolution, we found it scattered throughout the (Cu, Ni)-Sn compound layer formed when Ni is added, mainly at grain boundary.

It may act to suppress diffusion within the compound layer and promote more dense compound formation[2-9-2-10]. Ge could not be detected, due to the low volumes added.

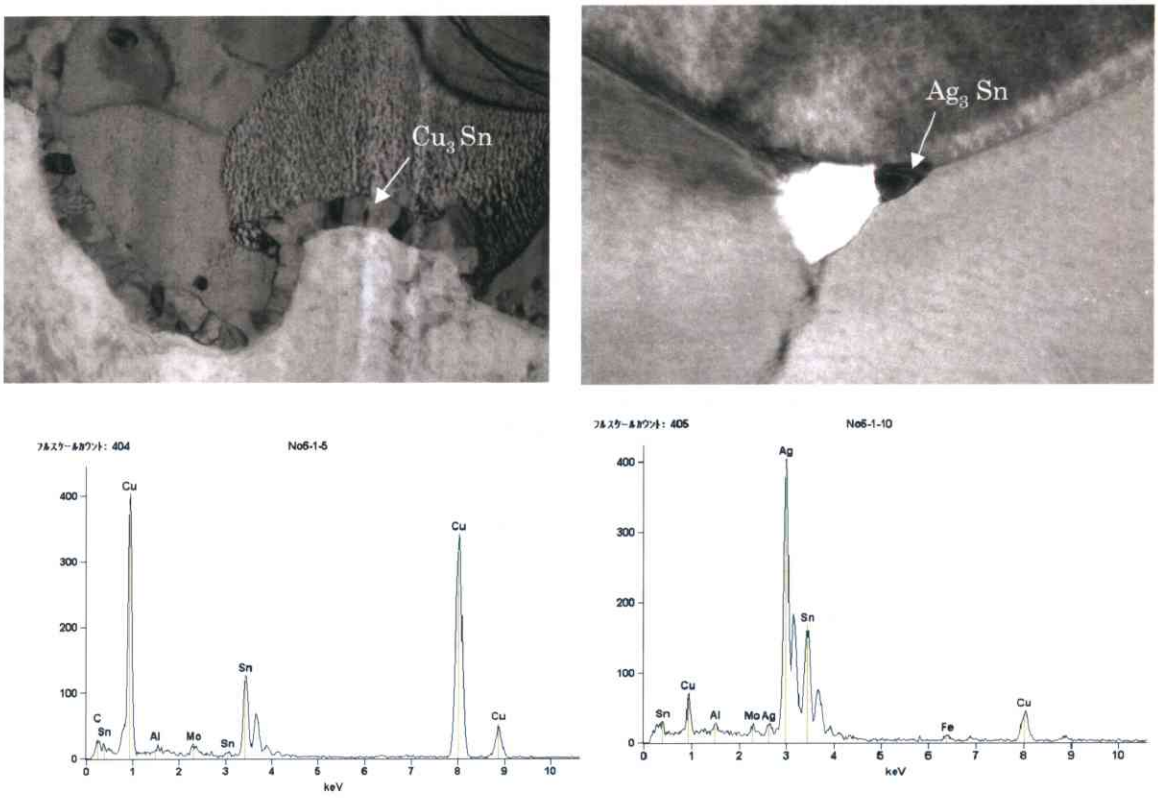

Fig.2-14. TEM and EDX analysis in cross section after Cu erosion tests at 255℃ , S1ACNG

2.4. Drossing (Sn oxidation)

Because the melting point has become higher than before, Sn element in the Sn-Ag system lead-free solder is easily oxidized. To prevent this, Ge was added in the lead-free solder alloys. The effect of Ge element on preventing Sn oxidation of Sn-Ag-Cu lead-free solder alloy was investigated.

2.4.1. Experimental Procedures

Drossing, oxide formed in the atmosphere on the surface of the molten solder, was collected from the wave soldering.

Figure 2-15 is a schematic cross-section view of wave soldering equipment. Drossing depositedon the surface of the molten solder was extracted at 250℃ in the atmosphere, and the elements in the drossing of the solders were analyzed by Inductively Coupled Plasma-Atomic Emission Spectroscopy (ICP-AES).

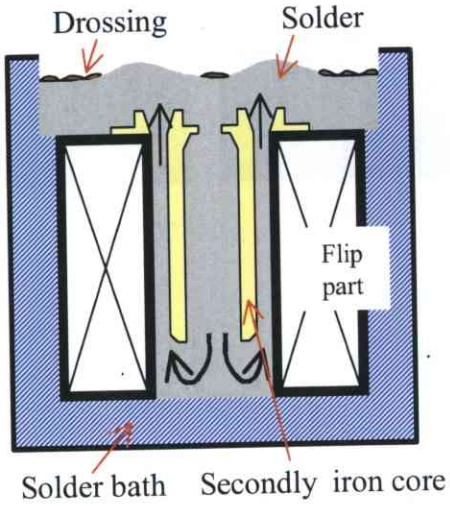

Fig.2-15. The schematic cross-section view of wave soldering equipment

2.4.2. Results

Figure 2-16 shows the amount of drossing of both solders in the atmosphere on the surface of the molten solder after different times(2~8 h) at250℃ in wave soldering. In this case, the amount of Ge was 0.02wt%. From this graph, the amount of drossing of the S3.5ACNG solder was about 1/2 or less comparedwith the S3AC solder. As a result, drossing was greatly decreased by adding the small amount of Ge. Therefore, it is very effective to prevent drossing added Ge into the solder[2-11-2-12].

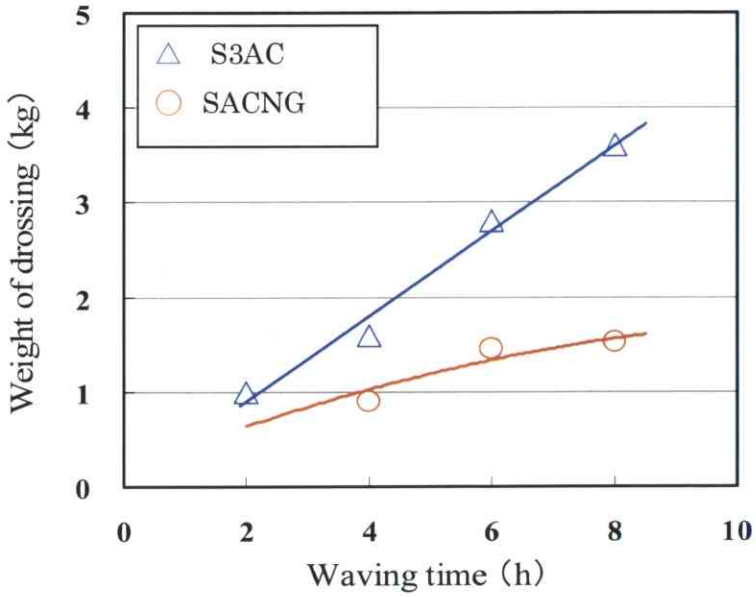

Fig.2-16. Amount of drossing of two kinds solder

Table 2-3 shows the result of analyzing the component of drossing after waving the molten solder in the atmosphere for eight hours. From the results, the amount of Ge concentrated to the drossing was 10 times compared to that ofthe S3.5ACNG solder.

Table 2-3. The results of analyzing the component of drossing. (wt.%)

Alloy. No		Sn	Ag	Cu	Ni	Ge
S3.5ACNG	Solder	95.98	3.46	0.47	0.07	0.02
	Drossing	95.84	3.42	0.47	0.07	0.20
S3AC	Solder	96.54	2.97	0.49	—	—
	Drossing	96.70	2.85	0.45	—	—

2.4.3. Discussion

To analyze the surface oxidation of two kinds of solders, the specimen oxidized in atmosphere at 250℃ for 2hrs in the molten state was used. Each specimen, the size of which were 8mmf×2mm, was cleaned for 10min with supersonic waves in an organic solvent prior to investigation with X-ray Photoelectron Spectroscopy (XPS). An aluminum anode X-ray source producing Al K α X-rays at 1486.6 eV was used. The x-ray spot size was 100 μ mf; and analysis area was 1mm□. The cross-section of soldered specimen was polished with 0.25□m diamond and cleaned with Ar ion. The distributed form of Ge in solder alloy was analyzed with Scanning Auger Electron Spectroscopy (AES), for which the acceleration voltage was 20kV and the beam size was 50nmf.

The XPS depth profiles Sn, O, Ge on S3.5ACNG and S3AC are shown in Fig.2-17, Fig.2-18 respectively. Moreover, Sn narrow scanning spectrum analysis results of these solders are shown in Fig.2-19, Fig.2-20, and Ge narrow scanning spectrum on the surface of S3.5ACNG is shown in Fig.2-21.

Figure 2-17 shows that the density of Ge is high from the surface to a 20nm depth, and the density of oxygen decreases rapidly around 20nm from the surface.

Moreover, Figure 2-19 and Figure 2-21 show that the oxide layers of Ge and Sn are only near the surface. Therefore, the XPS analysis results of S3.5ACNG show that Ge has been concentrated to the surface and a very thin oxidation layer (20nm~30nm) of Ge was formed on the surface of the S3.5ACNG solder. It is believed that the thin oxide layer (film) of Ge is very effective to prevent the oxidation of the SACNG solder.

On the other hand, the results of S3AC solder show rather long tail oxygen and Sn oxide profile (over 100nm), which indicate that oxidation diffusion does occur in deeper regions (Fig.2-18, Fig.2-20).

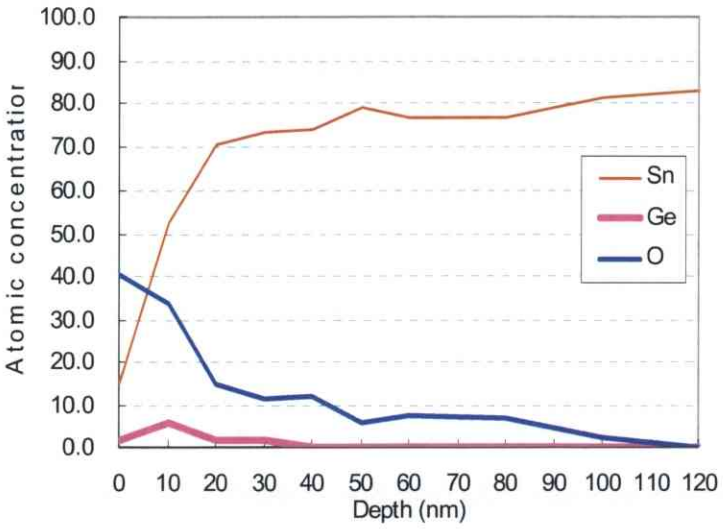

Fig.2-17. XPS depth profiles of SACNG

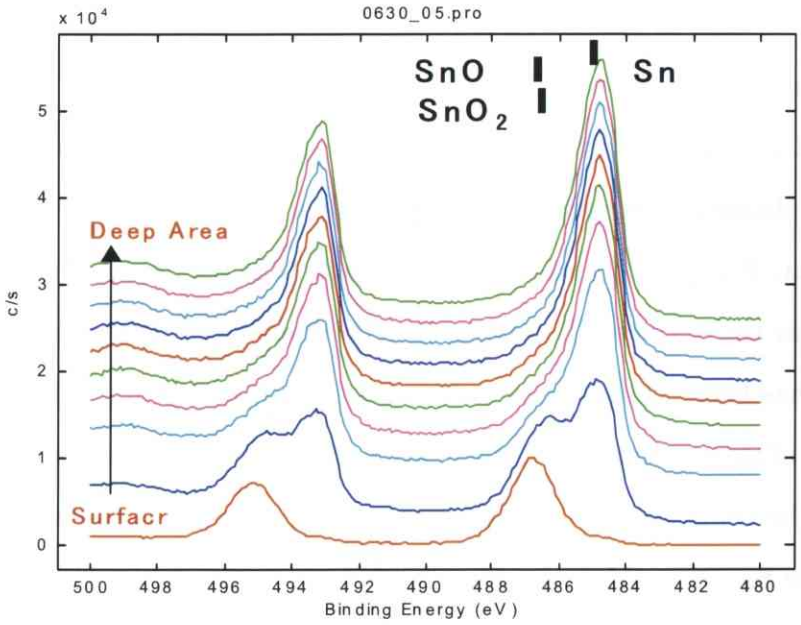

Fig.2-18. XPS narrow scanning spectrum of Sn3d on the surface of SACNG

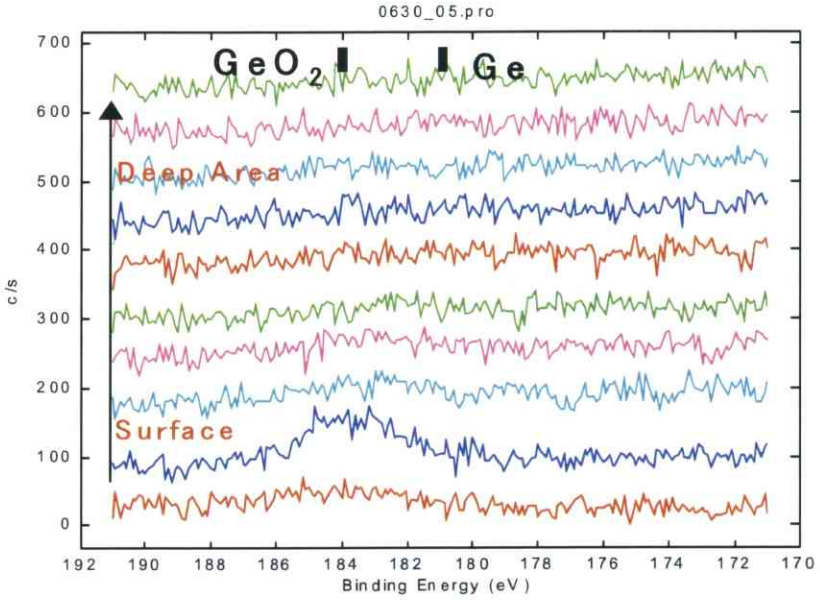

Fig.2-19. XPS narrow scanning spectrum of Ge3s on the surface of S3.5ACNG

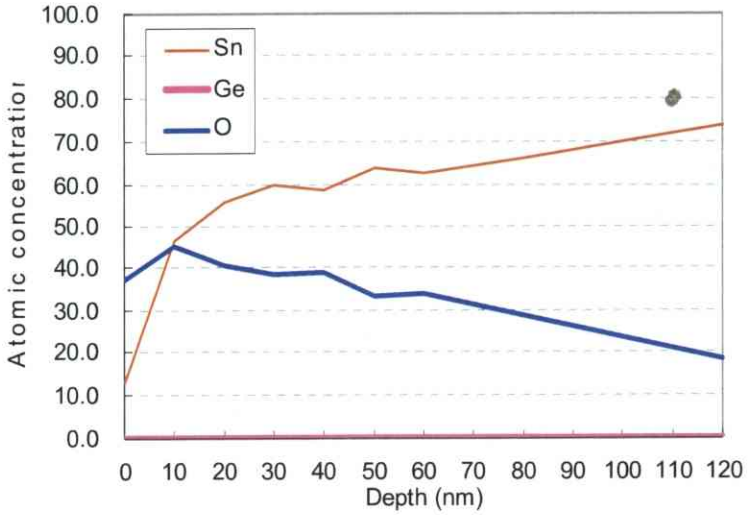

Fig.2-20. XPS depth profiles of S3AC

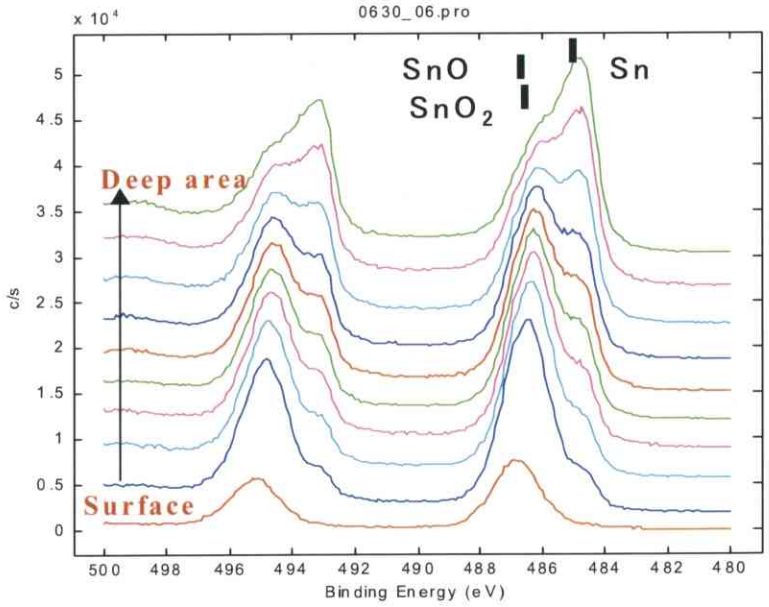

Fig.2-21. XPS narrow scanning spectrum of Sn3d on the surface of S3AC

Distribution Form of Ge in S3.5ACNG Solder

The distribution form of Ge in the cross-section of jointed Cu electrode parts was analyzed by AES.

Figure 2-22 shows a scanning electron image and an auger electron image of S3.5ACNG solder, and the schematic elemental distribution is shown in Fig.2-23. The results show that enriched Ge was found in the grain boundary region of the Sn-rich phase in the solder alloy.

It is considered that the enhanced Ge around grain boundary region was formed due to the surface diffusion of Ge in Sn-rich phase of the solder[2-13-2-14].

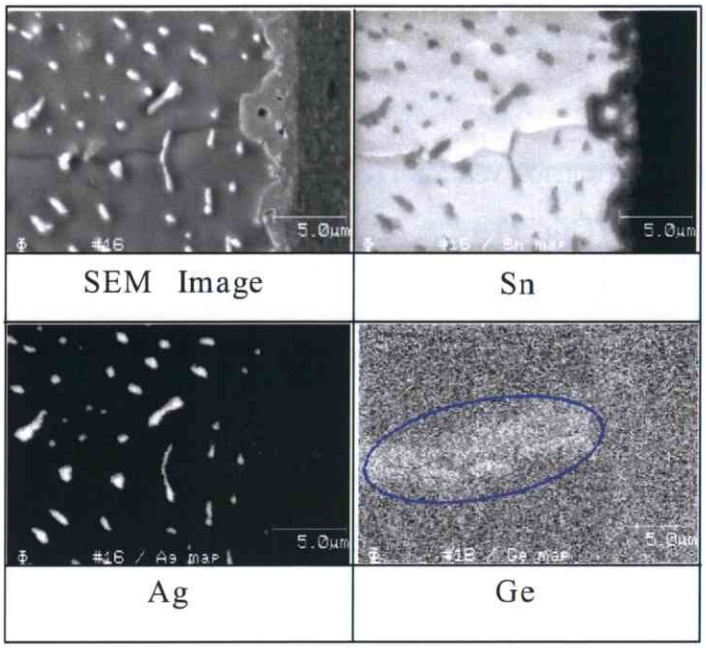

Fig.2-22. AES mapping analysis of S3.5ACNG

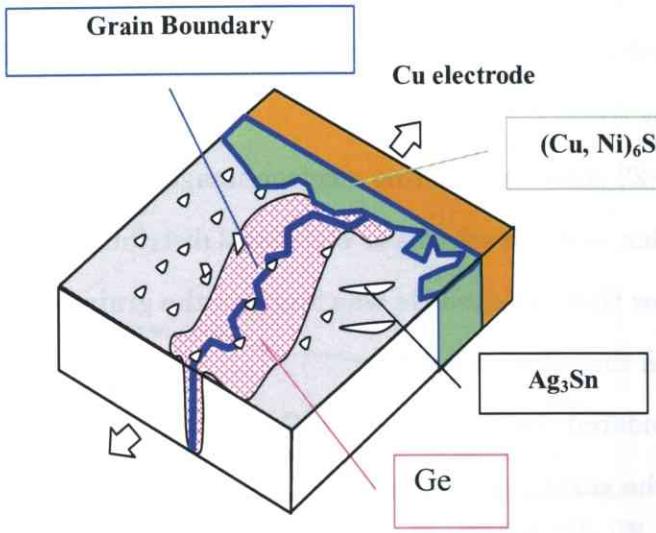

Fig.2-23. Schematic elemental distribution

Whether the oxidation reaction occurs or not, is generally evaluated by the oxidation free energy (ΔG°)[2-15-2-16]. ΔG° is shown in eq.(1).

$$\Delta G^\circ = \Delta H - T\ \Delta S \quad \text{---------- (1)}$$

At high temperature, the heat capacity ΔCp is considered, and the equation is shown in (2).

$$\Delta G^\circ = \Delta H298 + \int \Delta Cp\, dT - T\Delta S298 - T\int (\Delta Cp/T)\, dT \quad \text{---------(2)}$$

Where : $\Delta H298$: Enthalpy at 25℃(298K), $\Delta S298$: Entropy at 25℃(298K),

ΔCp : Heat capacity, T : Temperature (K)

Table 2-4. Oxidation free energy at 250 ℃ (kJ/mol)

SnO_2	SnO	Ag_2O	CuO	Cu_2O	NiO	GeO_2
- 474	- 235	(+)	- 108	- 131	(+)	- 477

Table 2-4 shows the oxidation free energy ΔG° estimated at 250℃(523K). The oxidation reaction of various elements is the following: Ge>Sn>Cu. From these results, the element of Ge is effective to prevent oxidation of SACNG solder.

The oxidation prevention mechanisms of Ge are considered as the following and shown in Fig.2-24.

- The element of Ge is easier to diffuse into the surface of the molten solder, because Ge was distributed in the region of the grain boundary of Sn-rich phase.
- The element of Ge is the easiest to react with oxygen, because it has the lowest oxidation free energy of the three elements (Sn, Cu, Ge) at 250℃ (523K) in the molten solder.
- The stable film of GeO2 was easily formed on the surface of the molten solder because the element of Ge had a clear advantage over the others elements.

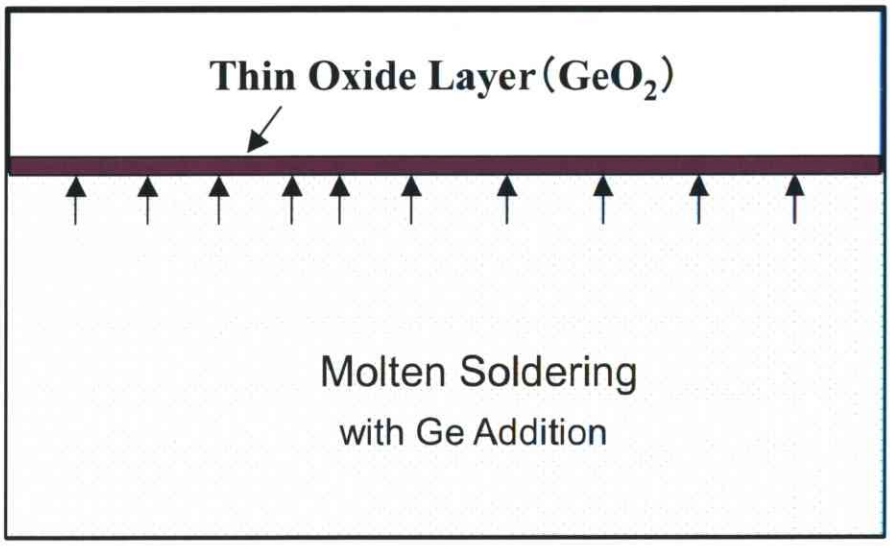

Fig.2-24. Schematic of GeO_2 layer formation in molten soldering

2.5. Conclusions

This chapter pulled together behaviors test results, which includes wettability and spreadability, dissolution of Cu, and dross (Sn oxidation).

- Based on the results of wetting evaluations performed by the eniscograph method, we found that wetting zero cross time declines as Ag content rises from 0% to 3%, due primarily to the lowering of the liquidus line temperature of the Sn-Ag alloy. The current study showed no clear consequences of adding 0.07% Ni or 0.01% Ge. With respect to wetting spreading characteristics, solder alloys with higher Ag content were found to exhibit increased spreadability.
- A Cu wire rupture test was performed to examine Cu dissolution. At 300°C, rupture times were nearly half those observed at 255°C. When no Ni was added, erosion significantly reduced the diameter of the Cu wire. In these cases, we detected only extremely thin compound layers on the surface.
- With respect to the addition of Ag, Cu, Ni, and Ge and rupture times, adding Ni significantly extended rupture times. Ni formed a thick (Ni, Cu)-Sn compound layer on the external surface of the Cu wire.
- Higher concentrations of both Ni and Ag were found toward the exterior, while Ag exhibited a scattered distribution in the (Ni, Cu)-Sn compound layer and at the grain boundary.
- The amount of drossing of the S3.5ACNG solder was about 1/2 or less compared with S3AC solder alloy. Moreover, the Ge has been concentrated to the surface and a very thin oxidation layer(20~30nm) of Ge was formed on the surface of S3.5ACNG solder. In addition, enriched Ge was distributed in the grain boundary region of the Sn-rich phase in the solder alloy. In the SACNG solder, the thin oxide layer (film) of Ge was very effective to prevent the oxidation of Sn.

2.6. References

2-1. JEITA: "Lead-free Roadmap", 2002 ver.1.0,2002.

2-2. P.Borgesen, T.Bieler, L.P.Lehman, and E.J.Cotts: "Pb-free solder: New Materials Consideration for Microelectronics Processing" Mrs Bulletin, Vol.32 ,2007, pp.360-364.

2-3. D.Shangguan, G.Gao: "Lead-Free & No-Clean Soldering for Automotive Electronics", Solder. Surf. Mt. Technol., 26,1997, pp.5-8.

2-4. R.W.Johnson, J.L.Evans, P.Jacobsen, J.R.Thompson, and M.Christopher: "The Changing Automotive Environment: High-Temperature Electronics", IEEE Transactions on electronics Packaging Manufacturing, Vol.27, No.3, 2004,pp.164-175.

2-5. JIS Z3198-4: [Test Method for Lead-free Solder, PartⅣ], 2003.

2-6. JIS Z3198-3: [Test Method for Lead-free Solder, PartⅢ], 2003.

2-7. Y.S.Lai, J.M.Song, H.C.Chang, T.T.Chiu: "Ball Impact Responses of Ni- or Ge-Doped Sn-Ag-Cu Solder Joints", J. Electron.Mater., Vol.37, No.2, 2008.

2-8. T.H.Chuang,S.F.Yen,H.M.Wu: "Intermetallic formation in Sn3Ag0.5Cu and Sn3Ag0.5Cu0.06Ni0.01Ge solder BGA Packages with immersion Ag surface finish", J. Electron. Mater., Vol.36, No.2, 2006, pp.310-318.

2-9. T.Matsumura, T. Yamamoto: "Assembly Technology Using Lead-free Solder", FUJITSU, Vol 56, No.6, 2005, pp.545-551.

2-10. T.H.Chuang, S.F.Yen, M.D.Cheng: "Intermetallic reactions in Sn3Ag0.5Cu and Sn3Ag0.5Cu0.06Ni0.01Ge solder BGA Packages with Au/Ni surface finishes", J. Electron.Mater., Vol.36, No.2, 2006, pp.302-309.

2-11. C.M.Chuang, K.L.Lin: "Effect of Microelements Addition on the Interfacial Reaction between Sn-Ag-Cu Solders and the Cu Substrate", J. Electron. Mater., Vol.32, No.12, 2003, pp.1423.

2-12. K.Habu,N.Takeda,H.Watanabe,H.Ooki,J.Abe, T.Saito,Y.Tanigachi,and K.Takayama: "Development of Highly Reliable Pb-free Solder Alloys of the Ge Doped Sn-Ag-Bi System", Proc. of 5th Symposium on Microjoining and Assembly Technology in Electronics,1999,pp.397-402.

2-13. T.Takemoto, Y.J.Joo, T.Nishimura, S.Oki, and K.Fujimoto: "Suppression of DrossFormation in Lead-free Wave Soldeering", Proc. of 5th Symposium on Microjoining and Assembly Technology in Electronics,2001,pp.491-496.

2-14. M. Nagano, N. Hidaka, M. Shimoda and H. Watanabe: "Effect of Germanium Content on Oxidation Prevention of Sn-Ag-Cu Lead-free Solser", Proc. of New Frontiers of Process Science and Engineering in Advanced Materials, PSEA'04, 2004, pp.256-261.

2-15. O.Kubaschewski, E.Ll.Evans, and C.B.Alcock: "Metallurgical Thermo -chemistry", 1967.

2-16. K.Hauffe: "Oxidation of Metals", 1965.

Chapter 3 Mechanical Properties (Tensile Strength and Low-Cycle Fatigue) of Lead-free Sn-Ag-Based Solder Alloys

3.1. Introduction (Purpose)

3.1.1. Tensile Strength

This chapter presents a quantitative analysis of solder joint reliability data for lead-free Sn-Ag-based solder alloys. In order to keep the reliability of the solder joint, it is necessary to understand the various properties in which affect those of the whole joint.

The chapter will focus on the fundamental aspect of time-independent deformation mode in lead-free Sn-Ag-based solder alloys. In the laboratory, time-independent deformation is typically generated by the stress-strain experiments. The tests are carried out under either strain-rate control or stress-rate control, but most often, the experiments are performed under strain-rate control.

3.1.2. Low- Cycle Fatigue

As described, In general, the long-term reliability of electronic solder joints is determined by the creep and fatigue properties of the solder alloy[3-1-3-3)].

Fatigue deformation results when a cyclic stress or cyclic strain is applied to the material. When the deformation is caused by a defined range of applied stress, then fatigue is said to be stress controlled. On the other hand, fatigue that results from a repeated strain displacement is said to be strain controlled. Nearly all fatigue conditions that are applicable to soldered interconnections, whether it be thermal mechanical fatigue that is generated by the combination of temperature variations and thermal expansion mismatch of fatigue that is caused by mechanical vibration, result in strain controlled, cyclic deformation.

The chapter will also focus on thermal fatigue that affects the performance of solder interconnections. Thermal fatigue is another critical parameter in lead-free Sn-Ag-based solder alloys. Constraint of thermal expansion is causes thermal stresses, which may eventually initiate and propagate fatigue. Thermal fatigue may be

classified under the more general heading of low-cycle fatigue, because thermal fatigue cracks usually start in less than 50,000 cycles. In addition, a thermal fatigue cycle usually contains significant inelastic strain[3-4].

3.2. Experimental Procedure

3.2.1. Tensile Test

The evaluation of time-independent deformation of bulk solder properties can be carried out in tension test. The test sample dimensions are typically large, relative to the microstructural features of the material. Test procedures and data analysis regiments have been established in the JIS standard (JIS-Z3198) specifications[3-5].

Tensile test is constructed as shown in Fig.3-1 by potting the stress determined by dividing the axial load P by the original area of cross section A_0 as ordinate versus the strain $\varepsilon_0 = \triangle L_0/L_0$ as abscissa where $\triangle L_0$ is the increment of the original gage length L_0. The strain ε_0 is thus determined from axial strain measurements by the use of one of the strain gages available commercially.

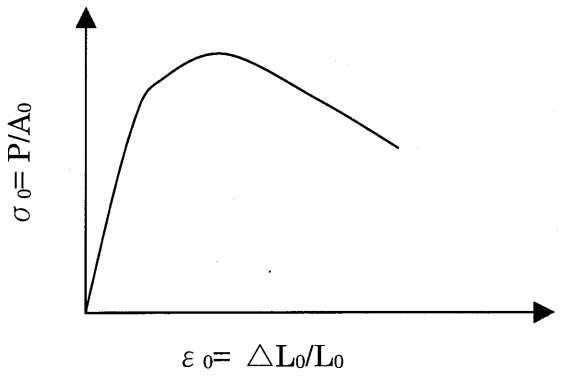

Fig.3-1 Ordinary stress-strain curve for solder alloy

Multiple extensometers or strain gages can be used to measure deformation along several directions with respect to the stress axis, thereby providing the mean to determine the bulk modulus of the material.

Rapidly cooled, as-cast, specimens of Sn-Ag-based solder alloys were used in this study. Tensile tests were carried out in an Instron Model electro-hydraulic servo machine at temperatures among 25 ℃(298K)to 125℃(398K).

The bulk specimens consisted of cast ingots of Sn-Ag-based solders (shown in table 3-2) purchased from NIHON HANDA. Solder bars prepared by the manufacturer were melted in air in an electric furnace at 330℃(603 K) for two hours. The melt was then chill-cast as an ingot in a stainless steel mold measuring 14 mm in diameter and 160 mm in length. The solder rods were machined into round shape of creep specimen measuring 15 mm in length and 3 mm in diameter (Fig.3-2). All specimens were heat-treated at 60℃(333 K) for 24 h to remove residual stress and defects induced during specimen forming.

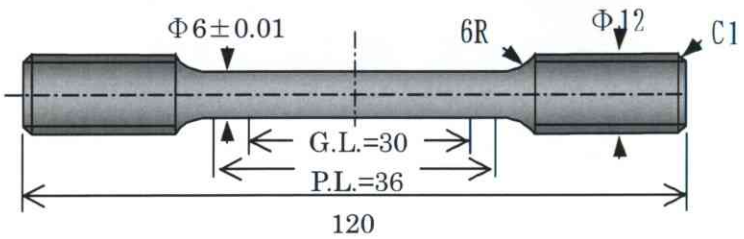

(a) Specimen shape (JIS Z 3198-2)

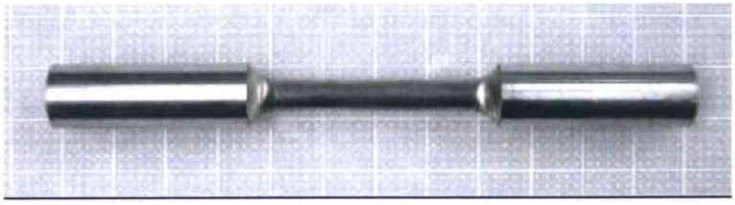

(b) Appearance

Fig.3-2 Tensile test specimen

Fig.3-3 Tensile test machine

Table 3-1. Comparison of the Various Solder Alloys

No.	Element					Reference
	Sn	Ag	Cu	Ni	Ge	
7	Bal	3.0	0.5	0.07	0.01	Compared with Ag content
6	Bal	3.5	0.5	0.07	0.01	
8	Bal	4.0	0.5	0.07	0.01	
6	Bal	3.5	0.5	0.07	0.01	Compared with Cu content
9	Bal	3.5	0.75	0.07	0.01	
10	Bal	3.5	1.25	0.07	0.01	
11	Bal	3.5	1.5	0.07	0.01	
12	Bal	3.5	2.0	0.07	0.01	
13	Bal	3.5	0.5	0.0	0.01	Compared with Ni content
6	Bal	3.5	0.5	0.07	0.01	
14	Bal	3.5	0.5	0.1	0.01	
15	Bal	3.5	0.5	0.2	0.01	

Table 3-2. Composition of the Solder Alloys

No.	Element					Alloy codes
	Sn	Ag	Cu	Ni	Ge	
1	Bal	0.3	0.5	-	-	S03AC
2	Bal	1	0.5	-	-	S1AC
3	Bal	1	0.5	0.07	0.01	S1ACNG
4	Bal	3	0.5	-	-	S3AC
5	Bal	3	0.5	-	-	S3.5AC
6	Bal	3.5	0.5	0.07	0.01	S3.5ACNG (SACNG)

3.2.2. Low-cycle Fatigue Test

As solder joints become smaller, to accommodate the increased miniaturization of electronic products, the test was performed with smaller size test piece.

Figure 3-4 shows the miniature size specimen. The specimen is 1.0 mm in diameter and 2.5 mm in length of parallel section.

Figure 3-5 shows the Fatigue machine of LMH207 Micro Load Test System (Saginomiya). Electromagnetic Linear Actuator System with air bearing, which is characterized low friction and high stiffness, has exceptionally good features for Micro Fatigue Test. This serves precise micro force and micro displacement, which is achieved by advanced digital servo controller.

(a) Appearance of machine

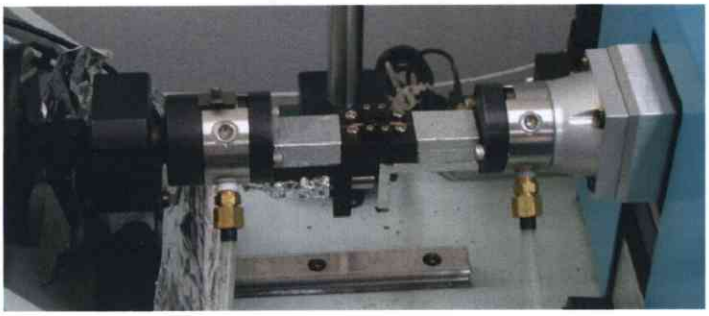

(b) Appearance of the guide of specimen

Fig.3-5 Fatigue test machine

3.3. Experimental Results and Discussion

3.3.1. Effects of Ag, Cu, and Ni Elements With the Content of Ag Over 3.0wt%

The effects of Ag, Cu, and Ni elements on tensile strength, elongation are gave in following. The base material was Sn3.5Ag0.5Cu0.07Ni0.01Ge (SACNG) solder alloy. The tensile speed was 0.2%/s. The Ag content was changed from 3.0wt% to 4.0wt%. The Cu content was changed from 0.5wt% to 2.0wt%. The Ni content was changed from 0.07wt% to 0.25wt%. The effects of adding Ag element on tensile strength and elongation are shown in Fig.3-6, Fig.3-7.

Although Ag content was increased from 3% to 4%; the tensile strength was in same level. The elongation also was in same level. Moreover, if it dares to say, the strength and elongation of the solder alloy with 3.5%Ag content was best one in the three of the solder alloys with the content of Ag from 3.0% to 4.0%.

The tensile strength and elongation were also compared among those solder alloys, which the content of Cu changed from 0.2wt% to 2.0wt%.

Figure 3-8 shows result of the tensile strength and Figure 3-9 shows the elongation result of which the content of Cu changed from 0.2wt% to 2.0wt%. There are not clear deference of strength and elongation in these solder alloys.

Figure 3-10 shows result of the tensile strength and Figure 3-11 shows the elongation result of which the content of Ni changed from 0.07wt% to 0.25wt%.

The tensile strength and the elongation are also in same levels, which the content of Ni changed from 0.07wt% to 0.25wt%.

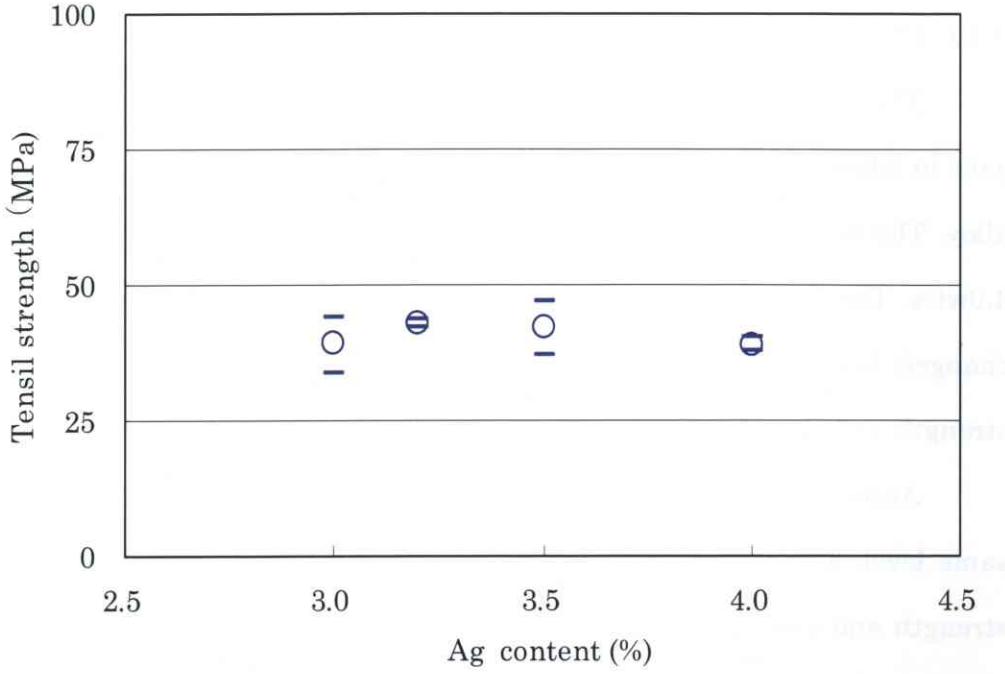

Fig.3-6 Effect of Ag content in Sn0.5Cu0.07Ni0.01Ge (mass%) solder alloy on the tensile strength.

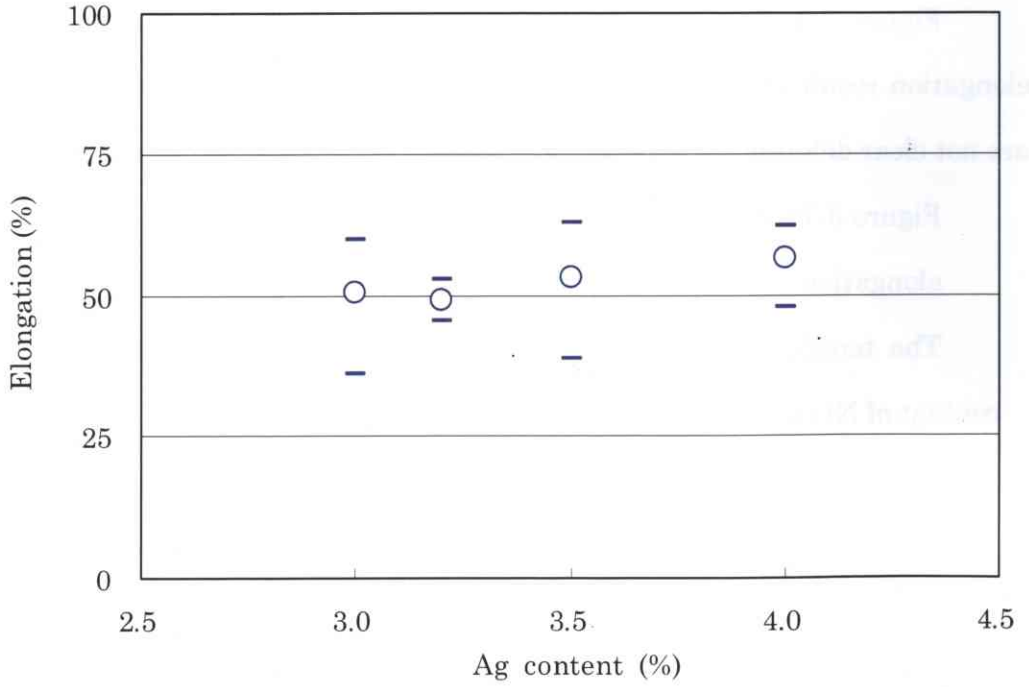

Fig.3-7 Effect of Ag content in Sn0.5Cu0.07Ni0.01Ge (mass%) solder alloy on the elongation.

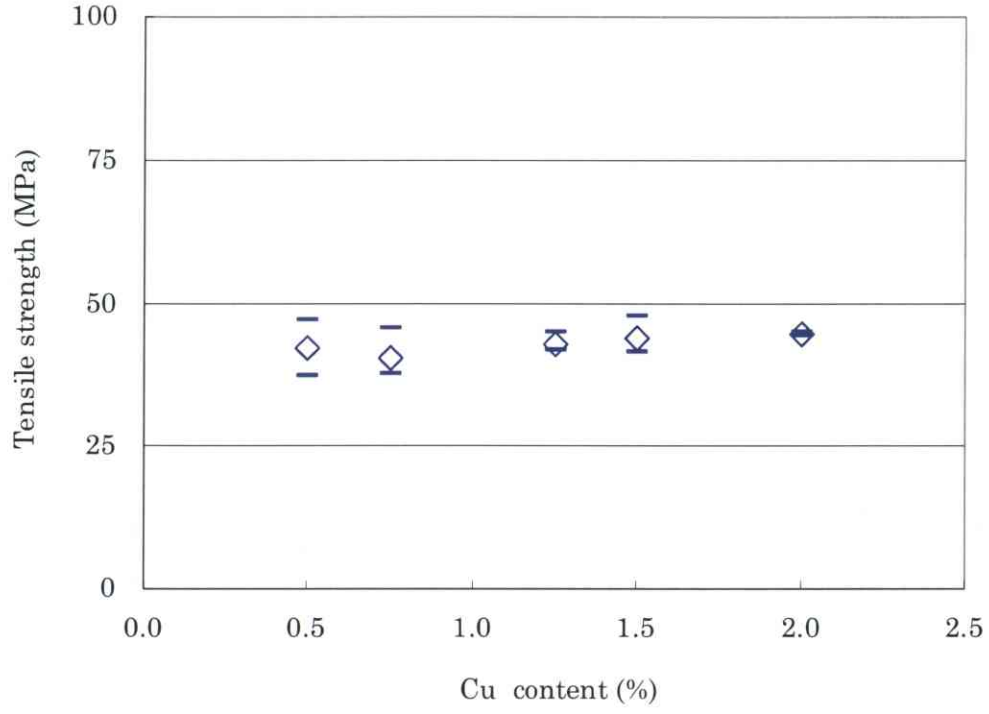

Fig.3-8 Effect of Cu content in Sn3.5Ag0.07Ni0.01Ge (mass%) solder alloy on the tensile strength.

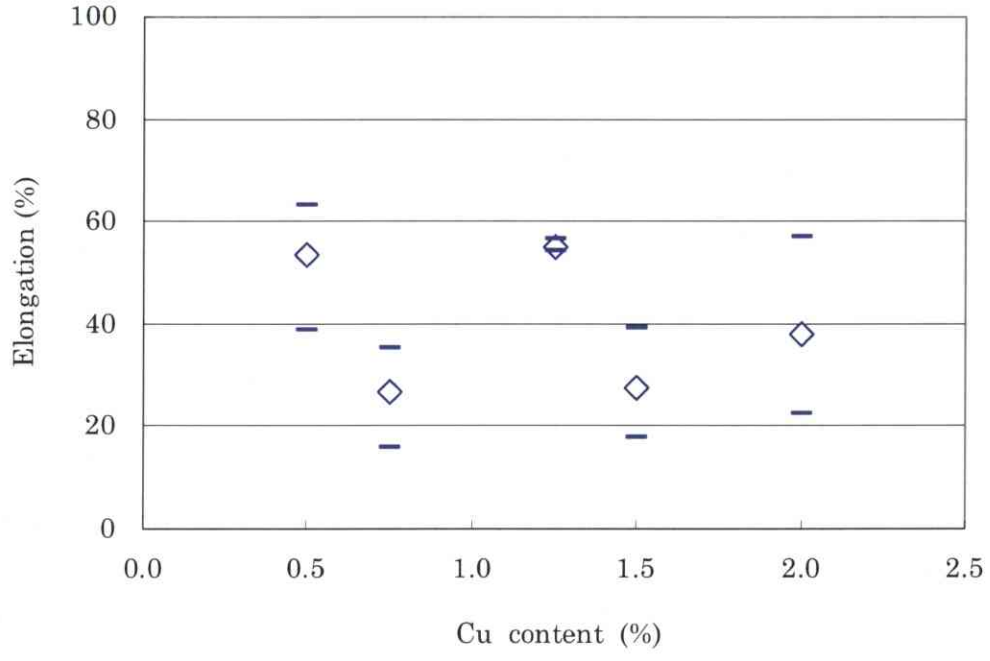

Fig.3-9 Effect of Cu content in Sn3.5Ag0.07Ni0.01Ge (mass%) solder alloy on the elongation.

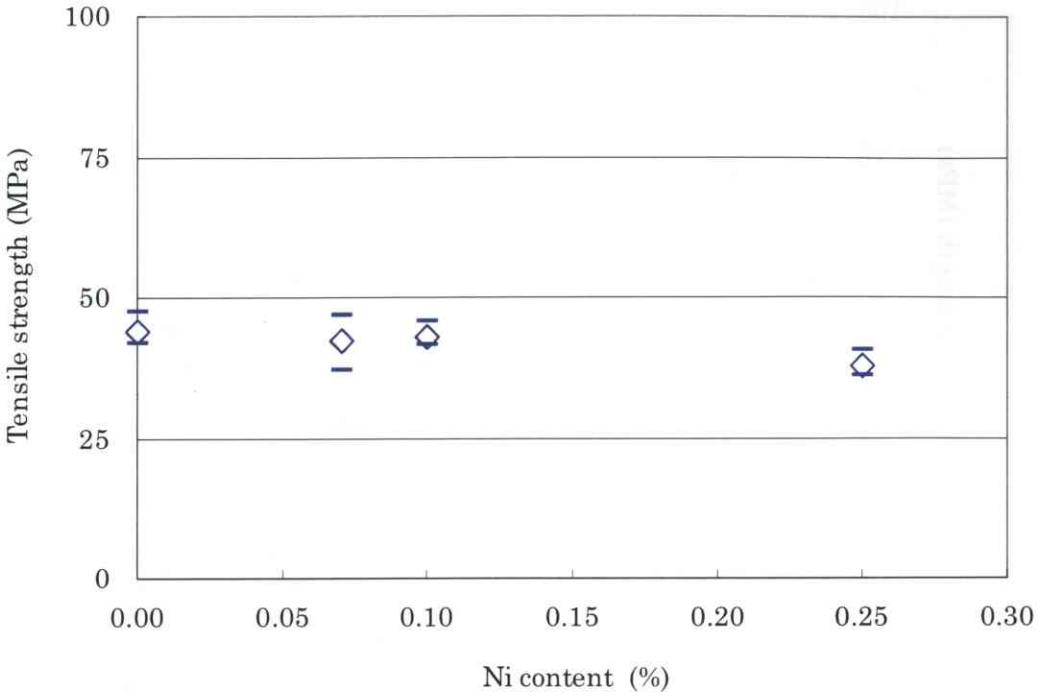

Fig.3-10 Effect of Ni content in Sn3.5Ag0.5Cu0.01Ge (mass%) solder alloy on the tensile strength.

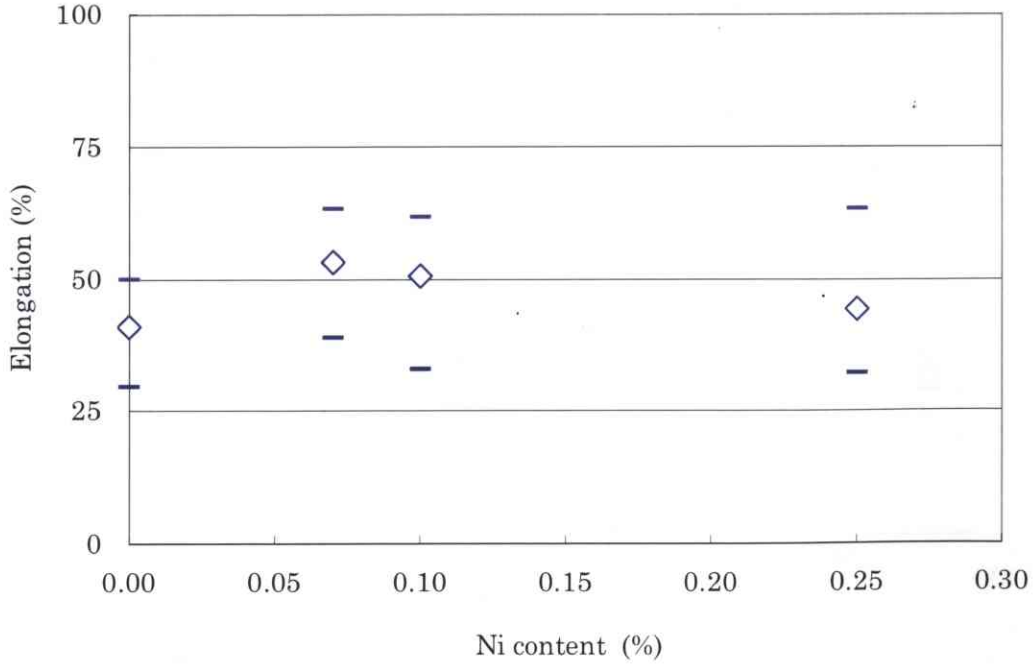

Fig.3-11 Effect of Ni content in Sn3.5Ag0.5Cu0.01Ge (mass%) solder alloy on the elongation.

3.3.2. Effects of Ag, and Ni Elements With the Content of Ag Below 3.0wt%

To understand the effect of adding Ag, Ni, the tensile test was also performed at the temperatures of 25℃,75℃,and 125℃ with strain rate at 0.002%/s.

Figure 3-12 shows relationship between tensile strength and temperature of S0.3AC, S1.0AC, S1.0ACNG, and S3.5ACNG. The tensile strength decreases with increasing temperature. The tensile strength increases with increasing the content of Ag from 0.3wt% to 3.5wt%. The tensile strength increases with adding Ni into the solder alloy, although the effect is smaller.

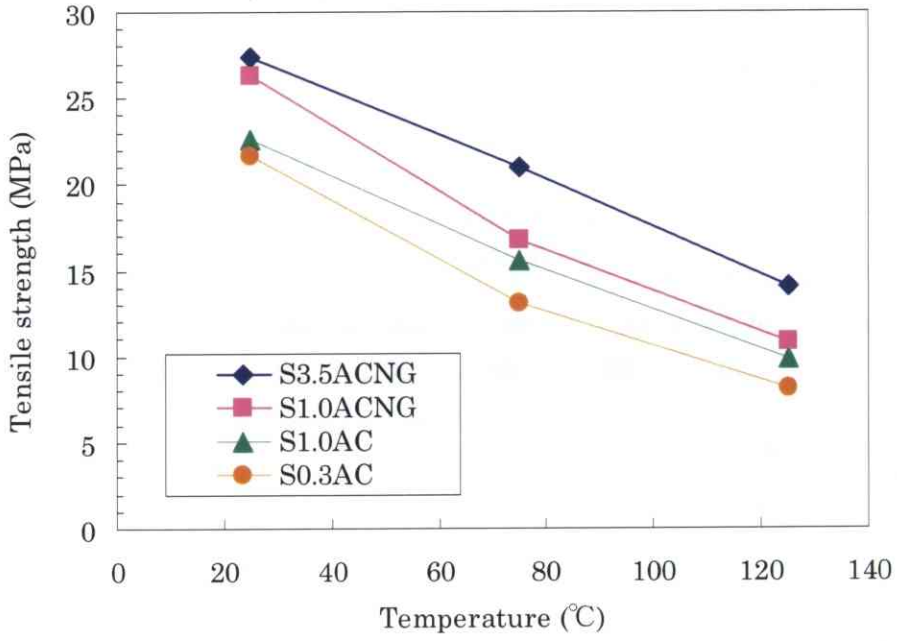

Fig.3-12 The relationship of tensile strength and tensile test temperature in various lead-free Sn-Ag-based solder alloys.

Figure 3-13 shows relationship between yield strength and temperature of S0.3AC, S1.0AC, S1.0ACNG, and S3.5ACNG. The yield strength shows a similar tendency with tensile strength. The Yield strength decreases with increasing temperature and increases with increasing the content of Ag from 0.3wt% to 3.5wt%. Also, the yield strength increases with adding Ni into the solder alloy.

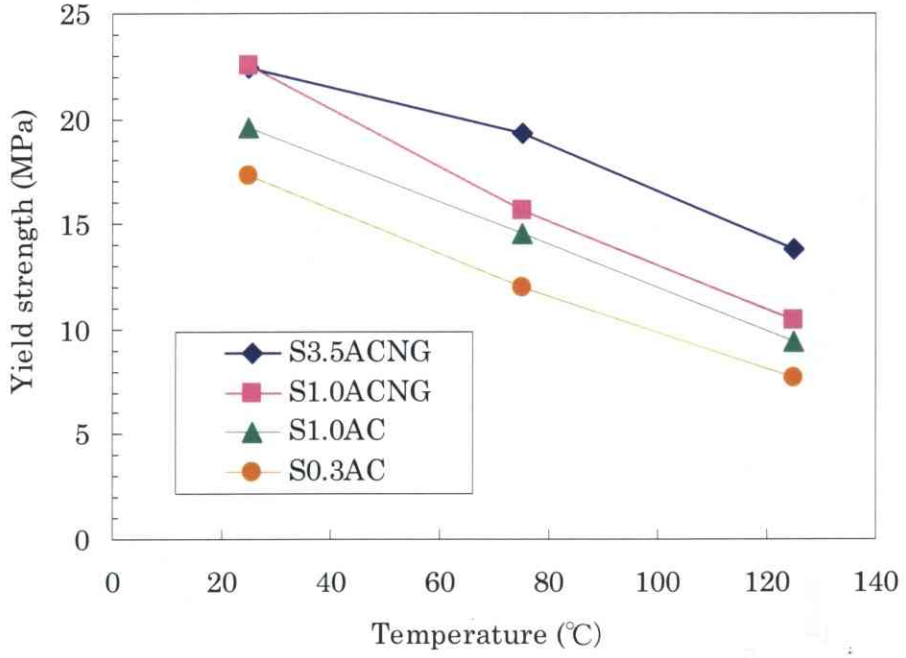

Fig.3-13 The relationship of yield strength and tensile test temperature in various lead-free Sn-Ag-based solder alloys.

Figure 3-14 shows relationship between elastic modulus E and temperature of S0.3AC, S1.0AC, S1.0ACNG, and S3.5ACNG. The elastic modulus E decreases when the temperature increase from 25℃ to 125℃. The elastic modulus E decreases when the temperature increase from 25℃ to 125℃.

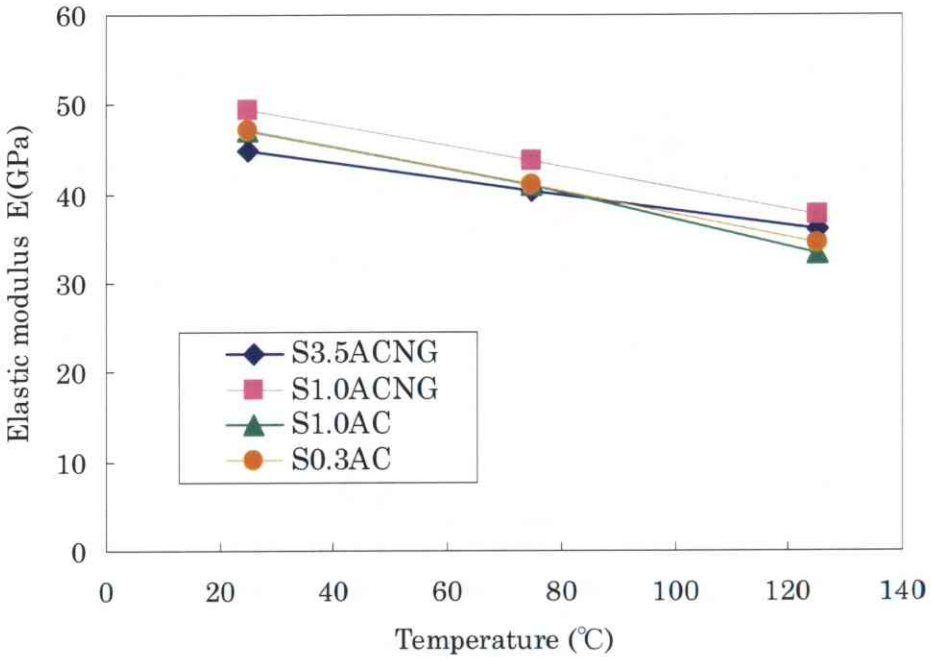

Fig.3-14 The relationship of elastic modulus and tensile test temperature in various lead-free Sn-Ag-based solder alloys.

Figure 3-15 shows relationship between elongation and temperature of S0.3AC, S1.0AC, S1.0ACNG, and S3.5ACNG. The elongation decreases when the temperature increase from 25℃ to 125℃. The elongation of the S0.3AC is the best among the four kinds of solder alloys.

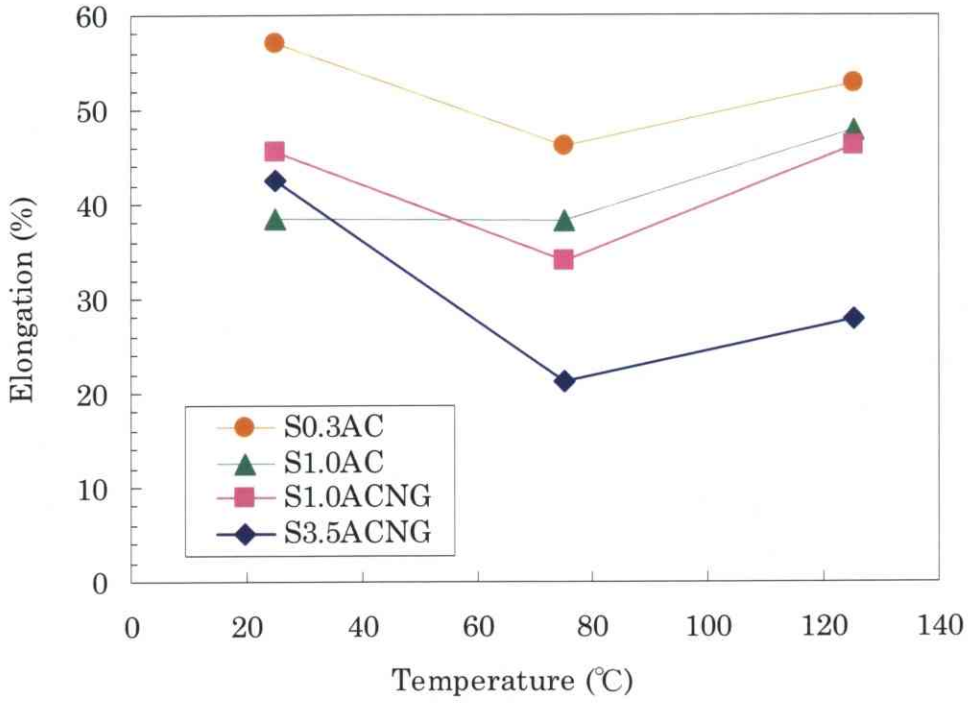

Fig.3-15 The relationship of elongation and tensile test temperature in various lead-free Sn-Ag-based solder alloys.

3.3.3. Low Cycle Fatigue

Figure 3-16 shows the low-cycle tested results of lower Ag solder alloys of S0.3AC, S1.0AC, and S1.0ACNG at room temperature(25℃). The plastic strain $\triangle \varepsilon_p$ is 90% or more in the total strain. Moreover, no significant difference can be observed in those solder alloys. in the other word, The fatigue life is in same level in three kinds of Sn-Ag-based solder alloys.

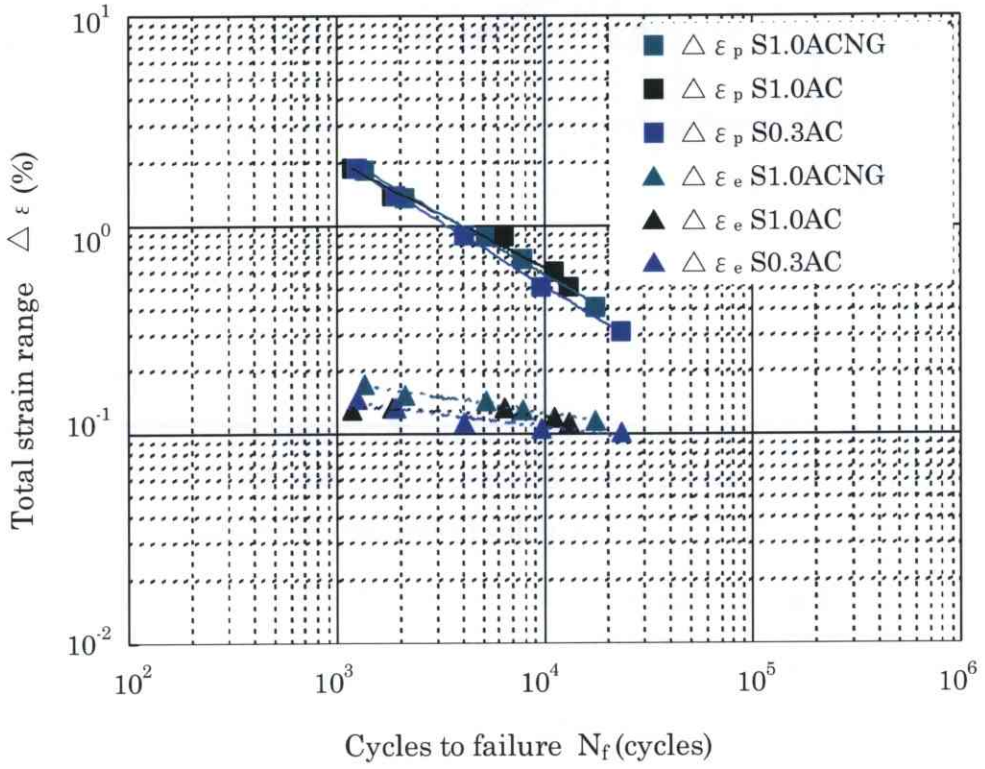

Fig.3-16 Cycles-to-failure (N_f) versus strain range
for S0.3AC, S1.0AC,S1.0ACNG solder alloys at 25℃

Figure 3-17 shows the low-cycle tested results for S0.3AC, S1.0AC, and S1.0ACNG at 125. The fatigue life at 125℃has similar tendency to that of at 25℃.

It shows that no significant difference exit in those solder alloys.

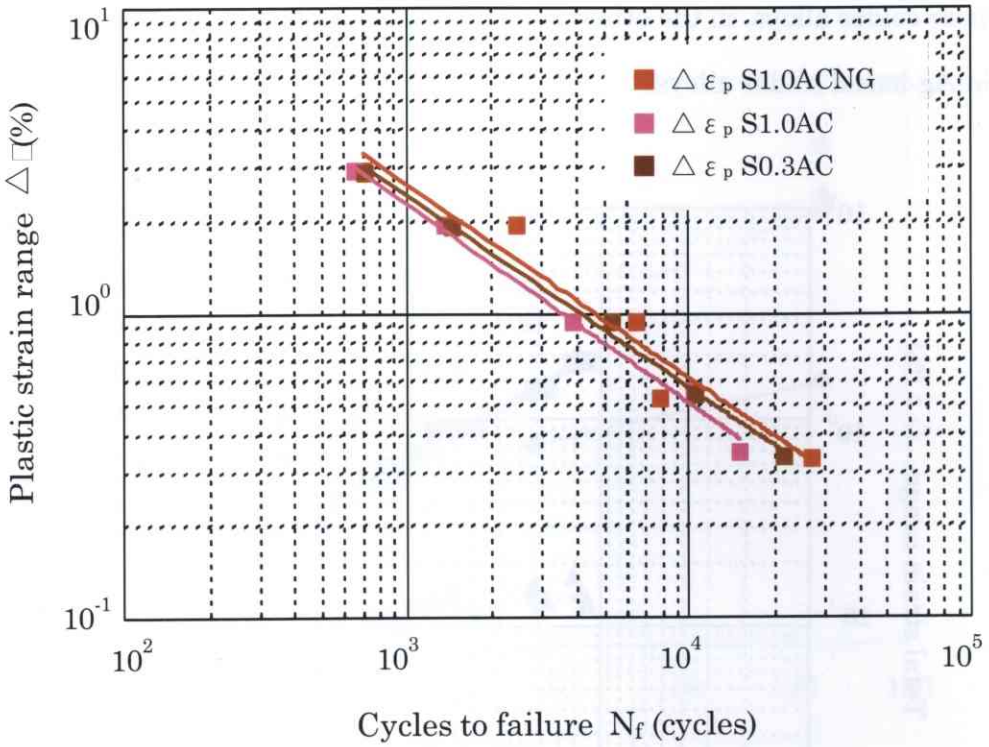

Fig.3-17 Cycles-to-failure (N_f) versus plastic strain range for S0.3AC, S1.0AC,S1.0ACNG solder alloys at 125℃

To compare the difference of the fatigue life between the temperature at 25℃,and 125℃, the cycles-to-failure of those solder alloys was plotted in Fig3-18 together. Fatigue life of the SACNG solder alloy was also plotted at Fig3-18.

From the results, the life of low-cycles fatigue is in same level for three kinds of S0.3AC, S1.0AC, and S1.0ACNG solder alloys between the temperature of 25℃ and 125℃. Moreover, the life of the lower Ag solder alloys is better than that of higher Ag solder alloy (SACNG).

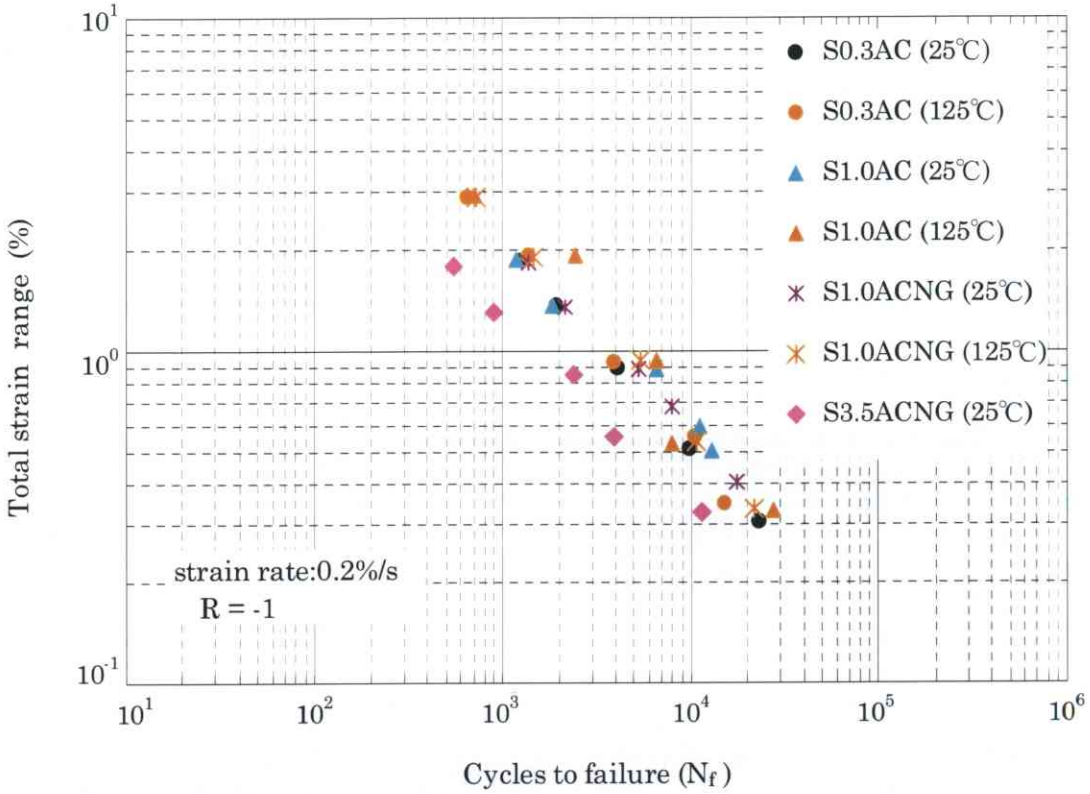

Fig.3-18 Cycles-to-failure (N_f) versus plastic strain range for various Sn-Ag-based solder alloys.

3.3.4. Microstructure

The mechanical properties of Sn-Ag-based solder alloys are determined by the microstructure of the material[3-6-3-9]. Microstructural features that affect mechanical performance include: grain size, sub-grain structure (low-angle boundaries, cells, etc.) [22-26], the distribution of matrix and particle phases, the atomic structure of the matrix phase (e.g., single element or solid solution), dislocation line defects (density and mobility), and point defects such as vacancies and interstitial atoms.

The lead-free Sn-Ag-based solder alloys have second and third phase particles distributed in the microstructure[3-10-3-13]. In the case of the Sn-Ag-Cu alloys, those particles are comprised of the Cu_6Sn_5 and Ag_3Sn intermetallic compounds[3-14-3-15]. Precipitate particles serve as barriers to the motion of dislocations.

Figure 3-19 shows the initial stage microstructure of Sn0.3AC, S1.0AC, S1.0ACNG, and S3.5ACNG (SACNG) solder alloys.

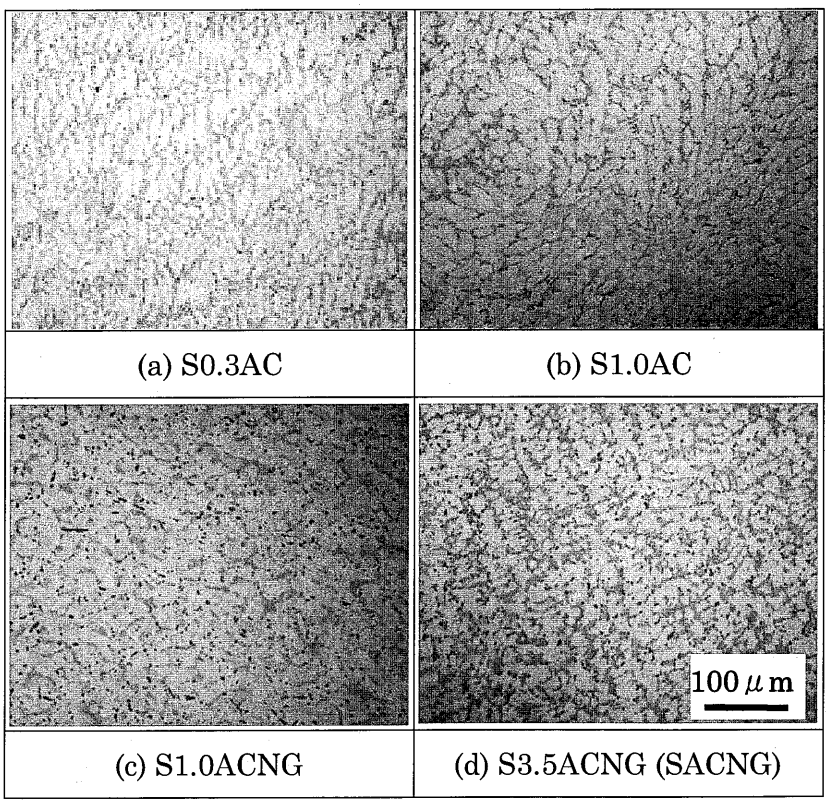

Fig.3-19 Optical image of microstructure for four kinds of solder alloys.

The microstructure of the alloys consists of eutectic regions of fine dispersed spherical Ag_3Sn intermetallic compounds (IMCs), together with the copper present as intermetallic Cu_6Sn_3 within a β-Sn matrix and large precipitate-free β-Sn regions. The microstructure of the four kinds of lead-free solder alloys is fine.

Figure 3-20 shows SEM micrographs of the alloys S0.3AC, S1.0AC, S1.0ACNG, and S3.5ACNG (SACNG). The density of particles of the Ag_3Sn and Cu_6Sn_3 IMCs are difference which can be observed among the Fig.3-19 (a), (b), (c), (d).

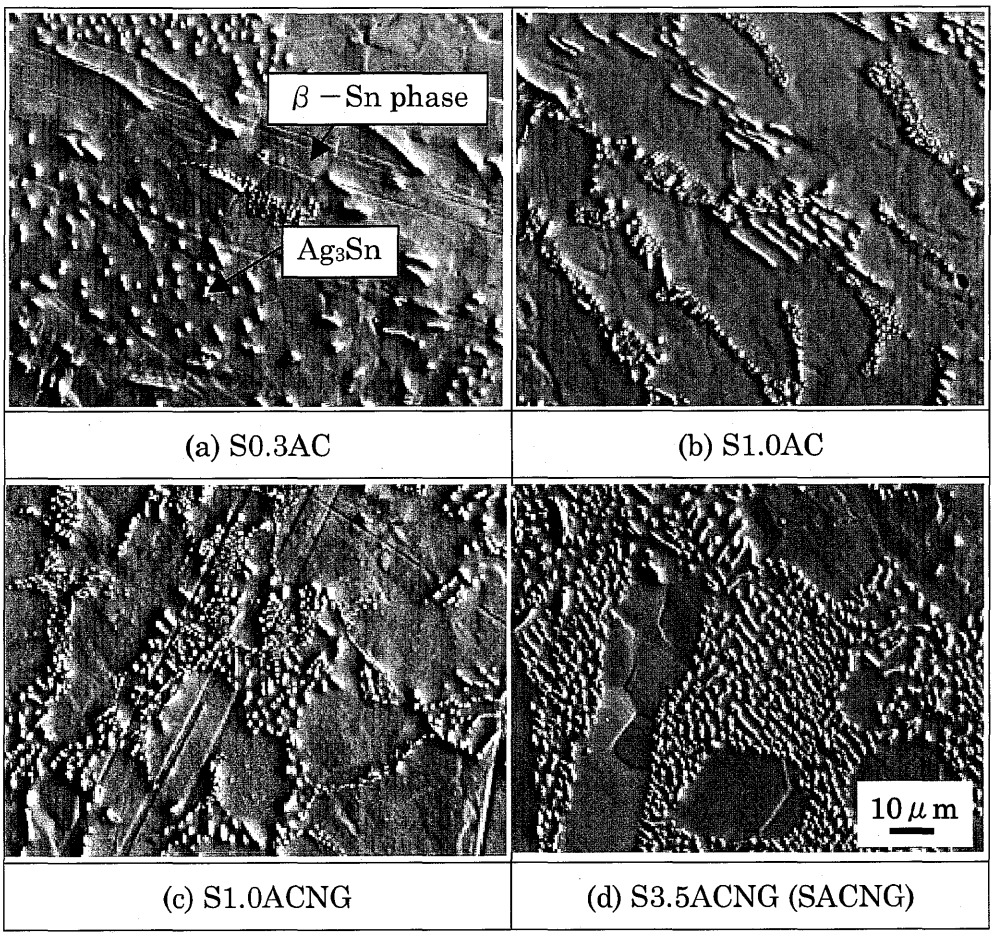

(a) S0.3AC (b) S1.0AC

(c) S1.0ACNG (d) S3.5ACNG (SACNG)

Fig.3-20 SEM photo of microstructure for four kinds of solder alloys.

It is considered that the dispersion of these particles strengthen (Ag_3Sn or Cu_6Sn_5) the β-Sn phase which is a major part of matrix in the lead-free solder alloys.

Figure 3-21 shows the schematic of microstructure and the mechanical properties for the Sn-Ag-based solder alloys. The tensile strength constants the strength of the β-Sn phase and the particles strengthen phase. The tensile strength increased when the density of the particles of Ag_3Sn increased in the eutectic area. The density of the particles of Ag_3Sn in the eutectic area also increased when the content of adding Ag increased. On the other hand, the tensile elongation decreased when the density of the particles of Ag_3Sn increased in the eutectic area. Accordingly, these particles are also considered to be an important factor to contribute to the significant improvement of the creep and rupture strengths of the solder alloys.

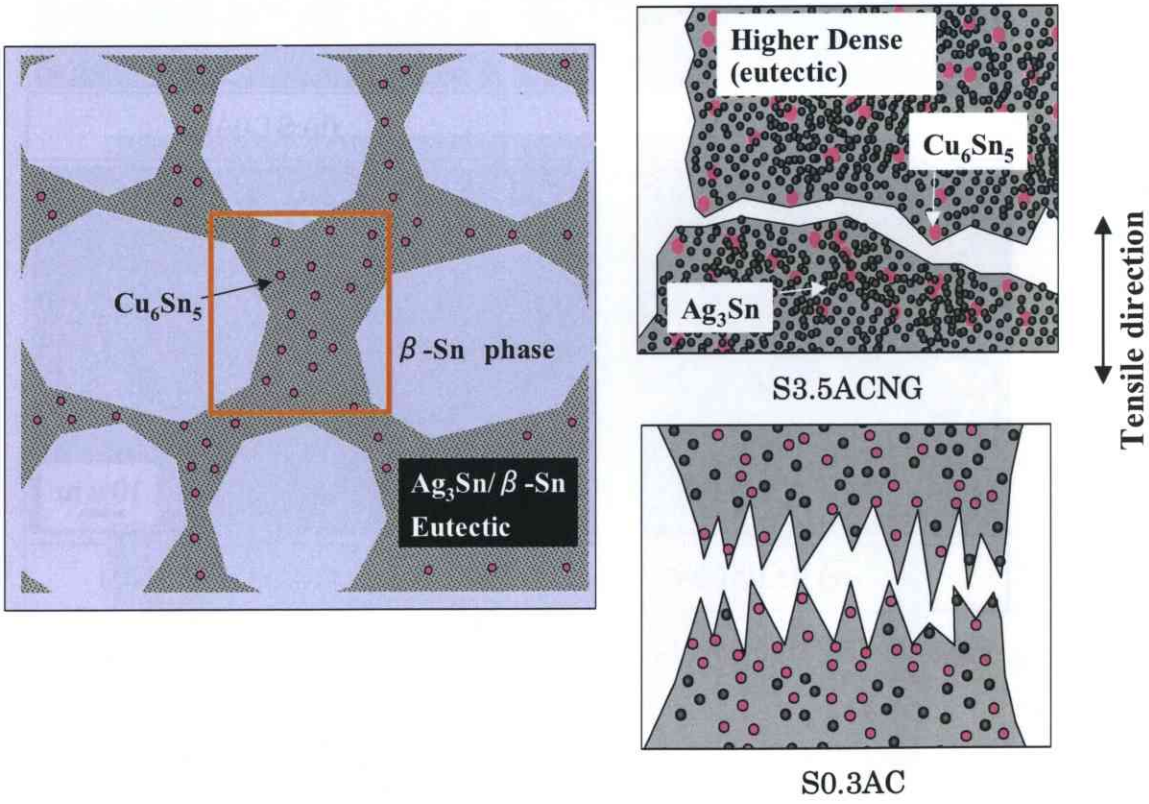

Fig.3-21 Schematic of microstructure and the tensile properties for the Sn-Ag-based solder alloys.

3.4. Life Prediction Models for Lead-Free Sn-Ag-Based Solder Alloys

Coffin-Manson type equations are commonly used to predict the low-cycle fatigue life of solder alloys[3-16-3-17]. The general form of the Coffin-Manson equation is as follows:

$$(N_f)^m \ \triangle \varepsilon_p = C \text{ ---------- } 3\text{-}4\text{-}(1)$$

Where N_f is the number of cycles to failure, $\triangle \varepsilon_p$ is the plastic (inelastic) strain range per cycle, and m and C are constants. From above results, the constants of various Sn-Ag-based solder alloys can be given in table 3-3.

Table3-3 the constants of A and m for the four kinds of solder alloys (Coffin-Manson equation)

Constant	S0.3AC	S1.0AC	S1.0ACNG	SACNG
m	0.61	0.51	0.58	0.56
C	146.8	66.4	119.4	59.9

The life prediction method, an example, can be shown as Fig 3-22.

The plastic strain between the chap and Cu electrode can be calculated by stress-strain graph in various temperatures. The life of soldering joint can be predicted by potted the plastic strain into the fatigue life curve.

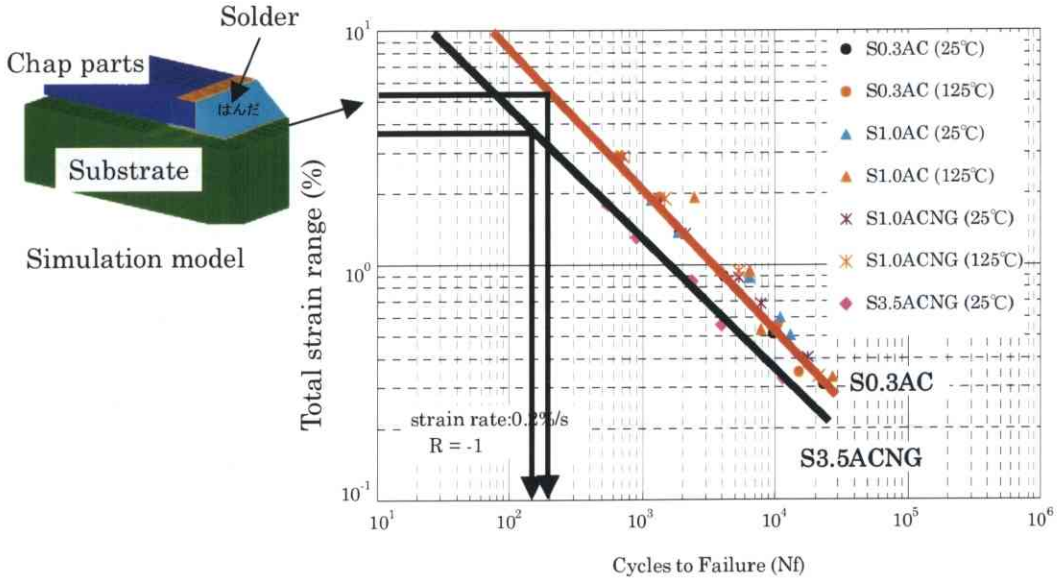

Fig.3-22 An example for life prediction method.

3.5. Conclusions

The effects of Ag, Cu, and Ni elements on tensile strength, elongation are gave in following.

- In the case of content of Ag is over 3.0wt% in Sn-Ag-based, No significant difference can be found on the tensile strength and the elongation, although changed the content of Cu, Ni elements.
- In the case of content of Ag is below 3.0wt%, the tensile strength increases with increasing content of Ag. On the other hand, the elongation decrease with increasing content of Ag.
- The tensile strength of S1.0ACNG solder alloy with adding 0.07wt% Ni is better than that of S1.0AC without Ni.
- The mechanical properties of Sn-Ag-based solder alloys are determined by the microstructure of which dispersed the particles of the Ag_3Sn and Cu_6Sn_3 IMCs.
- It was considered that dispersion of these particles strengthen the Sn phase which is a major part of matrix in the lead-free solder alloys.
- Accordingly, these particeles are also considered to be an important factor to contribute to the significant improvement of the creep properties and rupture strengths of the lead-free Sn-Ag-based solder alloys.
- The life of low-cycles fatigue is in same level for three kinds of S0.3AC, S1.0AC, and S1.0ACNG solder alloys between the temperature of 25℃ and 125℃.
- The life of the lower Ag solder alloys is better than that of higher Ag solder alloy (SACNG).

3.6. Reference

3-1. D.Shangguan: "Lead-Free Solder Interconnect Reliability", ed. by D.Shangguan, ASM, 1995, pp.191-196.

3-2. T.Takemoto, M.Takahashi, R.Ninomiya, and A. Matsunawa,"Mechanical Properties and Estimation of Thermal Fatigue Properties of Lead-free Solders", Advances in Electronic Packaging, EEP-Vol.19-2, 1997, pp.1623-1628.

3-3. Y.Yoshiura, H.Chake, T.Takemoto, and Y.Kikuchi: "Improvement of Thermal Fatigue Propertis of Sn-Pb Solder by Addition of Several Elements", Proc. of 2th Symposium on Microjoining and Assembly Technology in Electronics, 1996, pp.167-172.

3-4. D.A.Spera and D.F.Mowbray: "Thermal Fatigue of Materials and Components", ASTM, 1976,pp.3-9.

3-5. JIS Z3198-2:[Tensile Test for Lead-free Solder Alloy Part□]

3-6. T.Takahashi, S.Hioki, I.Shohji, and T.Yoshida: "Mechanical Properties of Various Lead-free Solders", Proc. of 9th Symposium on Microjoining and Assembly Technology in Electronics,2003,pp.223-228.

3-7. Y.Kariya, T.Asai, and T.Suga: "Mechanical Properties of Lead-free Sloder Alloys Evaluated by Miniature Size Specimen", Microjoining Commission(JWS), MJ-455-2004, 2004.

3-8. Y.Kariya, T.Asai, T.Suga, and M.Otsuka: "Mechanical Properties of Lead-free Sloder Alloys Evaluated by Miniature Size Specimen", Proc. of 9th Symposium on Microjoining and Assembly Technology in Electronics,2004,pp.61-64.

3-9. M.McCormack, and S.Jin: "Improved Mechanical Properties in New, Pb-free Solder Alloys", J. Electron. Mater., Vol.23, No.8, 1994, pp.715-720.

3-10. F.Ochoa, J.J.Williams, and N.Chawla: "Effects of Cooling Rate on the Microstructure and Tensile Behavior of a Sn-3.5wt.%Ag Solder", J. Electron.Mater., Vol.32, No.12, 2003,pp.1414-1420.

3-11. R.Ninomiya, Y.Nakahira, and T.Takemoto: "Microstructure and Mechanical Property of Sn-Ag-Bi-In Solder", Proc. of 4th Symposium on Microjoining and Assembly Technology in Electronics,1998,pp.249-252.

3-12. K.Habu, N.Sato,and H.Nagasawa: "The Effect and Stability of Composition in Pb-free Solser Alloys of the Sn-Ag-Cu-Bi System with a Small Amount of Additives", Proc. of 6th Symposium on Microjoining and Assembly Technology in Electronics, 2000,pp.287-292.

3-13. M.Nagano, N.Hidaka, M.Shimoda, and M.Ono: "Mechanical Properties and Microstructure of Sn-Ag-Cu-Ni-Ge Lead-free Solser", J.Japan. Institite of Electron. Packaging, Vol.8, No.6,2005,pp.495-501.

3-14. Y.Kariya, and W.J.Plumbridge: "Mechanical properties of Sn-3.0mass%Ag -0.5mass%Cu alloy", 7th Symposium on [Microjoining and Assembly Technology in Electronics], 2001,pp.383-388.

3-15. C.M.L.Wu, D.Q.Yu, and L.Wang: "Microstructure and Mechanical Properties of New Lead-Free Sn-Cu-RE Solder Alloys", J. Electron. Mater., Vol.31, No.8, 2002,pp.928-932.

3-16. Y.Kariya: "Mechanical Reliability of Solders in Small Volume" J.Japan. Institute of Electronics Packaging, Vol.9, No.3,2006,pp.138-142.

3-17. S.Terashima, Y.Kariya, and M.Tanaka: "Improvement on Thermal Fatigue Properties of Sn-1.2Ag-0.5Cu Flip Chip Interconnects by Nickel Addition", Mater.Trans., Vol.45, No.3, 2004,pp.673-680.

Chapter 4 CREEP PROPERTIES AND DEFORMATION MECHANISM OF LEAD-FREE SN-AG-BASED SOLDER ALLOYS

4.1. Introduction

In the Chapter 3, the tensile strength has been discussed. However, on the other hand, relatively low stresses (below the yield stress) that are applied at reduced loading rates cause the deformation to shift into the solder material[4-1-4-3].

The long-term reliability of electronic solder joints is determined by the creep and fatigue properties of the solder alloy.

This chapter focuses on the creep deformation of the Sn-Ag-based solder alloys. As described, creep deformation is the most common and critical deformation mechanism in solder joints, due to their higher homologous temperatures. This significant contribution is a result of the low solidus temperature of solder alloys.

The solidus temperature (T_s) of nearly all lead-free solder alloys are in the range of 215 to 225℃. The homologous temperature, defined as $T_h = T/T_s$, where T is the "use" temperature, will be in the range of $0.60 < T_h < 0.87$ for use temperature of 25 to 150℃. By comparison, these temperature would be equivalent to those experienced by advanced superalloys in the hot-section of an operating jet aircraft engine (700 to 900℃). Therefore, even at room temperature, solder alloys are considered to be in high-temperature service.

Phemenologically, creep is defined as strain (deformation) versus time, which results from the application of an applied stress[4-4-4-6]. The general strain-time creep response is shown in Fig.4-1. Three stages are identified: the primary or transient stage is characterized by a gradually decreasing strain rate time; the secondary or steady-state stage that exhibits a time independent strain rate; and lastly,

the tertiary stage in which the strain rate increase with time, to the point of failure or creep rupture.

Primary or transient creep is a relatively complex phenomenon because the underlying mechanism and microstructure, and therefore, the strain rate, change with time. The defects required for deformation may be created at the moment that the stress is applied.

On the other hand, an adequate density of defects may already be present in the microstructure to provide deformation in response to the applied stress.

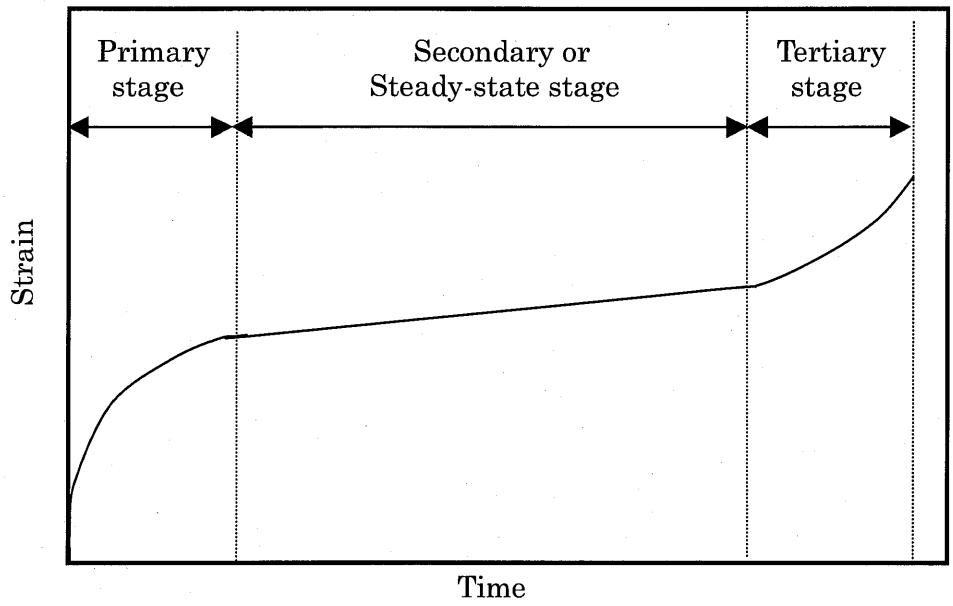

Fig.4-1 Typical creep curve in an alloy material.

Steady-state or secondary creep (Fig.4-1) is characterized by a constant or minimum strain rate, $d\varepsilon/dt_{min}$. Two theories have typically been used to explain the constant strain rate[4-7-4-12]: (a) there is a balance between the creation and annihilation of defects during steady-state creep. The rate processes are thermally activated and dependent upon the applied stress. The defect velocity is assumed to be a constant; and (b) there is a relatively constant supply of defects having a

constant velocity that establishes the creep rate. The creep rate is determined by the stress level and temperature and is also a thermally activated process.

Because of the relatively high temperatures that are required to establish steady-state creep in metals and alloys, diffusion-controlled mechanisms typically underlie the resulting deformation. Those mechanisms include the simple diffusion of point defects-vacancies and interstitials-as well as diffusion-controlled, dislocation motion resulting from cross slip and/or jog-screw mechanisms.

Diffusion–controlled process include self-diffusion or bulk (lattice) diffusion, in which atomic movements occur within the lattice structure, as well as fast or short-circuit diffusion in which atomic transport occurs along grain boundaries, interfaces, or other defect structures in the microstructure. Therefore, the apparent activation energy values for creep often reflect one of these two mechanisms. When self –or bulk-diffusion is the controlling mechanisms, apparent activation energy will have values that are over 90kJ/mol for Sn-based solder alloys[4-9-4-10].

For example, the cross slip of dislocations and the movement of screw dislocations by jogs are based specifically on the diffusion of vacancies in the bulk lattice. Therefore, the apparent activation energy for creep, in the event that either of these two processes are rare controlling, will be similar to that of lattice self-diffusion. On the other hand, when the controlling mechanism is fast or short-circuit diffusion, the value of the apparent activation energy is typically 0.4 to 0.6 of the bulk diffusion value, or about 40kJ/mol to 60kJ/mol[4-10, 4-11]. Fast or short-circuit diffusion often controls creep deformation in the Sn-Pb solder alloys [43].

Two properties are important to the creep behavior of Lead-free solder alloys. First, the Lead-free alloys have low solidus temperature so that, even at

temperature as low as –55℃, 21the homologous temperature is still in excess of 0.5. Therefore, diffusion-controlled mechanisms can dominate the creep behavior. Secondly, the Sn-Ag-(Cu) system solder alloys can be characterized as precipitation hardened alloys having essentially a 100% Sn matrix phase and tow precipitate particle phases, Ag_3Sn, and Cu_6Sn_5. In general, precipitate particles will improve the creep resistance of metal and alloys, particularly when the creep mechanism is based upon dislocation glide, and to a lesser magnitude, dislocation climb. The magnitude of the effect depends upon the size, distribution, volume fraction, and coherency of the particle phases[4-13-4-15]. However, it is expected that precipitate particles will have a lesser impact on creep that is diffusion-controlled, especially when the particles are incoherent, because of the contribution of thermally-activated atom and vacancy transport to deformation, whether these point defects are the sole source of mass transport or assisting dislocation climb[4-16-4-19].

As described, Sn-Ag (-Cu) system solder alloys are subject to creep and recrystallization even at room temperature. In response, various techniques have been developed that involve the addition of trace amounts of Ni or Ge, which is believed to improve the high temperature performance of solder alloys. Chapter2 has described the effects of adding Ge, which can prevent Sn oxidation and suppress dross formation in wave soldering[4-20].

This chapter reports an investigation of the creep behavior of both bulk specimens and TH joints of SACNG solder alloy, comparing this alloy to S3.0AC solder alloy and addressing stress dependency and activation energy for creep in connection with microstructure observations to clarify the mechanism of deformation during creep. And also discusses investigations of particles growth

behavior based on transmission electron microscopy (TEM HITACHI H H9000UHR-I). Moreover, several important materials parameters were studied, such as the T_d and Larson-Miller Parameter (L·M · P). T_d is the temperature at which the material transforms from a relatively rigid or stable state to a more deformable or softened state, and the properties of the solder alloy are different above the T_d as compared with below the T_d. To acquire the T_d, the relationship between creep deformation and temperature were conducted on several kinds of Sn-Ag system solder alloys.

So that, creep characteristics such as stress exponent and activation energy were investigated on several kinds of Sn-Ag system solder alloys. In addition, according to the creep deformation mechanisms of each solder alloys; the limit coverage of several kinds of Sn-Ag system solder alloys was discussed.

4.2. Experimental Procedure

Table 4-1 gives the chemical composition of Sn-Ag system solder alloys used.

Table 4-1. Composition of the Solder Alloys

No.	Element					Alloy codes
	Sn	Ag	Cu	Ni	Ge	
1	Bal	3.5	0.5	0.07	0.01	SACNG
2	Bal	3.0	0.5	-	-	S3.0AC
3	Bal	1	0.5	0.07	0.01	S1ACN
4	Bal	1	0.5	-	-	S1AC
5	Bal	0.3	0.5	-	-	S0.3AC

4.2.1. Bulk Sample

The bulk creep specimens consisted of cast ingots of SACNG and Sn3.0AC solder alloys purchased from NIHON HANDA. Solder bars prepared by the manufacturer were melted in air in an electric furnace at 330℃ for two hours. The melt was then chill-cast as an ingot in a stainless steel mold measuring 14 mm in diameter and 160 mm in length. The solder rods were machined into round shape of creep specimen measuring 15 mm in length and 3 mm in diameter (Fig.4-2).

Tests were conducted by using a miniature creep test machine as shown in Fig.4-3. All specimens were heat-treated at 60℃ for 24 h to remove residual stress and defects induced during specimen forming. Creep life testing was performed at 40℃, 80℃, and 125℃, representing homologous temperature η (η = T/Tm, where Tm is the melting point of the solder alloys) of 0.63 to 0.81 for the Sn-Ag system solder alloys. The stress range in the tests fell within 5-20 MPa, corresponding to a normalized stress of $\sigma / E = 10^{-5}$ to 10^{-3}, where E is Young's modulus.

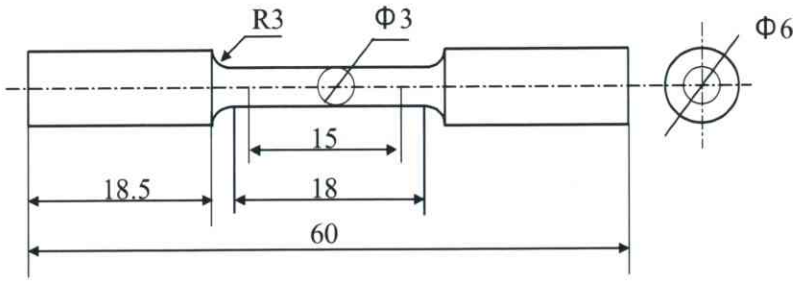

(a) Specimen geometry.

(b) Photo of the specimen.

Fig.4-2 Appearance of the test specimen.

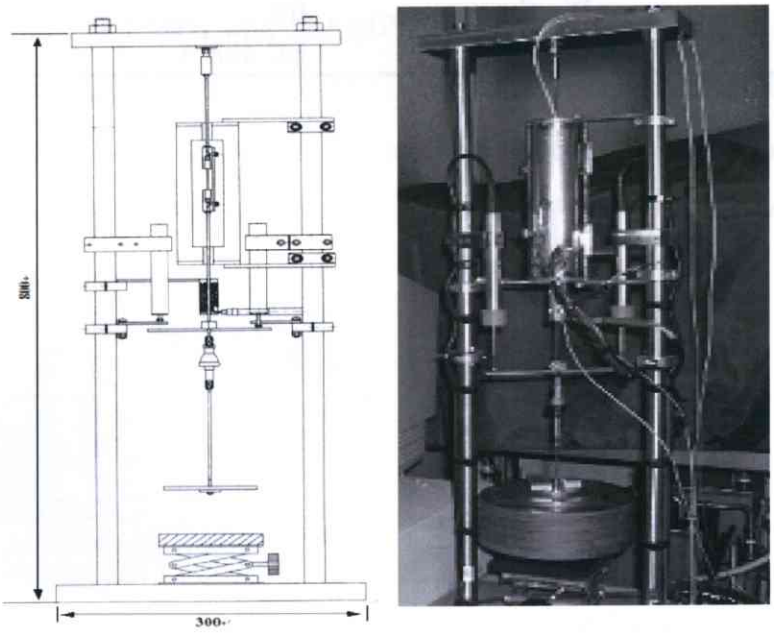

(a) Geometry. (b) Photo of the machine.

Fig.4-3 Miniature creep testing machine for bulk specimen.

4.2.2. Through Hole Sample

Figure 4-4 shows the TH test specimen. Given the wide prevalence of through-hole (pin-in-hole) technology in the electronics industry, our study also incorporated creep tests of TH joints. The substrate material used for the TH test was a standard FR-4 epoxy-glass laminate of 195 mm × 120 mm × 1.6 mm. The Cu pads on the FR-4 substrate were 0.85 mm in diameter. The Cu pin measured 0.5 mm × 0.55 mm. Table 4-2 gives wave-soldering conditions. The wave-soldering temperature was set to 250℃, approximately 30℃ above the melting point of the solder alloys.

Table 4-2. Wave soldering condition

Surrounding	Atmosphere
Soldering temperature	250 ℃
Conveyor speed	16.7 mm/s
Conveyor speed	4 deg.
Dip time	6 s
Flux	EC-19S-A

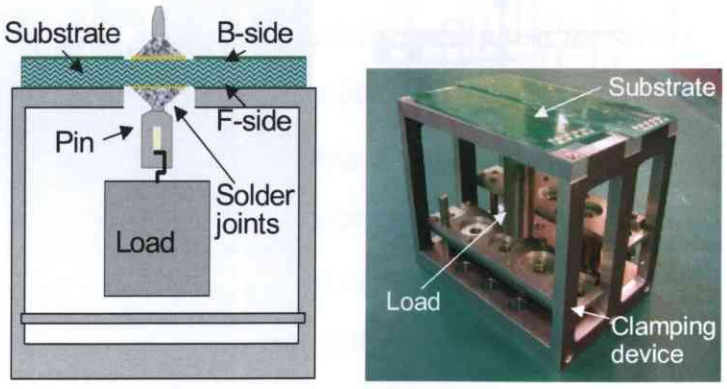

(a) Schematic. (b) Appearance.

Fig.4-4 Schematic diagram of TH joints creep test
(a) Schematic, (b) Appearance.

4.2.3. Microstructural Examination

The samples were prepared for scanning electron microscopy (SEM) by wet grinding to #2400-grit sandpaper, followed by diamond particle polishing down to 0.25 μm, and a final polishing stage with a colloidal silica suspension. After polishing, samples were etched by Ar^+ ion milling and observed via SEM (Hitachi S 4300). I performed microstructural analyses of initial and creep-tested samples with TEM at an acceleration voltage of 300 kV. I also performed element mapping with an electron probe X-ray microanalyzer (Shimadzu EPMA 1610) to determine particle compositional characteristics.

4.3. Results and Discussion

4.3.1. Creep Properties

Figure 4-5 shows creep curves up to the rupture times for the SACNG and S3.0AC solder alloys at temperatures of 40℃, 80℃, and 125℃ at applied stresses of 5 MPa, 9.8 MPa, 14.7 MPa, and 19.8 MPa, respectively. TH creep tests were performed at temperatures of 40℃, 80℃, and 125℃under loads of 300 g, 400 g, 2000 g, and 3000 g, respectively. Only the creep rupture time was recorded for the TH solder joints. At the lower temperatures of 40℃-80℃ and higher stresses of 9.8 MPa-19.8 MPa, creep rupture times for the Sn3.0AC solder alloy were longer than for the SACNG solder alloy.

However, at the higher temperature of 125℃ and lower stress of 5 MPa, the creep rupture time for the SACNG solder alloy was approximately three times that of the S3.0AC solder alloy.

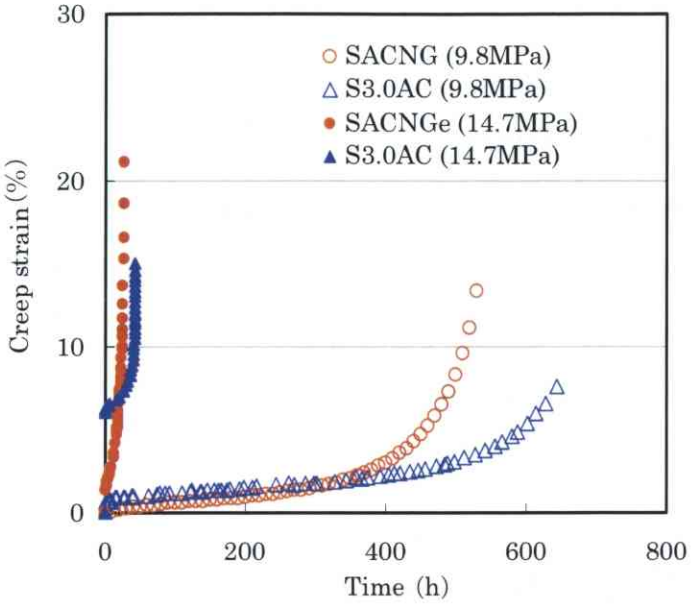

(a) Creep tested at 40℃.

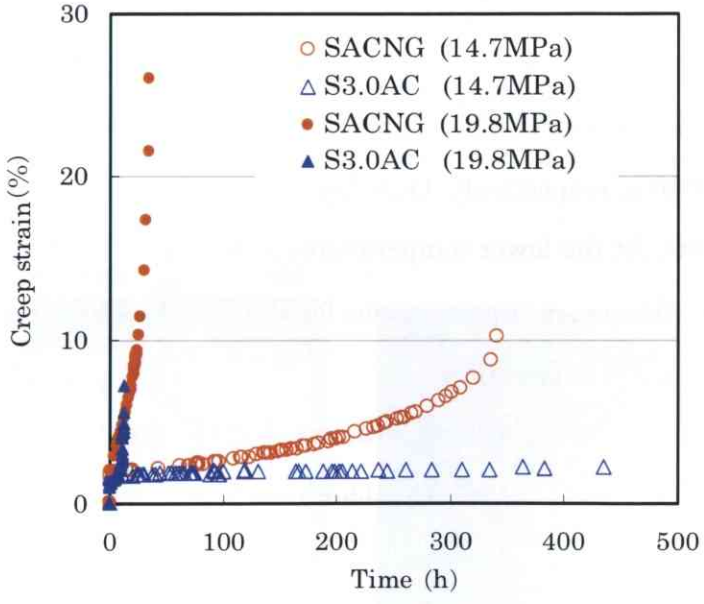

(b) Creep tested at 80℃.

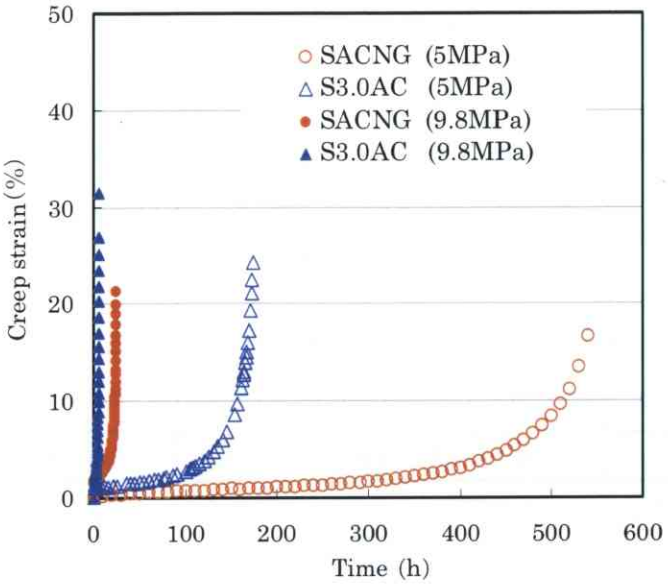

(c) Creep tested at 125℃.

Fig.4-5 Creep curves of the bulk of both solder alloys
(a) creep tested at 40℃, (b) 80℃, and (c) 125℃.

Figure 4-6 shows the relationship between creep stress and creep-rupture time for the SACNG and S3.0A0C solder alloys at each temperature. Table 4-3 gives the creep results for the TH joints of both solder alloys at 125℃. These results show that adding Ni improved creep strength for the S3.0AC solder alloy at higher temperatures.

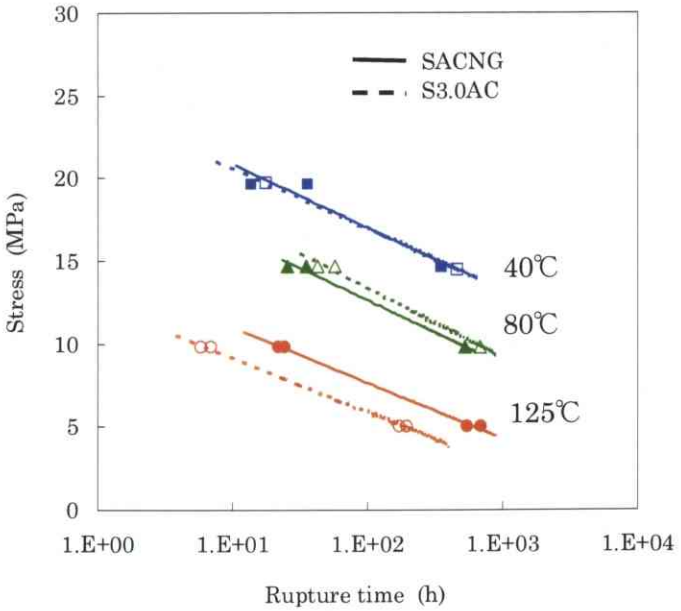

Fig.4-6 Creep rupture life of the SACNG and the S3.0AC solder alloys.

Table 4-3 Creep results of the TH joints of the both solder alloys at 125℃.

Load (g)	Creep rupture (h)			
	SACNG		S3.0AC	
300	500 (interrupted)		500 (interrupted)	
400	500 (interrupted)		500 (interrupted)	
2000	740	170 (interrupted)	168	153
3000	7	16	6	7

Creep behavior can normally be characterized by a stress-strain rate relationship. The minimum creep rate $\dot{\varepsilon}_m$ is one of the most significant parameters of creep resistance in engineering assessments. Stress dependence is often described by the power law equation:

$$\dot{\varepsilon}_m = A\ \sigma^n \text{ ----------4-3-(1)}$$

Here, $\dot{\varepsilon}_m$ is the minimum creep rate, while σ is applied stress, n is the stress exponent, and A is the material constant. Both A and n reflect temperature.

As expected, the creep rate increases progressively with stress at a given temperature and increases progressively with temperature at a given stress. the relationship is clearly illustrated by Fig.4-5.

Figure 4-7 shows the minimum creep rate as a function of applied stress of both solders at 40℃, 80℃, and 125℃, respectively. Figure 4-7 (a) shows that the stress exponent of the SACNG solder alloy declines with increasing temperature (from n = 11.3 at 40℃to n = 8.6- 6.9 at 80- 125℃). On average, the stress exponent is approximately 8.9.

Figure 4-7 (b) also illustrates a tendency similar to that seen in Fig.4-5 (a) for the S3.0AC solder alloy. The stress exponents of the S3.0AC solder alloy are 5.1 at 125℃, 9.4 at 80℃ and 12.3 at 40℃. The creep mechanism of Sn-base solder alloys in the homologous temperature range from 0.63 to 0.81 and stress range from $\sigma/G = 10^{-5}$ to 10^{-3} is in the dislocation-creep region[4-21-4-23]. The higher the n value of the stress exponent, the better the strengthening effect of the second phases in matrix Sn. Comparing both solder alloys shows that the n value for the stress exponent for the SACNG solder alloy is larger than that of the S3.0AC solder alloy at 125℃, but less at 80℃ and 125℃.

It was concluded that the microstructure of the SACNG solder alloy is more stable than the S3.0AC solder alloy at 125℃.

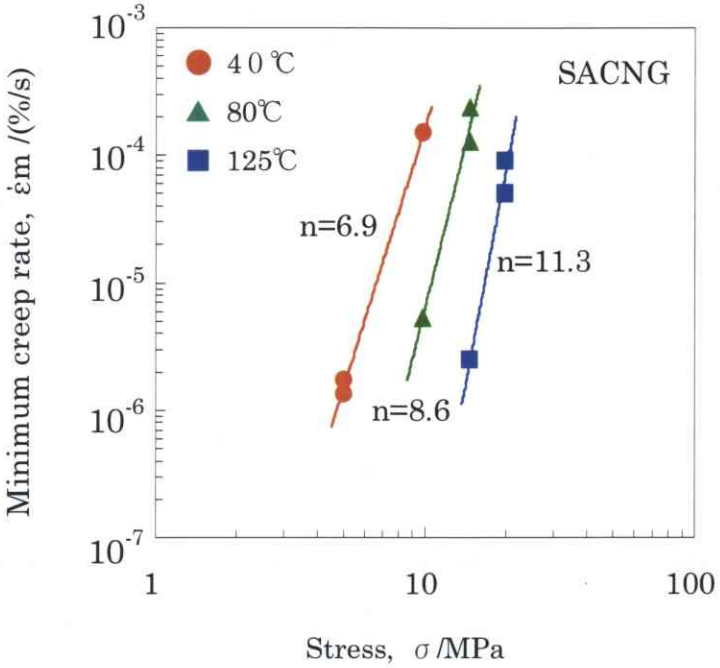

(a) SACNG.

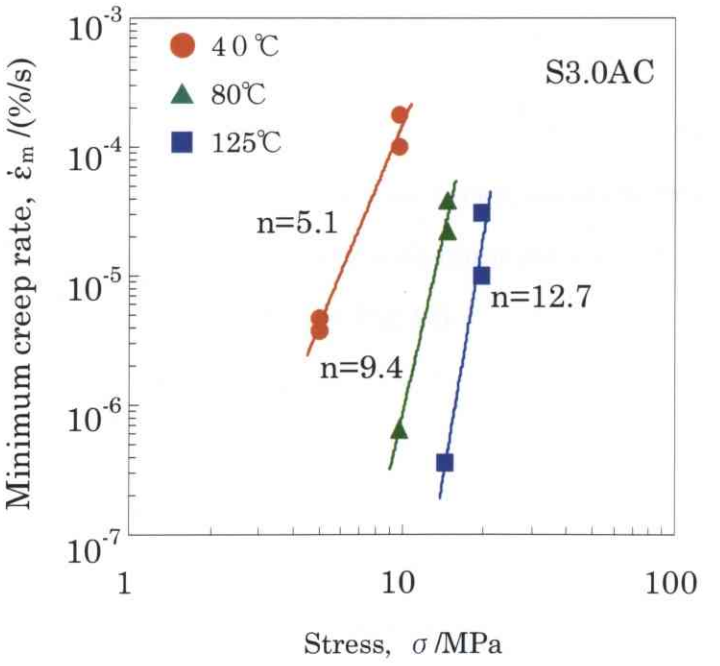

(b) S3.0AC.

Fig.4-7 Relationship between the stress and minimum creep rate of (a)SACNG, and (b) S3.0AC.

The apparent activation energy Q for creep can be calculated from the ln ($\dot{\varepsilon}_m$)-1/T plot, based on an Arrhenius type equation 4-3-(2).

$$\dot{\varepsilon}_m = A\,(\sigma/G)^n \exp(-Q/RT) \quad \text{----------4-3-(2)}$$

Where $\dot{\varepsilon}_m$ is the minimum creep rate, A is a material constant, σ is applied stress, G is temperature-dependent shear modulus, n is the stress exponent, Q is the apparent activation energy for creep, R is the universal gas constant, and T is absolute temperature.

Figure 4-8 shows the results. The apparent activation energy of creep for the SACNG and the S3.0AC solder alloys is 48 kJ/mol and 68 kJ/mol, respectively, under a constant stress of 9.8 MPa. In general, the lattice self-diffusion activation energy of pure tin is 102 kJ/mol[4-8-4-12], while dislocation-pipe diffusion activation energy is about 0.6 times the lattice self-diffusion activation energy[4-11-4-12].

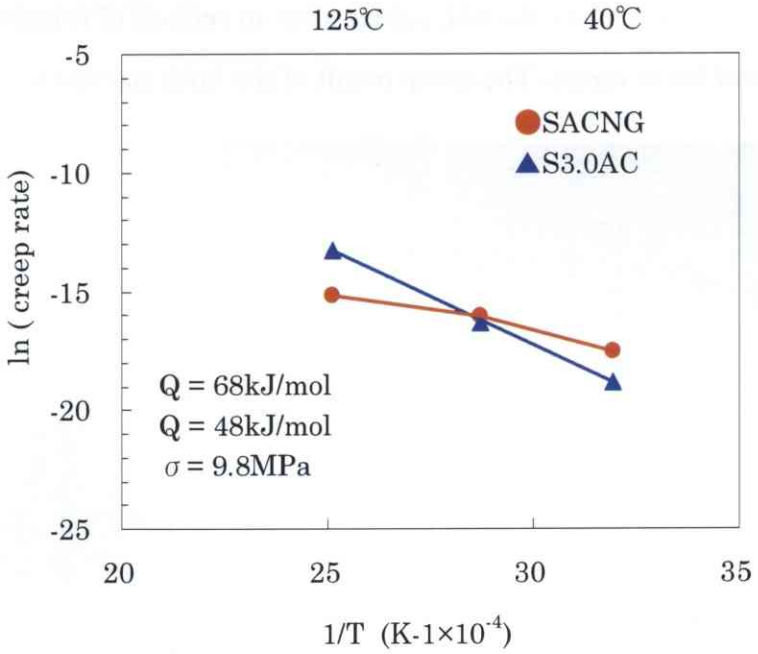

Fig.4-8 Arrhenius plots of creep rate and reciprocal temperature of the SACNG and the S3.0AC solder alloys.

The apparent creep-activation energies for both solder alloys are lower and close to dislocation pipe diffusion. Moreover, the apparent activation energy for the S3.0AC solder alloy is higher, implying that the microstructure of the S3.0AC solder alloy is highly sensitive to creep temperature. The microstructure of the SACNG solder alloy also appears more stable in the temperature range[4-24-4-25].

The relationship among applied stress, temperatures, and creep rupture times for bulk and TH joints in both solders can be plotted using Larson-Miller[4-26-4-27] plots. Fig.4-9 reflects all data. The Larson-Miller Parameter (LMP) can be expressed as follows:

$$LMP = T\,(C + \log(t)) \text{----------} 4\text{-}3\text{-}(3)$$

Where T is absolute temperature, C a constant (here C = 11)[4-27], and t the creep rupture time. Figure 4-9 shows that the creep strength of the SACNG solder alloy is higher than that of the S3.0AC solder alloy in regions of relatively higher temperatures and lower stress. The creep result of the bulk specimen corresponds to the TH joints.

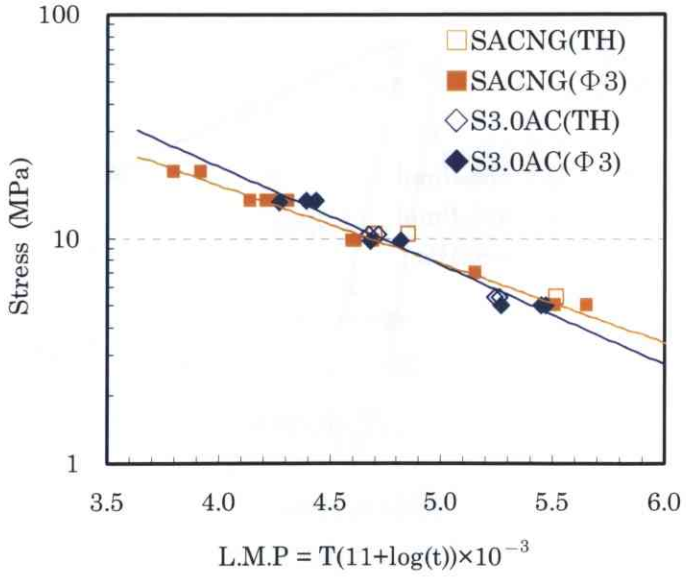

Fig.4-9 Correlation of creep strength with Larson-Miller parameter.

4.3.2. Microstructure

Microstructural observations were performed to clarify the relationship between creep strength and microstructure. Figure 4-10 is an SEM micrograph of bulk specimens of both solders at their initial state. The microstructure of the SACNG solder alloy shows two types of regions. The black-gray colored region is a dendritic β-Sn phase, while the light-colored region is a eutectic network band of dispersed Ag_3Sn and $(Cu, Ni)_6Sn_5$ intermetallic compounds within the β-Sn phase. This is finer and more uniform, and the hardness of the eutectic regions is approximately 0.45 GPa, as determined by nano-indentation testing.

On the other hand, we see segregated (larger block) eutectic regions of dispersed Ag_3Sn and Cu_6Sn_5 intermetallic within the β-Sn phase, which are dense microstructures, in the S3.0ACusolder alloy from Fig.4-10 (b), and the hardness of the segregated eutectic region is about 0.7 GPa. The deformation is unbalanced under applied stress[4-28-4-29].

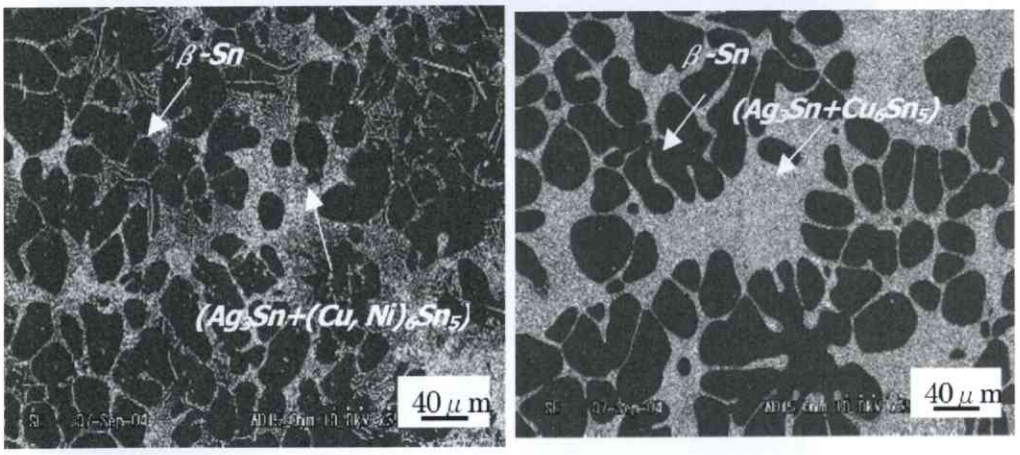

(a) SACNG. (b) S3.0AC.

Fig.4-10 Microstructure of the bulk specimen of the solder alloys, (a) SACNG, and (b) S3.0AC.

Figure 4-11 shows the microstructure of the TH joints for both solders after wave soldering. The microstructure of TH joints for S3.0AC is also segregated, similar to the bulk sample. Shrinkage cracking is clearly visible from the surface and cross-sections of TH joints, whereas the TH joint of the SACNG solder alloy shows a finer and more uniform microstructure than the S3.0AC solder alloy.

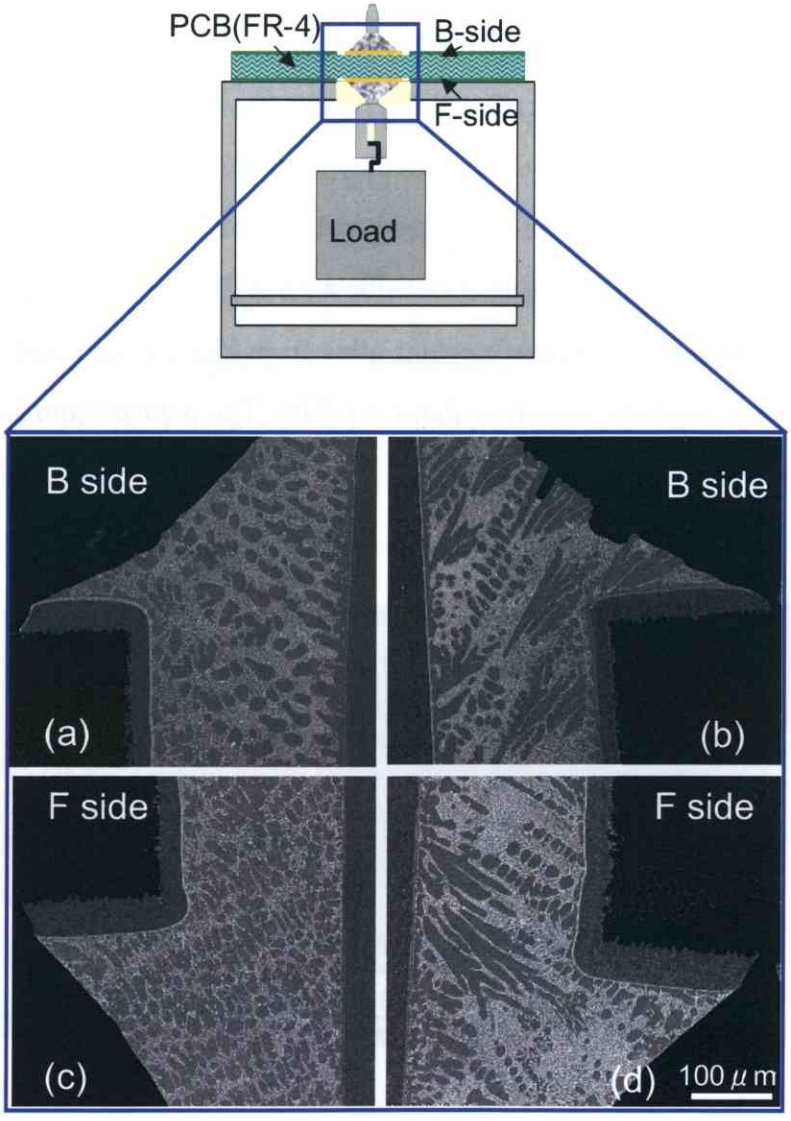

(a),(c) SACNG. (b),(d) S3.0AC.

Fig.4-11 Microstructure of cross-section of the TH joints for the both solder alloys. (a),(c) SACNG, and (b),(d) S3.0AC.

Figure 4-12 shows an SEM image of a eutectic region of the SACNG solder alloy and the S3.0AC solder alloy at the initial state and after the creep test at 125℃, 5 MPa. Before the creep test, although the microstructure of the S3.0AC solder alloy has a higher concentration of Ag_3Sn particles than the SACNG solder alloy, both solder alloys have fine microstructures in the eutectic regions. The particle size for both solder alloys became coarser after a creep test at 125℃, 5 MPa.

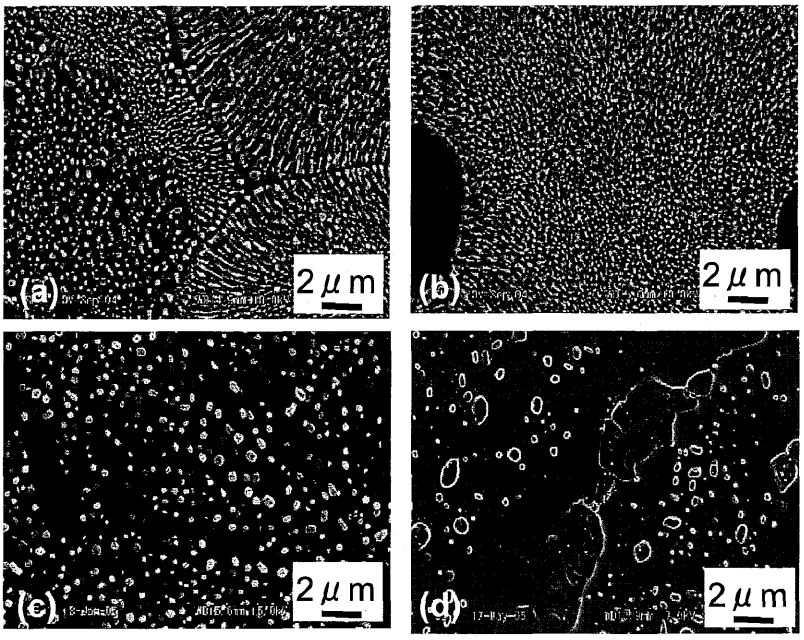

Fig.4-12 SEM graph of eutectic region of both solder alloys
(a) SACNG in initial state,(b) S3.0ACu in initial state,
(c) SACNG after crept at 125℃, 5 MPa for 200 h,
(d) S3.0AC after crept at 125℃, 5 MPa for 180 h.

Of special note here is the appearance and significant growth of Cu_6Sn_5 IMCs in the S3.0AC solder alloy. The apparent difference in creep rupture strength between the SACNG solder alloy and the S3.0AC solder alloy at high temperature (125℃) and low stress (5 MPa) depends on the size and the stability of the particles in the eutectic region. For cases of higher temperature and lower stress, Cu_6Sn_5 IMCs grow rapidly in the eutectic region of the S3.0AC solder alloy, while the

cavities or cracks generated by the coarser particles propagate, and creep rupture occurs within a shorter time. On the other hand, no particles resembling coarse Cu_6Sn_5 were observed in the SACNG solder alloy. This appears to be attributable to the addition of Ni to the S3.0AC solder alloy.

Figure 4-13 shows a similar comparison for TH joints of both solders after creep testing at 125℃, 2000 g for 170 h. We saw significant microstructural changes as well in the TH joints of the S3.0AC solder alloy. The particles of Cu_6Sn_5 IMCs in the S3.0AC solder grew faster than those of the (Cu, Ni) $_6Sn_5$ IMCs in the SACNG solder alloy.

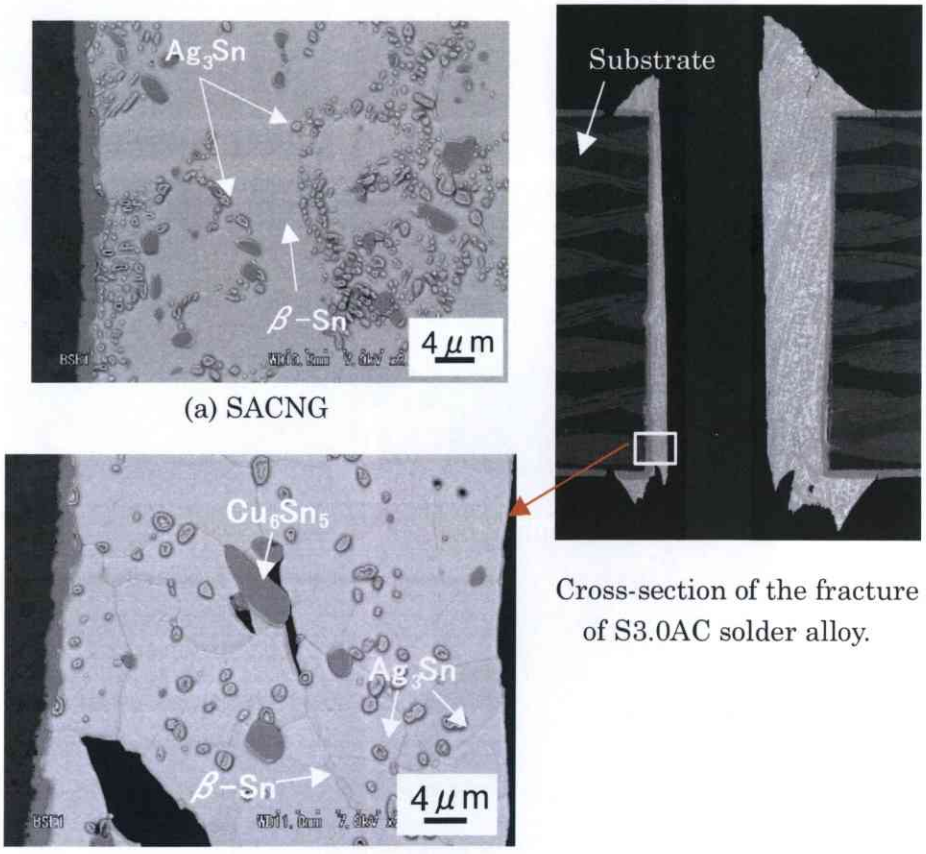

Fig.4-13 Back scattered images of the TH joints for the both solder alloys
(a) SACNG after crept at 125℃, 2000g for 170h,
(b) S3.0AC after crept at 125℃, 2000 g for170 h.

To analyze the elemental makeup of the particles, EPMA mapping analysis was performed in the same areas of the TH joints of the S3.0AC solder alloy.

Figure 4-14 shows the result of EPMA analysis. Cu, Sn elements were detected from markedly coarsened particles but the presence of Ni could not be confirmed. The coarsened particles are Cu_6Sn_5 IMCs[62].

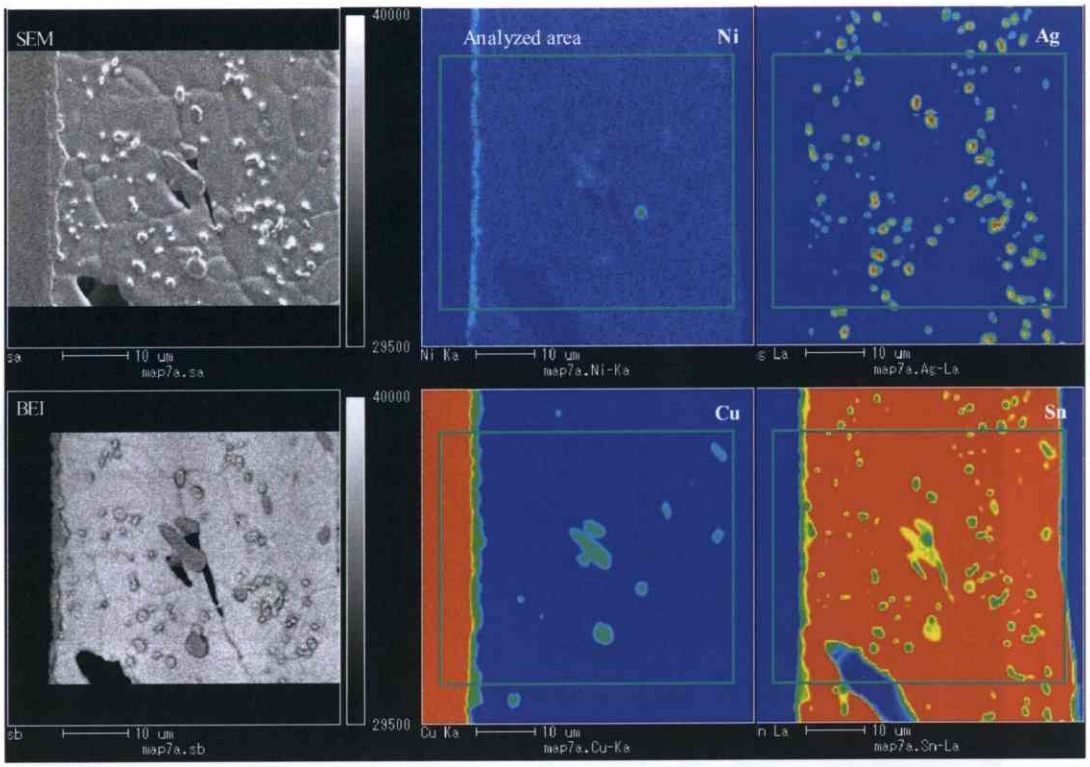

Fig.4-14 EPMA mapping analysis of the TH joints for the S3.0AC solder alloy after creep testing at 125℃, 2000 g for 170 h.

TEM analysis was performed to investigate the relationship between creep strength properties and precipitates. Figure 4-15 is a TEM image of a SACNG solder alloy in its initial state and after creep at 125℃. At the initial state, particle sizes are 0.1-0.2 μ m. These particles grow to 0.5-1.0 μ m after the creep test at 125℃ and 5 MPa for 550 h, with dimensions several-fold larger than at the initial state.

The particles blocking dislocations was also observed and the smaller particles appear to improve creep strength.

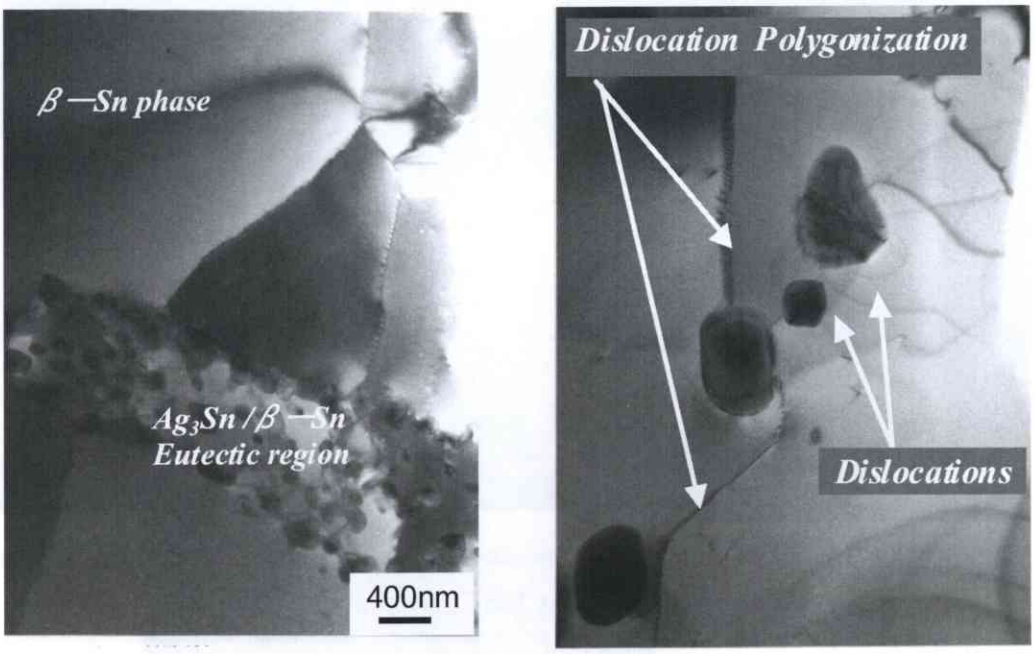

(a) (b)

Fig.4-15 TEM photograph of the SACNG solder alloy (a) initial state, and (b) after creep testing at 125℃, 5 MPa for 550 h.

To analyze the distribution of Sn, Cu, and Ni, EDX mapping was performed at selected areas of the SACNG solder alloy. Moreover, to identify these precipitates, electronic diffraction analysis was also carried out.

Figure 4-16 shows the result of EDX analysis. Elements Ni, Cu, and Sn were detected from the particles.

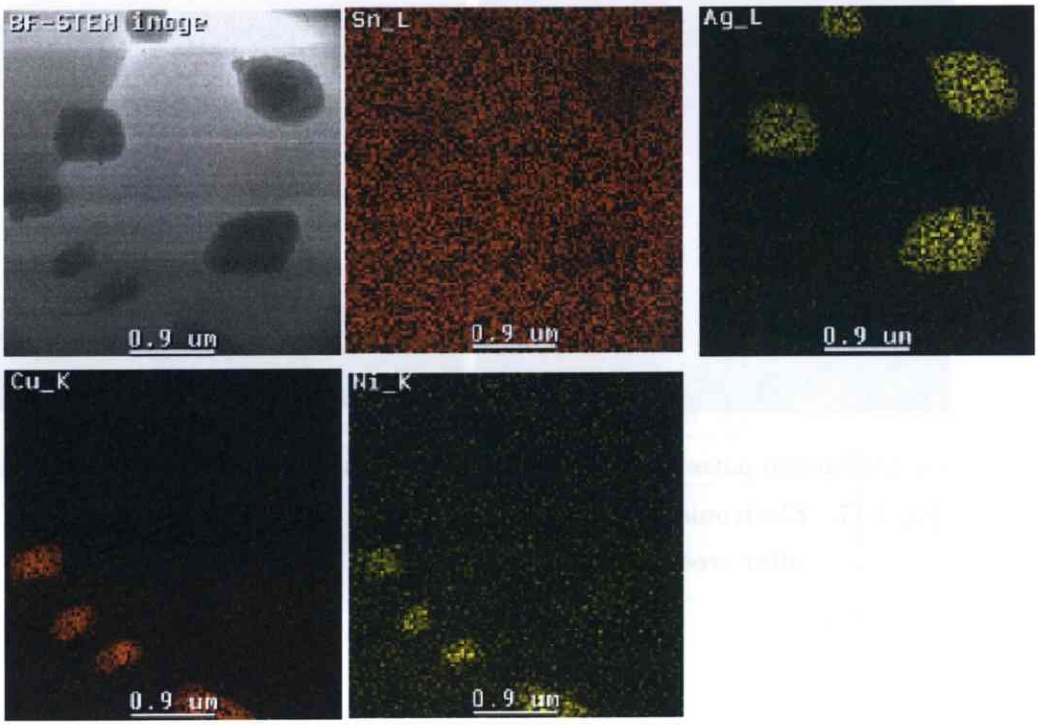

Fig.4-16 EDX mapping analyses of the SACNG after creep test at 125℃ for 550h.

Figure 4-17 shows the electron diffraction pattern of particles and □-Sn phase.

From these analyzed results of electronic diffraction pattern and EDX mapping, the particles, diameter of which are about 0.5 μ m, is a particle of the $(Cu, Ni)_6Sn_5$ confirmed that particles measuring approximately 0.5 μ m in diameter are $(Cu, Ni)_6Sn_5$ IMCs in the SACNG solder alloy[4-30-4-34].

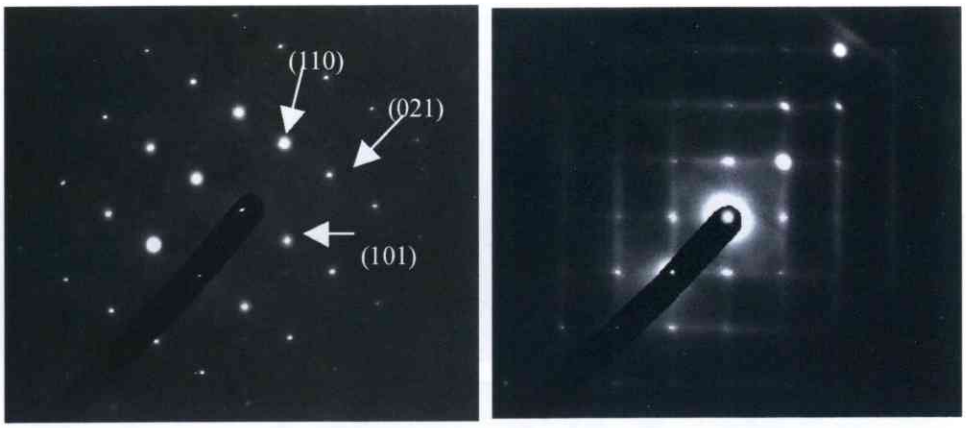

(a) Diffraction pattern of Particle (b) Diffraction pattern of β-Sn phase

Fig.4-17 Electronic diffraction pattern of the SACNG solder alloy after creep test at 125℃ for 550h.

4.3.3. Limit Range of the Sn-Ag-Based Solder Alloys

As described, to understand the limit range for "use", the creep strength of 10^5 h as limit strength, an accelerated testing was executed. Short time creep tests were also performed on S0.3AC, S1.0AC, and S1.0ACNG solder alloys. The test temperature was at 80℃, 125℃, and the applied stress was at the range of 5MPa, 9.8MPa, and 14.8MPa.

Figure 4-18 shows the results of creep life of 4 kinks of Sn-Ag-based solder alloys. From the results, the creep strength can be ordered as: S0.3AC＜S1.0AC＜S1.0ACNG≦S3.0AC＜SACNG.

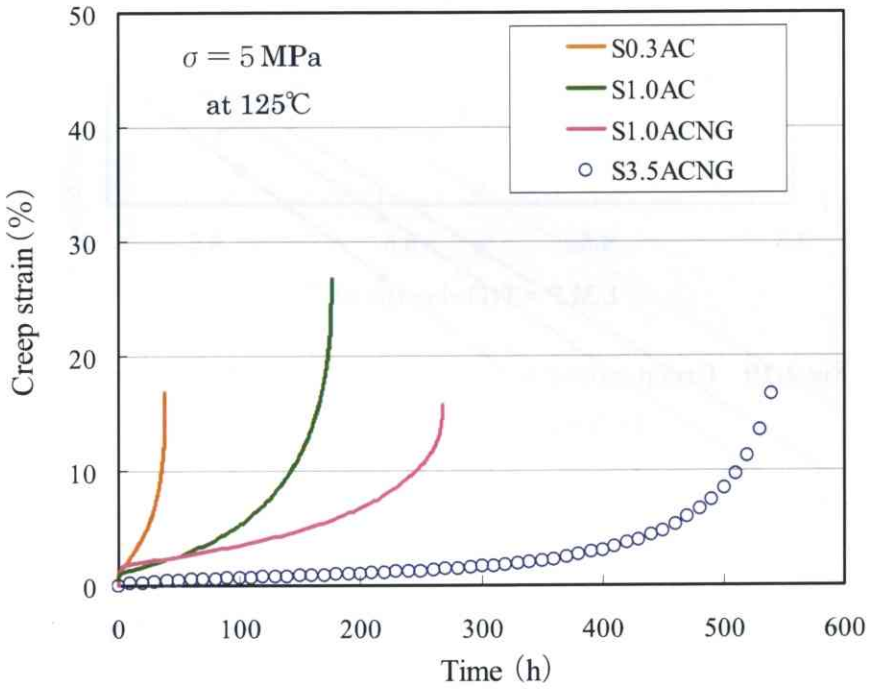

Fig.4-18 Creep curves of 4 kinds of Sn-Ag-based solder alloys

Moreover, Figure 4-19 shows the results of which plotted in Fig4-9 together Using the Larson-Miller Parameter (LMP), the lead-free solder alloys of S0.3AC, S1.0AC, S1.0ACNG, and SACN can get those limited range and can be as lineup solders to correspond the products (cost, reliability, etc).

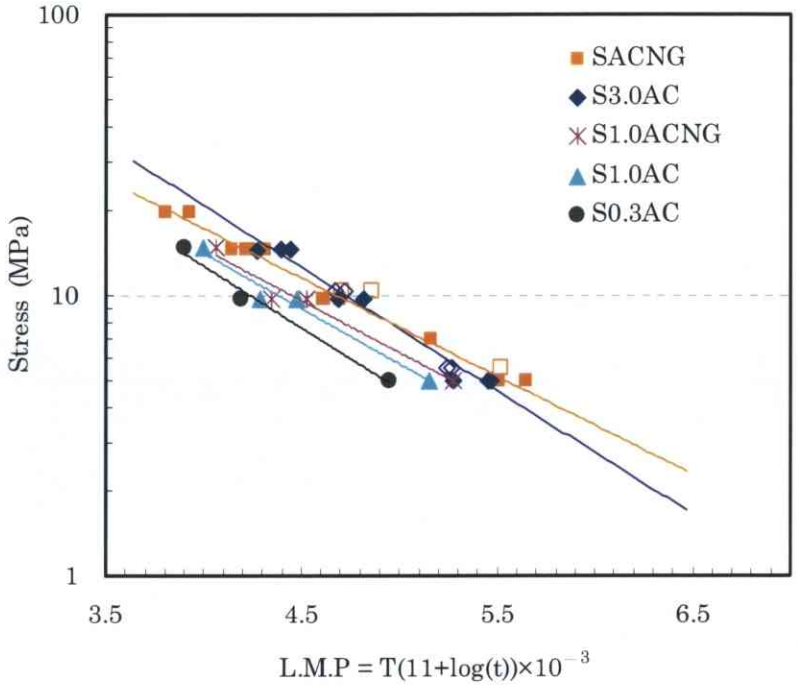

Fig.4-19 Creep strength using Larson-Miller parameter for the Sn-Ag-based solder alloys.

Figure 4-17 shows the relationship between the limited stress and temperature for the four kinds of solder alloys. When the life of the solder alloys is over ten years, the applied stress and temperature can be described by the equation 4-3-(4):

$$\sigma = A \times \exp(-B \times T) \text{----------} 4\text{-}3\text{-}(4)$$

Where T is absolute temperature, A, B is a constant, and σ is applied stress. The constant of A, B is shown in table 4-4 for the four kinds of solder alloys. So that, when the specification (use temperature, life, and applied stress) is cleared The solder can be selected by creep strength from Sn-Ag-besed solder alloys.

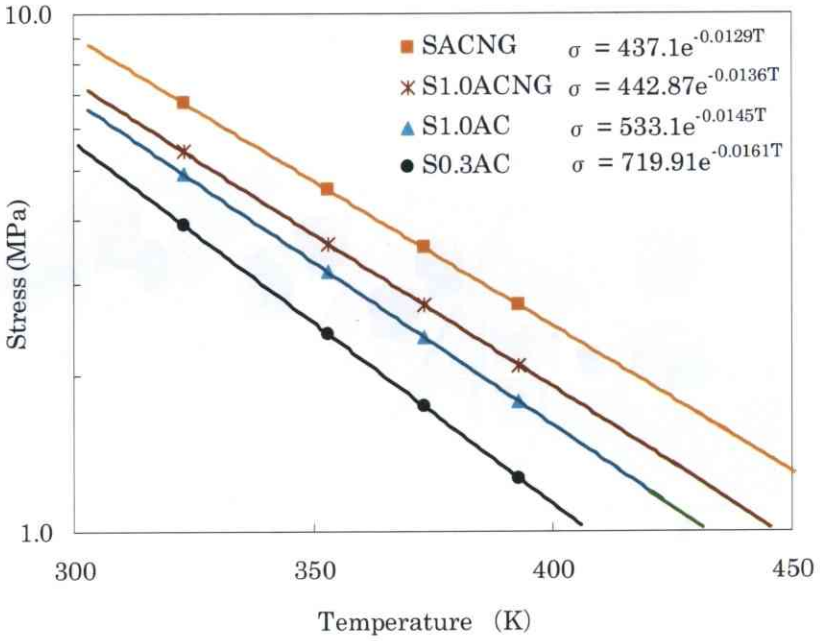

Fig.4-20 Relationship between the stress and temperature for S0.3AC,S1.0AC,S1.0ACNG,and SACNG solder alloys.

Table 4-4 A,B constant for the four kinds of solder alloys (S0.3AC, S1.0AC, S1.0ACNG, and SACNG)

Constant	S0.3AC	S1.0AC	S1.0ACNG	SACNG
A	437.1	442.8	533.1	719.9
B	0.0129	0.0136	0.0145	0.0161

4.4. Conclusions

The microstructure and creep behavior of bulk specimens and TH joints were investigated for Sn-Ag-based solder alloys. The conclusions are following.

- Creep strength of the bulk specimen and the TH joints sample can be plotted using LMP, a parameter of stress, temperature and rupture time. Moreover, the Sn-Ag-based solder alloys can be lineup by the creep properties. For example, the lineup mapping can be shown as Fig.4-21.

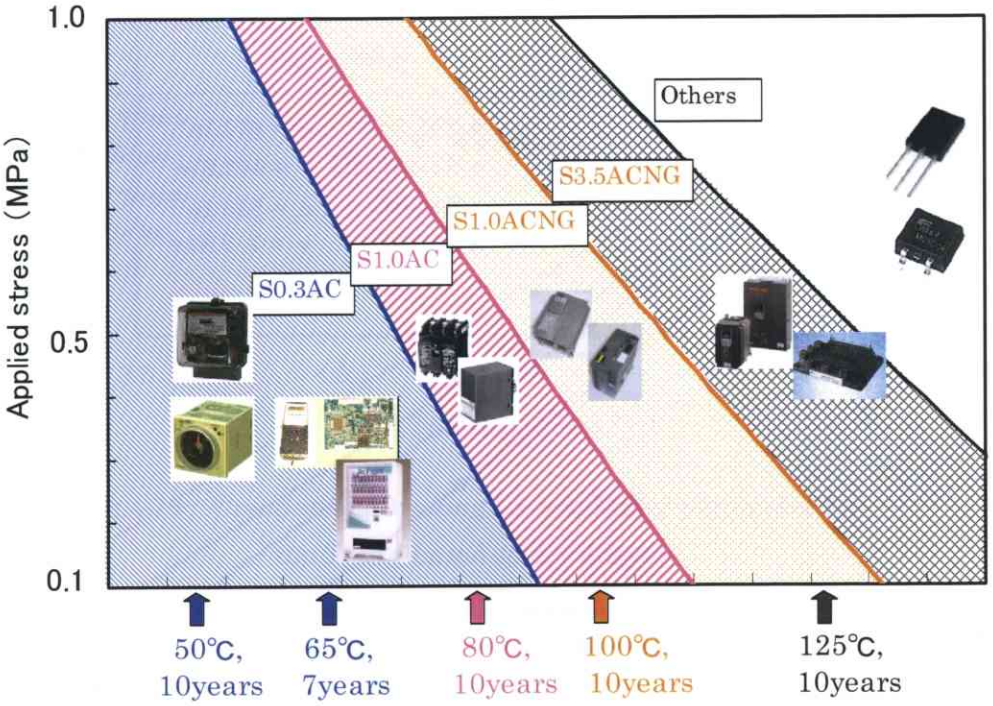

Fig.4-21 the lineup image of various Sn-Ag-based solder alloys and the products in Fuji.

- The stress exponents of the SACNG solder alloy and the S3.0AC solder alloy were 6.9 and 5.1, and their apparent activation energies at 9.8 MPa were 48 kJ/mol and 68 kJ/mol, respectively. The microstructure of the S3.0AC solder alloy appears quite sensitive to creep temperature.
- Creep strength of SACNG solder alloy at 125℃is approximately three times that of the S3.0AC solder alloy. The initial microstructure of the SACNG solder alloy is finer and more uniform than that of the S3.0AC solder alloy.
- Creep characteristics were apparently affected by IMCs growth in the eutectic region. The IMCs of the $(Cu, Ni)_6Sn_5$ formed after the addition of Ni showed improved creep strength at regions of higher temperature (125℃) and lower stress (5 MPa).

4.5. References

4-1. EITA: "Lead-free Solder Technologies", published by, CORONA, 2004,pp.19-22.

4-2.R. J. Mccabe, M. E. Fine, " High Creep Resistance Tin-Based Alloys for Soldering Applications", J. Electron. Mater. Vol. 31,No.11, 2002,pp.1276-1282.

4-3. V.I.Igoshev, and J.I.Kleiman: "Creep Phenomena in Lead-Free Solders", J. Electron. Mater., Vol.29, No.2, 2000, pp.244-250.

4-4. K.Wu, M.Aoyama, N.Wade, J.Cui, S.Yamada, and K.Miyahara: "Creep and Rupture Behavior of Cu Wire/Lead-Free Solder-Alloy Joint Specimen", J. Electron.Mater. Vol. 32,No.12, 2003,pp.1392-1397.

4-5. F.Garofalo: "Fundamentals of Creep and Creep Ruoture in Metals", MacMillian, 1965,pp.156-201.

4-6. K.Mariyama, and H.Nakasima: "Fundamentals of Creep in Metals and Alloys", Published by Uchida Rokakuho,2002.pp.8.

4-7. D.Shangguan: "Lead-Free Solder Interconnect Reliability", ed. by D.Shangguan, ASM, 1995, pp.88-89.

4-8. J.Askin: "Tracer Diffusion Data", Penum, 1970.

4-9. Y. Kariya, M. Otsuka, and W. J. Plumbride: "The Consititutive Creep Equation for a Eutectic Sn-Ag Alloy Using the Modified Theta-Projection Concept", J. Electron. Mater. 32, 2003, pp.1398-1402.

4-10. P.Shewmon: "Diffusion in solids", 2nd, ed., TMS, 1969,pp.189-199.

4-11. J.Christian: "The Theory of Transformations in Metals and Alloys: Part I Equilibrium and General Kinetic Theory", Pergamon,1975,pp.541-543.

4-12. J.Stephens, and D.Frear: "Time-Dependent Deformation Behavior of Near -Eutectic 60Sn-40Pb Solder", Metall.Mater.Trans.A, Vol.30A, 1999, pp.1301-1313.

4-13. T. T. Mattila, and J. K. Kivilahti, J. Electron. Mater.,Vol.34, 2005, pp.969-976.

4-14. S. Terashima, and M. Tanaka, Mater. Trans., Vol.45,2004,pp.681-688.

4-15. C. M. L. Wu and M. L. Huang: "Creep Behavior of Eutectic Sn-Cu Lead-Free Solder Alloy", J. Electron. Mater. 31, 2002,pp.442-448.

4-16. M. Kerr and N. Chawla:"Creep Deformation Behavior of Sn-3.5Ag Solder/Cu Couple at Small Length Scales", Acta.Metall., Vol. 52, 2004, pp.4527-4535.

4-17. R. J. Mccabe, M. E. Fine:"Creep of Tin, Sb-Solution-Strengthened Tin, and SbSn-Precipitate Strengthened Tin" Meta.Mate.Trans.,Vol.33A,2002, pp.1531-1538.

4-18. K. Atsumi, Y. Kariya, and M. Otsuka: "Creep Properties of Sn-3.5Ag-xBi and Sn-3.5Ag-xCu Solder Alloys", Proc. of 6th Symposium on Microjoining and Assembly Technology in Electronics, 2000,pp.281-286.

4-19. M.Nagano, N.Hidaka, M.Shimoda and H.Watanabe: "Effect of Germanium content on Oxidation Prevention of Sn-Ag-Cu Lead-Free Solder", Proc. of PSEA04, 2004, pp.256-261.

4-20. Z. Chen, Y. Shi, and Z. Xia: "Constitutive Relations on Creep for SnAgCuRE Lead-Free Solder Joints", J. Electron. Mater., Vol.33,No.9,2004,pp.964-971.

4-21. P. T. Vianco, J. A. Rejent, and A. C. Kilgo: "Creep Behavior of the Ternary 95.5Sn-3.9Ag-0.6Cu Solder-Part I: As-Cast Condition", J. Electron. Mater., Vol.33, No.11,2004,pp.1389-1400.

4-22 .Q. Xiao and W. D. Armstrong: "Tensile Creep and Microstructural Characterization of Bulk Sn3.9Ag0.6Cu Lead-Free Solder", J. Electron. Mater., Vol.34, No.7, 2005, pp.196-211.

4-23. W.J.Plumbridge, C.R.Gagg, and S.Peters: "The Creep of Lead-Free Solders at Elevated Temperatures", J. Electron. Mater.,Vol.30,No.9,2001, pp.1178-1183.

4-24. T. H. Chuang, S. F. Yen, and M. D. Cheng: "Intermetallic Formation in Sn3Ag0.5Cu and Sn3Ag0.5Cu0.06Ni0.01Ge Solder BGA Packages with Immersion Ag Surface Finish", J. Electron. Mater.,Vol.35,2006,pp.302-309.

4-25. T. H. Chuang, S. F. Yen, and M. D. Cheng: "Intermetallic Reactions in Sn3Ag0.5Cu and Sn3Ag0.5Cu0.06Ni0.01Ge Solder BGA Packages with Au/Ni Surface Finish", J. Electron. Mater.,Vol.35,2006,pp.302-309.

4-26. D. Mitlin, C. H. Raeder, and R. W. Messler, Jr: "Solid Solution Creep Behavior of Sn-xBi Alloy", Metall. Mater.Trans.Vol.30A, 1999, pp.115-122.

4-27. R. Ninomaya, Y. Nakahara, and T. Takemoto,: "Microstructure and Mechanical Property of Sn-Ag-Bi-In Solder", Proc. of 9th Symposium on Microjoining and Assembly Technology in Electronics, 1998,pp.249-252.

4-28. J.J.Sundelin, S.T.Nurmi, T.K.Lepisto, and E.O.Ristolainen: "Effect of PCB surface finish on creep properties of lead-free solder joints", Soldering & Surface Mount Technology, Vol.17, No.4, 2005,pp.3-9.

4-29. Q. Xiao, L.Nguyen, and W. D. Armstrong, "Anomalously High Tensile Creep Rates from Thin Cast Sn3.9Ag0.6Cu Lead-Free Solder", J. Electron. Mater., Vol.34,No.7, 2005,pp.1065-1075.

4-30. F.Ochoa, X.Deng, and N.Chawla: "Effect of Colling Rate on Creep Behavior of a Sn-3.5Ag Alloy", J. Electron. Mater., Vol.33, No.12, 2004, pp.1596-1607.

4-31. N.Hidaka, M. Nagano, M. Shimoda, H. Watanabe, and M. Ono: "Creep Properties and Microstructure of the Sn-Ag-Cu-Ni-Ge Lead-Free Solder Alloy", Proc. ASME, InterPACK, 2005,2005-73148.

Chapter 5 MICROSTRUCTURAL EVOLUATION AND INTERFACIAL INTERACTION IN LEAD-FREE SN-AG-BASED SOLDER ALLOYS

5.1. Introduction

In the Chapter 2, we have discussed the effect of adding Ni on dissolution of Cu electrode. It was considered that adding Ni formed a thin layer of the interfacial reaction phase of (Cu, Ni) Ag as a barrier to suppress the diffusion rate of Cu into molten soldering (Fig.5 -1).

In this chapter, the effects of adding Ni on the microstructures of the interfacial reaction phase will be investigated. Specially, the intermetallic reaction growth between the Sn-Ag-based solder alloys and the substrate Cu was investigated.

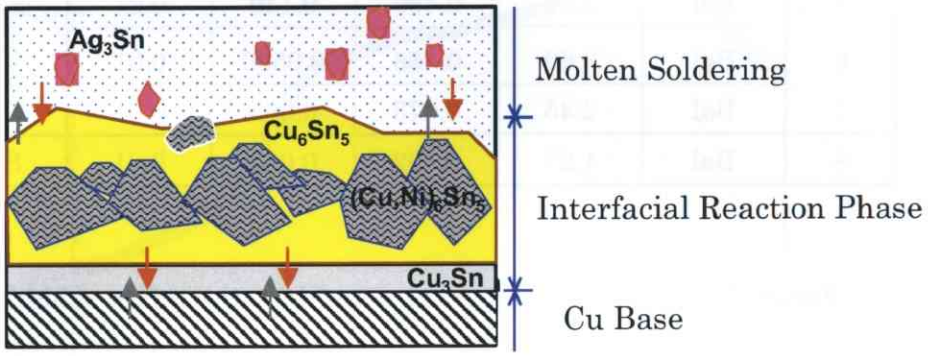

Fig.5-1 The schematic illustrative of the interface reaction layer.

5.2. Experimental Procedures

Seven tapes of solder alloys (ball solders) were used. The content of the Cu was fixed at 0.5 mass%, and the Ge was fixed at 0.01%, and the range of Ni was changed from 0.07mass% to 0.25mass%. The solder balls, the diameter of which is 300 μ m, were attached to Cu pads with a diameter of 200 μ m on a FR-4 substrate. The chemical compositions of the solder are shown in Table 5-1.

Table 5-1. Composition of various solder alloys

No.	Elements					Alloy Codes
	Sn	Ag	Cu	Ni	Ge	
1	Bal	3.55	-	-	-	S3.5A
2	Bal	3.66	0.492	-	-	S3.5AC
3	Bal	3.01	0.466	0.07	0.01	S3.0AC07NG
4	Bal	3.56	0.466	0.247	0.01	S3.5AC2.5NG
5	Bal	3.59	0.489	0.149	0.01	S3.5AC1.5NG
6	Bal	3.60	0.468	0.0590	0.01	S3.5AC07NG
7	Bal	2.45	0.473	0.065	0.01	S2.5AC07NG
8	Bal	1.27	0.462	0.063	0.01	S1.2AC07NG

Figure 5-2 shows the temperature profile in the reflow soldering. The peak temperature was set at 516K, and the time above 493K was 44s. After reflow soldering, the soldering ball joints were further aged at the temperatures of 353K, 373K and 393K for the times of 300h, 600h,and 1000h respectively.

The reflowed and aged samples were ground to #2400-grit sandpaper, followed by diamond particle polishing down to 0.25 μ m, and made to a final polishing stage using colloidal silica suspension. After polishing, cross sections of the samples were etched by Ar^+ ion milling and observed with Field Emission Scanning Electron Microscope

(FE-SEM: HITACHI S-4300). The FE-SEM was operated at 7kV in backscatter mode to measure η and ε IMCs-phase thickness. The distribution of the IMCs and its chemical compositions were analyzed using an Electron Probe Micro-Analyzer (EPMA) to determine solder composition distributions.

Moreover, the microstructure analysis of the initial samples were performed using TEM (HITACHI H-9000UHR model) at an acceleration voltage of 300kV.and Energy Dispersive X-ray (EDX) microanalysis was also used to determine the elemental composition at selected areas.

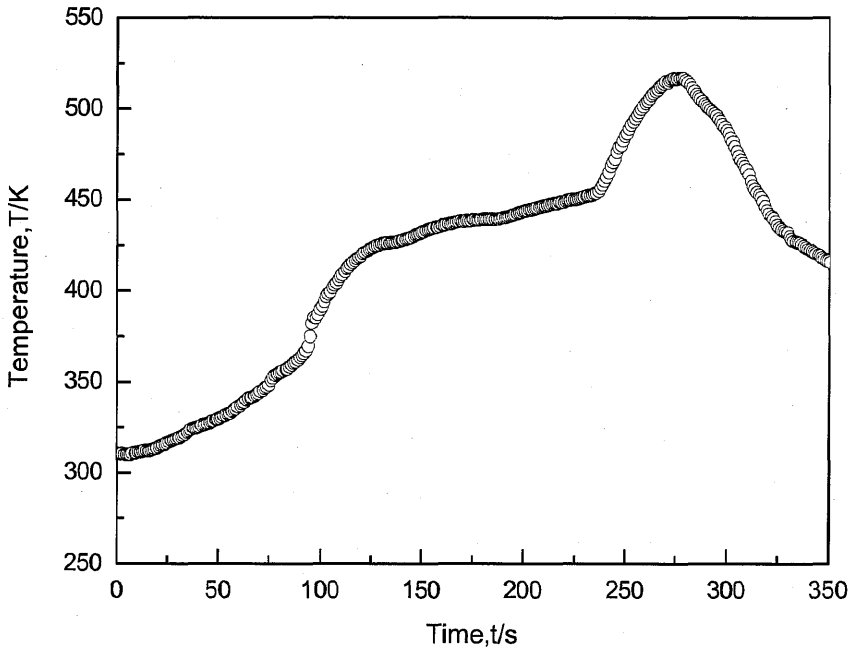

Fig.5-2 Temperature profile in reflow soldering.

5.3. Results and Discussion

Figure 5-2 shows TEM photograph of S3.5ACNG solder alloys in initial stage. Table 5-2 shows the analysis results of the point in the interfacial reaction phase.

Form the results, the composition of the IMCs in the interface reaction layer can be shown as the schematic.

Table 5-2 The results of EDX

	Sn	Ag	Cu	Ni	IMCs
1	47.2	1.0	47.7	4.0	$(Cu, Ni)_6Sn_5$
2	46.6	0.6	51.6	1.0	Cu_6Sn_5
3	45.8	0.8	48.9	4.3	$(Cu, Ni)_6Sn_5$
4	48.9	0.8	45.5	4.7	$(Cu, Ni)_6Sn_5$
5	47.1	0.3	47.9	4.5	$(Cu, Ni)_6Sn_5$
6	47.4	51.5	0.9	–	Ag_3Sn+Sn
7	74.1	25.2	0.7	–	Ag_3Sn+Sn
8	22.6	76.3	0.8	–	Ag_3Sn

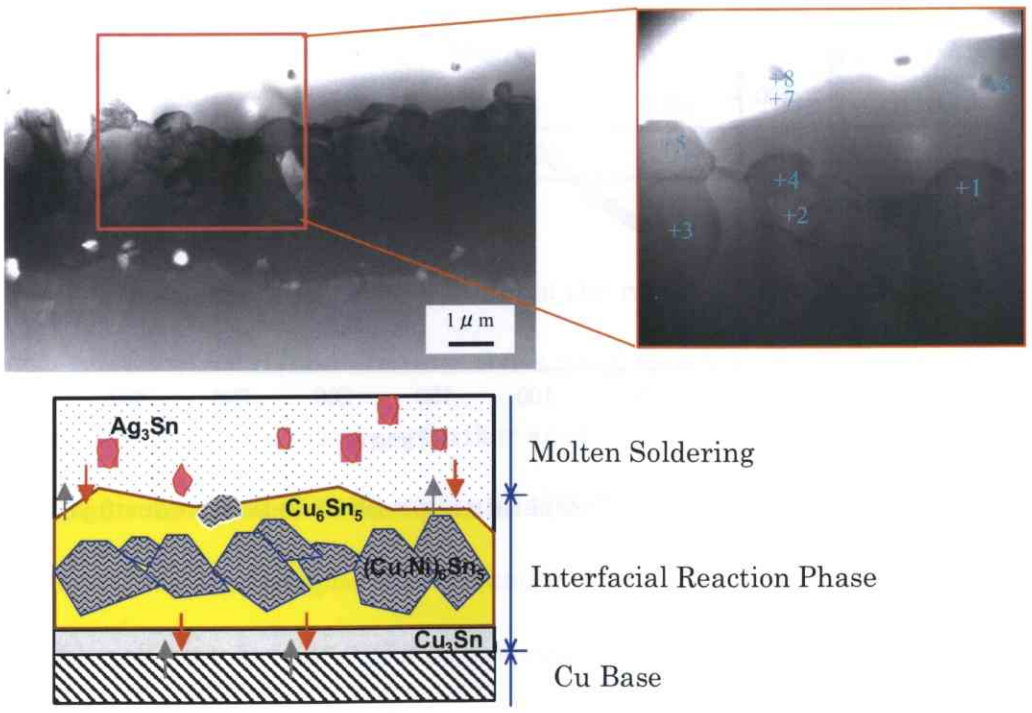

Fig.5-2 TEM photograph and schematic illustrative showing the reaction products of S3.5ACN solder alloy in initial stage.

5.3.1. Initial Microstructures of Solder Ball Joints

Figure 5-3 shows optical microstructures of various ball solders with polarized light. By viewing the reflected light through polarized light, the crystal, which has same orientation, can be observed clearly [5-1-5-3]. It was observed that the β-Sn phase of all the solder ball joints grew up to a large grain in size after reflowed in this temperature profile condition. Moreover, a lot of small grain of the β-Sn phase appeared in the interface reaction in the solder ball joints with adding Ni. Whereas, the smaller grain was not observed in the Sn-Ag and the Sn-Ag-Cu solder ball joints.

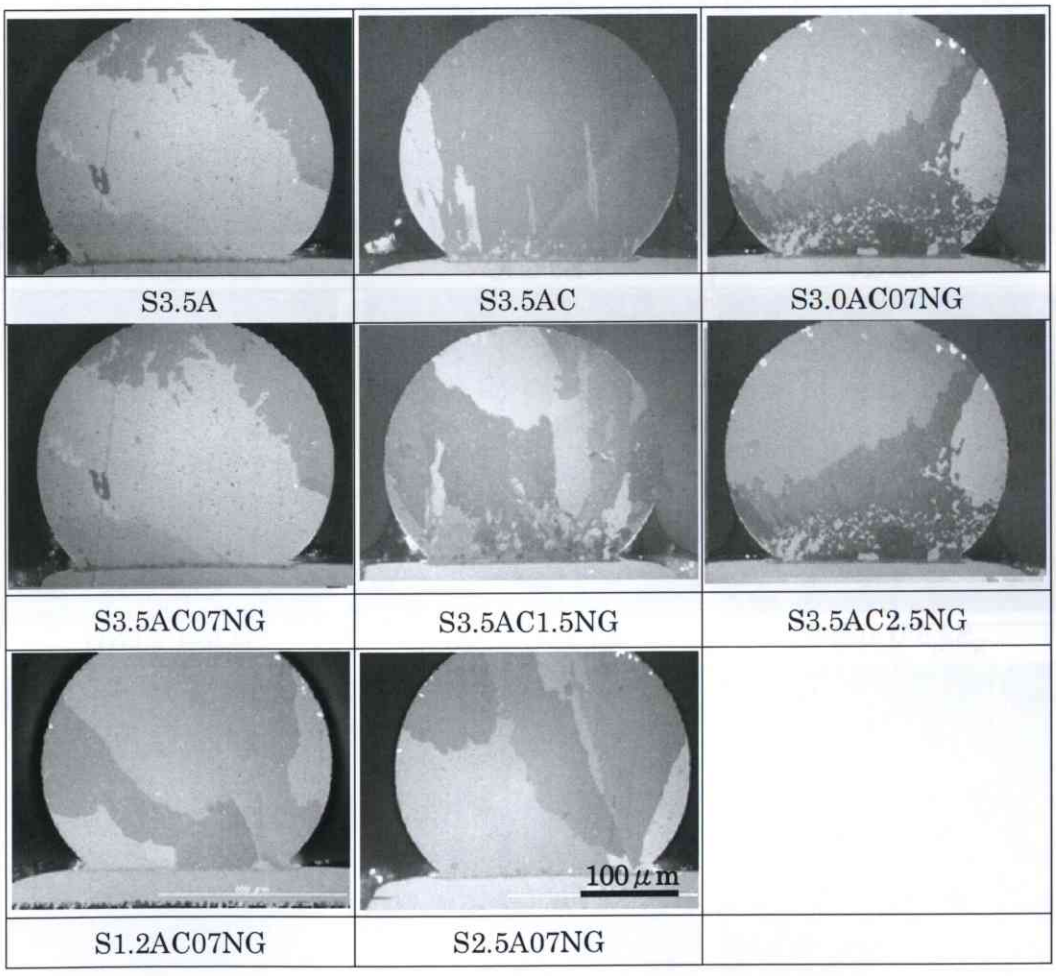

Fig.5-3 Polarized light micrographs of the solder ball joints.

Figure 5-4 shows the SEM images of the cross sections of the solder ball joints after reflow soldering. In the interfaces of the adding Ni solder alloys/Cu, the mop-haired of the IMCs reaction layer were formed regardless of the amount of Ag in the solder alloys. Moreover, the shape of the IMCs reaction layer is similar in the range of Ni content of 0.07-0.25 (mass)%.

In the SA and the SAC solder alloys; the coarse scallops of the IMCs were formed at the interface reaction layer. The shape of the IMCs reaction layer is greatly different compared with those of the solders with adding Ni.

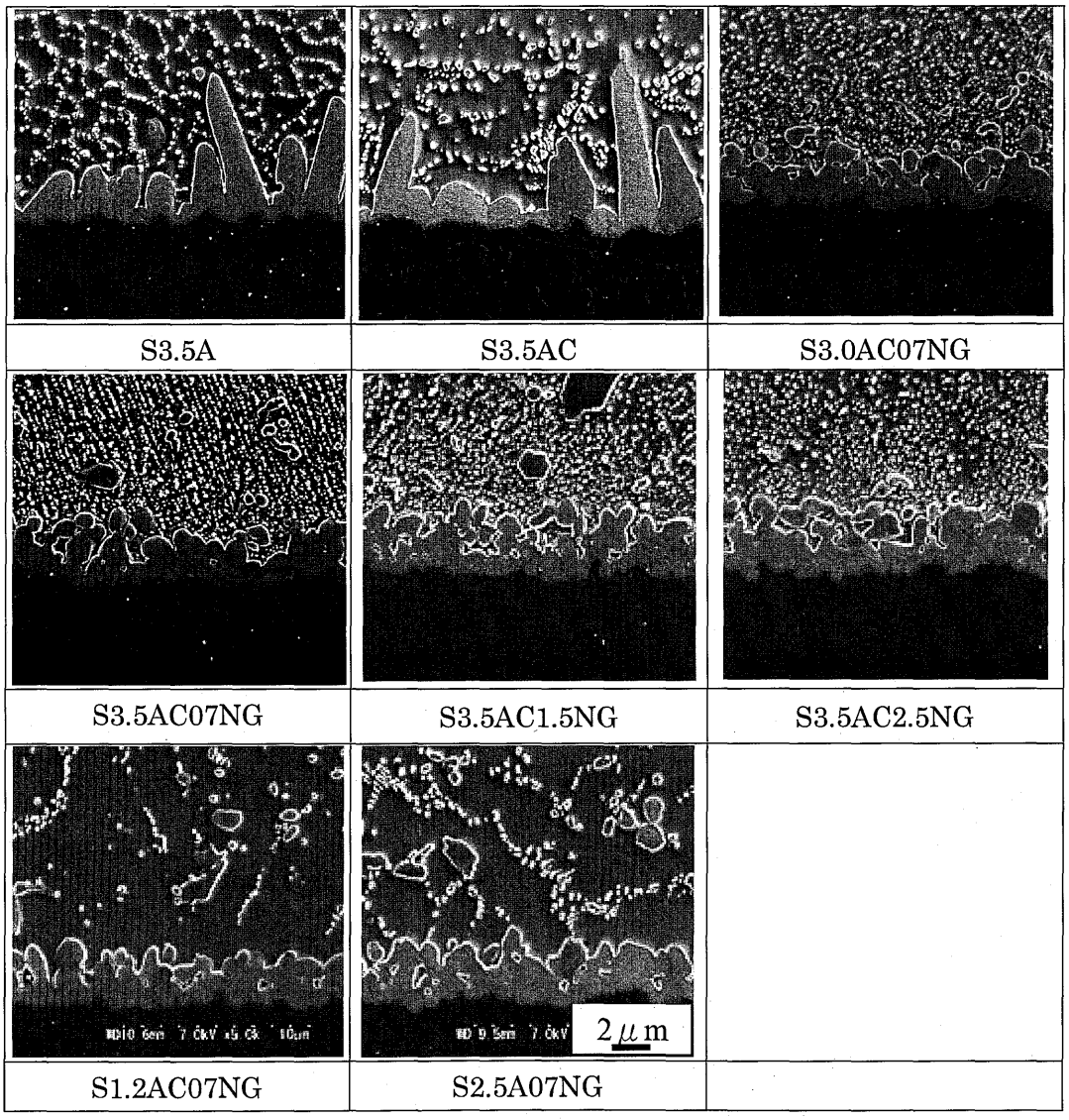

Fig.5-4 SEM photograph at the cross-sections of solder ball joints after reflow soldering.

5.3.2. Microstructure of the Solder Ball Joint after Heat Exposure

The interface of the solder ball joints was investigated with the back -scattered electron images after heat exposure at 353K, 373K and 393K for 1000h respectively. The growth of reaction layer in the interface of the all solders/Cu pad joints depends on the temperature. The growth rate of interface reaction layer increased as heat exposure temperature increased[5-4-5-7].

Figure 5-5 shows the reaction layers of the joints of the S3.5A and the S3.5AC solder alloys. The reaction layers that formed in the joints with the S3.5A and the S3.5AC solders were identified to be composed of Cu_6Sn_5 and Cu_3Sn by EPMA quantitative analysis. The reaction layer of Cu_3Sn can be observed clearly. The Cu_6Sn_5 that appeared scallop also was clearly observed and its shape was not greatly changed even though heat exposure.

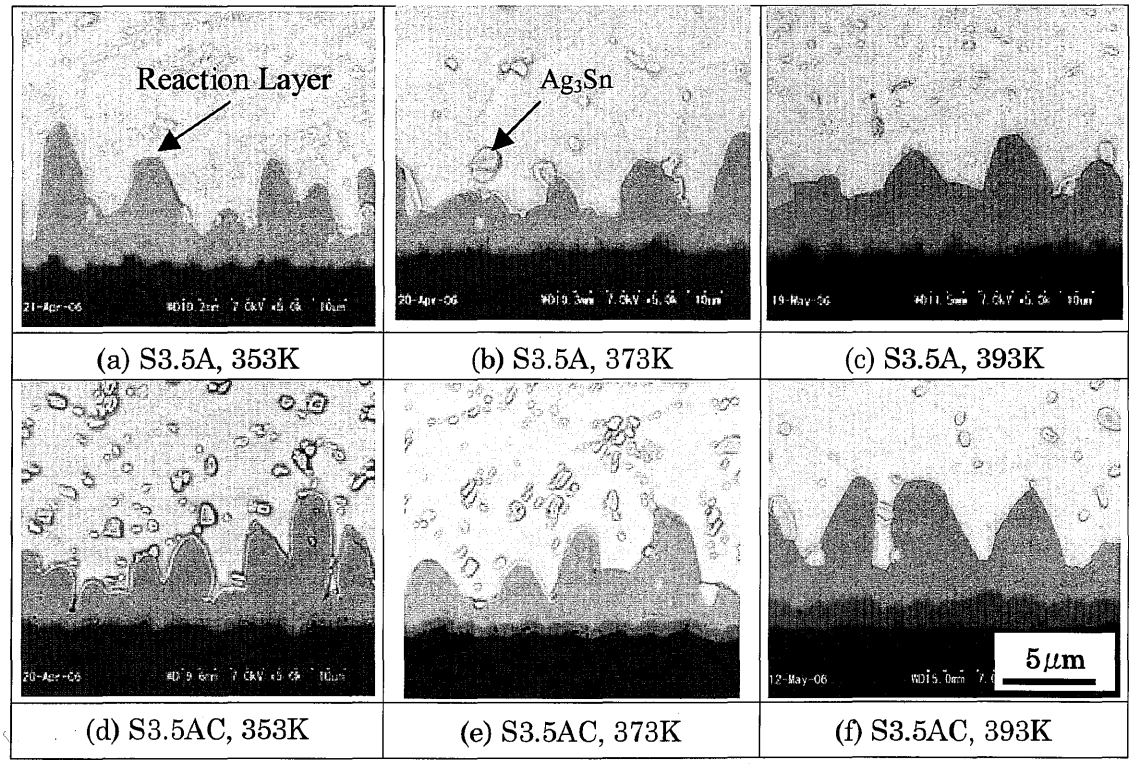

(a) S3.5A, 353K | (b) S3.5A, 373K | (c) S3.5A, 393K

(d) S3.5AC, 353K | (e) S3.5AC, 373K | (f) S3.5AC, 393K

Fig.5-5 BSE images of cross sections of solder ball joints after heart exposure at 353K, 373K, and 393K for 1000hr respectively.

Figure 5-6 shows the reaction layers of the joints with adding Ni. For the reaction layer formed at the joint with the adding Ni solders, S30ACNG, S3.5ACNG, S3.5AC15NG, and S3.5AC25NG, the layer consists of $(Cu, Ni)_3Sn$ and $(Cu, Ni)_6Sn_5$ by EPMA quantitative analysis[5-8-5-10].

The IMCs of $(Cu, Ni)_6Sn_5$ that appeared mop-haired were changed into a stable belt shape by heat exposure. Moreover, It was found that the Ag_3Sn IMCs dispersed in all solders, and the Cu-Sn-Ni IMCs dispersed in the adding Ni solders, S30ACNG, S3.5ACNG, S3.5AC15NG, and S3.5AC25NG by EPMA analysis.

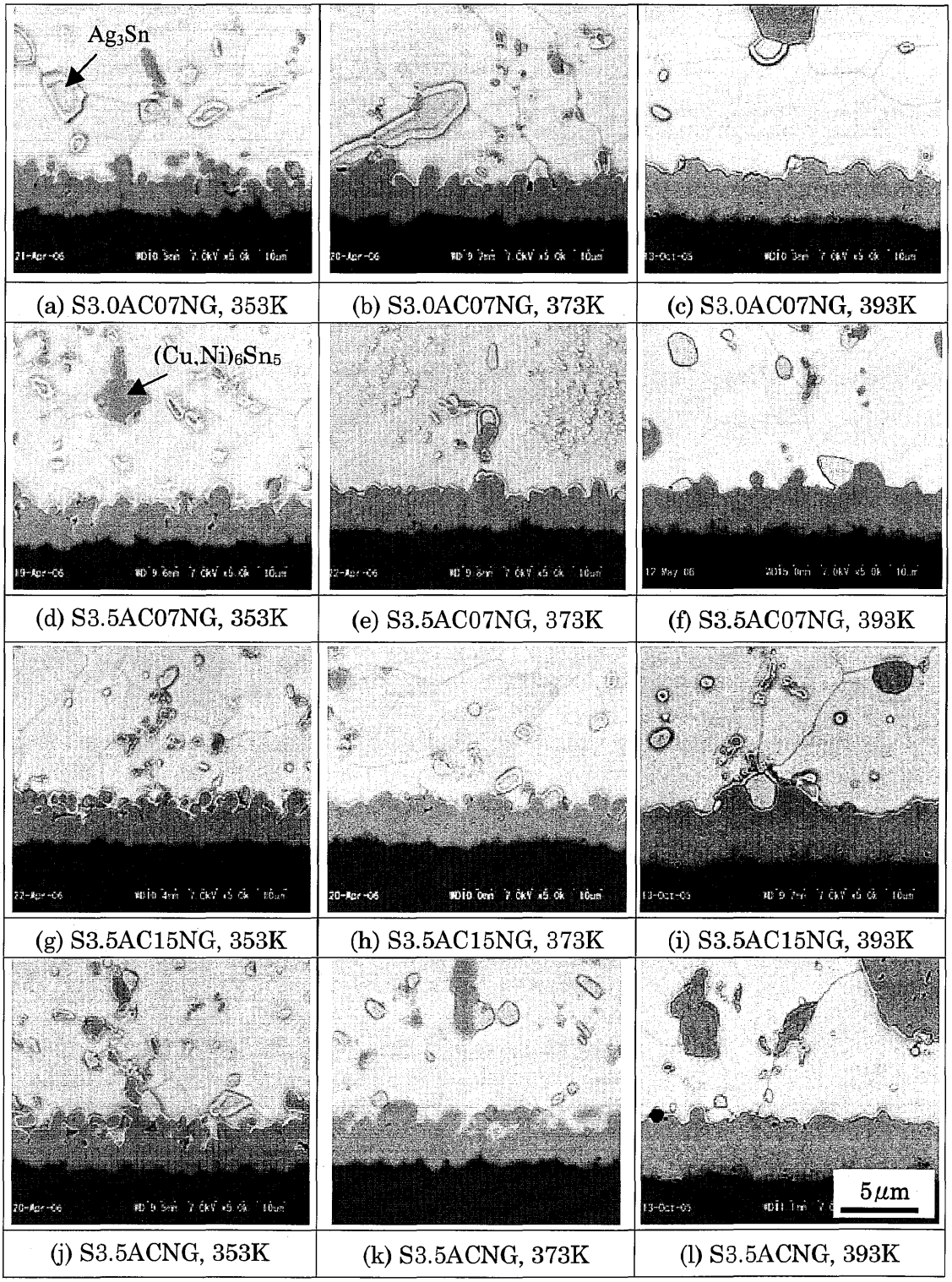

(a) S3.0AC07NG, 353K | (b) S3.0AC07NG, 373K | (c) S3.0AC07NG, 393K

(d) S3.5AC07NG, 353K | (e) S3.5AC07NG, 373K | (f) S3.5AC07NG, 393K

(g) S3.5AC15NG, 353K | (h) S3.5AC15NG, 373K | (i) S3.5AC15NG, 393K

(j) S3.5ACNG, 353K | (k) S3.5ACNG, 373K | (l) S3.5ACNG, 393K

Fig.5-6 BSE images at the cross-sectional surface zones of solder ball joints after heart exposure at 353K, 373K, and 393K for 1000hr respectively.

5.3.3. The Thickness of the Reaction Layer in Various Solder Ball Joints

During the reflow, the Cu dissolved into the molten solder by diffusion while an IMCs layer was formed by chemical reaction in the solder/Cu interface. During solidification, because the free energy of formation in the interface is less than that of the nuclei, the main IMCs that solidified from the molten solder was easily to combine with the IMCs layer that existed on the interface. As a result, an apparent reaction IMCs layer with different formation formed in the interface[5-11-5-13]. Here, the IMCs that formed in interface by chemical reaction were focused. To distinguish the IMCs, the etching rate by Ar^+ ion milling was adjusted. For each sample, 20 points of the maximum peak height, and the minimum trough height were measured, and the average layer thickness of the η-phase was calculated. The thickness of the ε-phase layer was also determined.

Figure 5-7 shows the relationship between the thickness of the reaction layer and the square root of the heat exposure time, since the reaction layer tends to increase according to the parabolic rate law. In the case of the SA and the SAC solders, the thickness of total (Cu_6Sn_5+Cu_3Sn) increased as thermal temperature increased. The reaction layer grows up to approximately 5 μm thicker than that of the solders with adding Ni after heat exposure at 393K for 1000h.

On the other hand, the reaction layers of solders with the adding Ni grow up to 3~4 μm regardless of the solder type in the same heat exposure condition. The growth of Cu_3Sn IMCs show similar trend as total IMCs. The thickness of the Cu_3Sn IMCs also increased as thermal temperature increased. Moreover, the thickness of the IMCs layer was not sensitive for changing the amount of Ni in the range of 0.07 to 0.25 (mass)%.

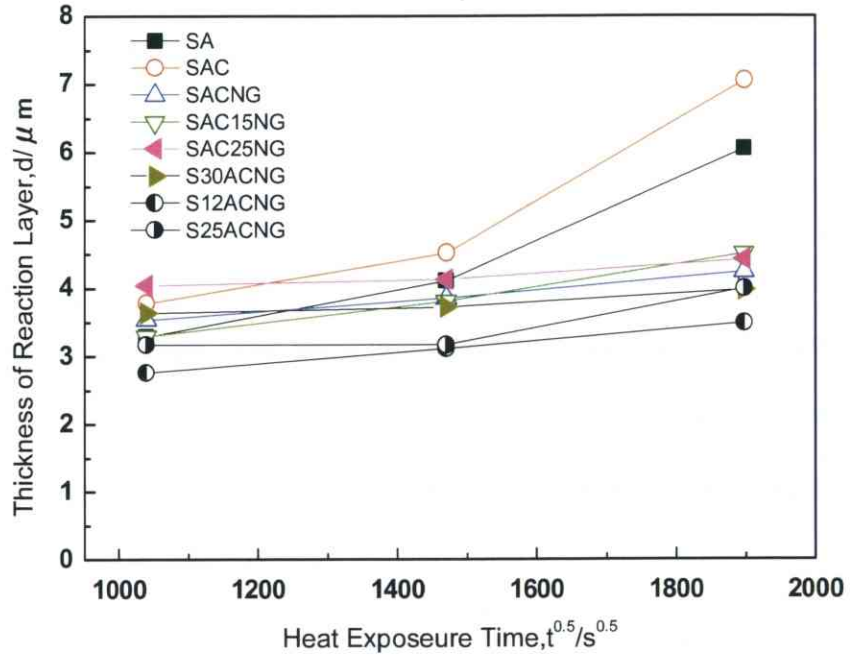

(a) The thickness of reaction layer of the Cu-Sn IMCs

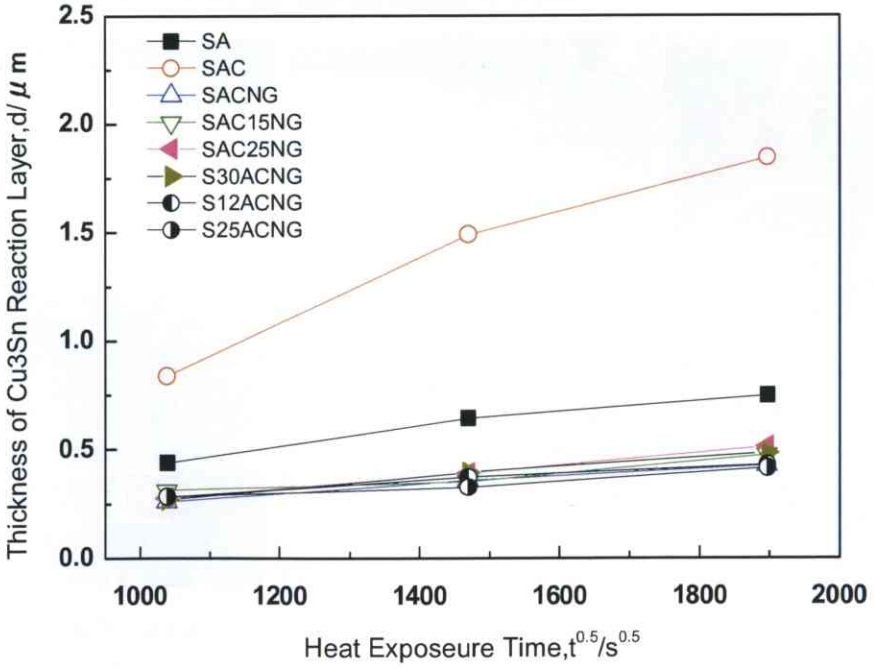

(b) The thickness of reaction layer of the Cu_3Sn IMCs

Fig.5-7 Growth kinetics of reaction layers at 393K (a) Total Cu-Sn, (b) Cu_3Sn

Figure 5-8 shows secondary electron images of the interface solder ball joints after heat exposure at 393K for 1000h. The thickness of Cu_3Sn IMCs layer shows greatly different between the solders with small amounts of Ni and the solders of S3.5A, S3.5AC. It indicates that the growth rate of Cu_3Sn IMCs layer in the SA, the SAC solder, was faster than these of solders with adding Ni. In adding Ni solders, the thickness of Cu_3Sn IMCs was about 0.5 μm after heat exposure at 393K for 1000h.

However, in the SA, SAC solders, the thickness of Cu_3Sn IMCs was about 0.5□m in the same heat exposure condition. The thickness of Cu_3Sn IMCs layers of the solders with adding Ni were apparently less than those values observed with SA, SAC solder. It was considered that adding Ni into the solder is very effective to reduce the growth rate of the Cu_3Sn IMCs in the interfaces of solder joints[5-14-5-16].

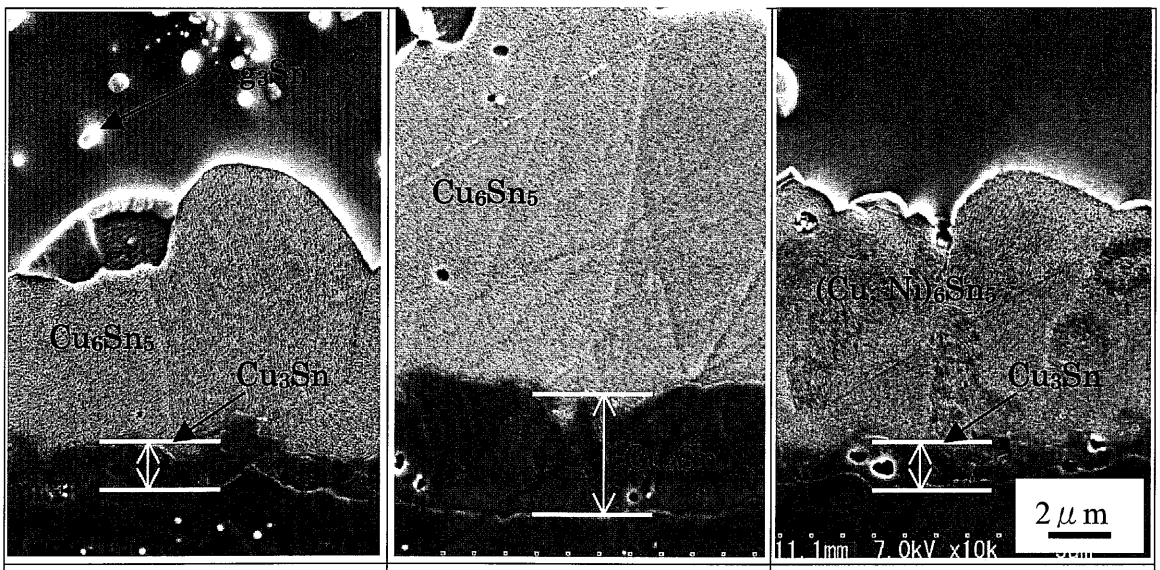

(a) S3.5A (b) S3.5AC (c) S3.5AC25NG

Fig.5-8 Comparison of the thickness of Cu_3Sn IMCs layers in the S3.5A, the S3.5AC, and the S3.5AC25NG solders after heat exposure at 393K for 1000h.

5.3.4. Growth Kinetics of Reaction Layer

The thickness (X (t)) of the reaction layer was expressed as a function[5-15-5-16] of heat exposure time, t.

$$X(t) = X_0 + (K t)^n \quad K = kD \text{ ----------5-3-(1)}$$

Where X (t) is the thickness of the reaction layer at, t; X0 is the thickness of the reaction layer before heat exposure treatment, the exponent, n is 0.5 for ordinary diffusional growth, K is the growth rate constant, t is the heat exposure time, D is the diffusion coefficient and k is a constant. The thickness of the IMCs layer as a function of square root of the heat exposure time for each temperature is shown in Fig.5-8.

The most thickness of the IMCs layer was linearly increased with the square root of heat exposure time and the growth was faster for higher heat exposure temperatures. This means that the layers growth is controlled by the volume diffusion mechanism.

The thickness data were further analyzed as a function of heat exposure temperature to determine apparent activation energy for the growth process. The activation energy of the growth of the reaction layer can be calculated by an Arrhenius plot for K, which is evaluated from the slope of the line shown in Fig.5-9 (a)-(e), and the results are shown in Fig.5-10.

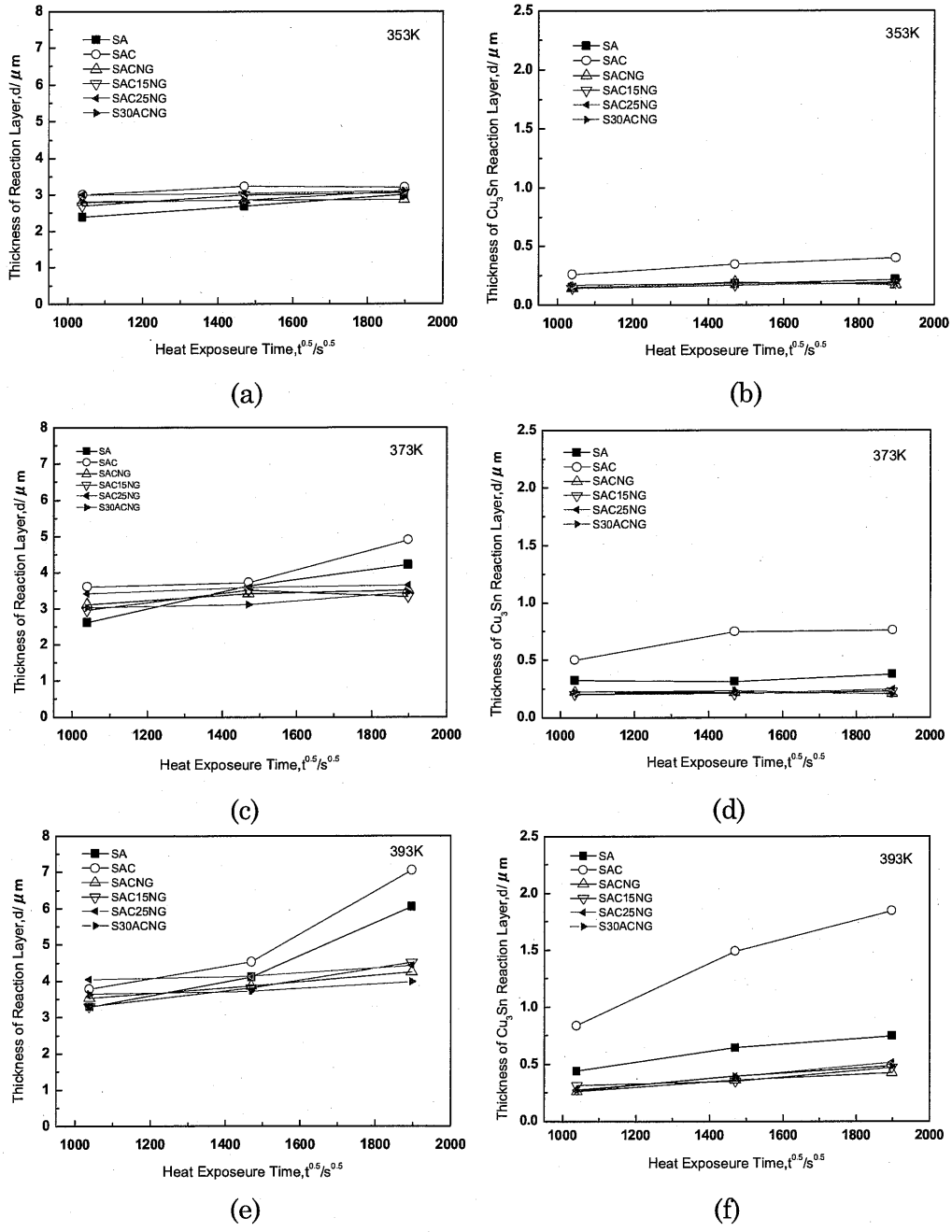

Fig.5-9 Growth of kinetics of total Cu-Sn(Cu_6Sn_5+Cu_3Sn) intermetallic reaction layers.

Figure 5-10 (a), (b) shows the Arrhenius plot results for the growth of the total IMCs (Cu_6Sn_5+Cu_3Sn), and Cu_3Sn in the joint interfaces of all solders.

Table 5-3 lists the values of the activation energy Q .the activation energy of the total Cu-Sn IMCs were investigated 40kJ/mol, 45kJ/mol and 15~20kJ/mol for the SA, the SAC and the solders with adding Ni respectively. Moreover, the Q-valus for the growth of the Cu_3Sn IMCs shows similar trend with total Cu-Sn IMCs and were investigated 71kJ/mol, 88kJ/mol and 52 ~ 66kJ/mol in those solders respectively. The values for the solders with adding Ni are much smaller than those of the SA, the SAC solder, and are close to the activation energy for grain boundary diffusion in solders[5-17-5-18].

Table5-3 Calculated activation energy (Q)

IMCs		SA	SAC	SACNG	SAC15NG	SAC25NG	S30ACNG
Q (kJ/mol)	Total Cu-Sn	38.9	44.3	20.4	20.3	18.5	14.1
	Cu_3Sn	70.8	88.1	52.7	51.4	62.2	55.7

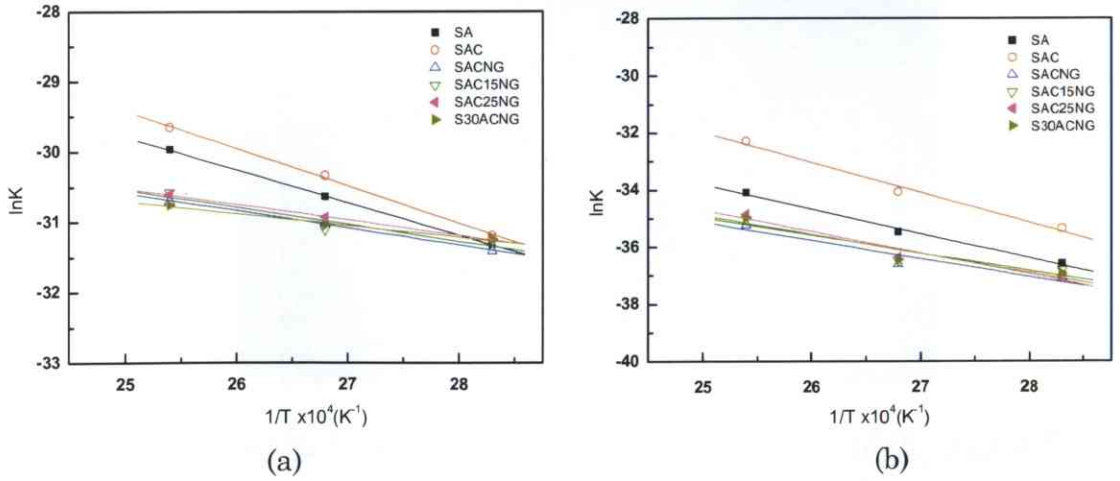

Fig.5-10 Arrehenius plots for growth of the reaction layers. (a) Total Cu-Sn, (b) Cu_3Sn.

Figure 5-11 shows EPMA mapping analysis results for the interfaces of the solder ball joints with the adding Ni solders and the Cu pads in initial state after reflow soldering. In the initial state for the adding Ni solder/Cu joint, a rich Ni region that distributed in the outer region of total IMCs layer and Ag dispersed in the IMCs layer can be observed in Fig.5-11. It indicated that the initial IMCs layer was consist by the Cu-Sn based region, the Cu-Sn-Ni region, and the Ag-Sn region.

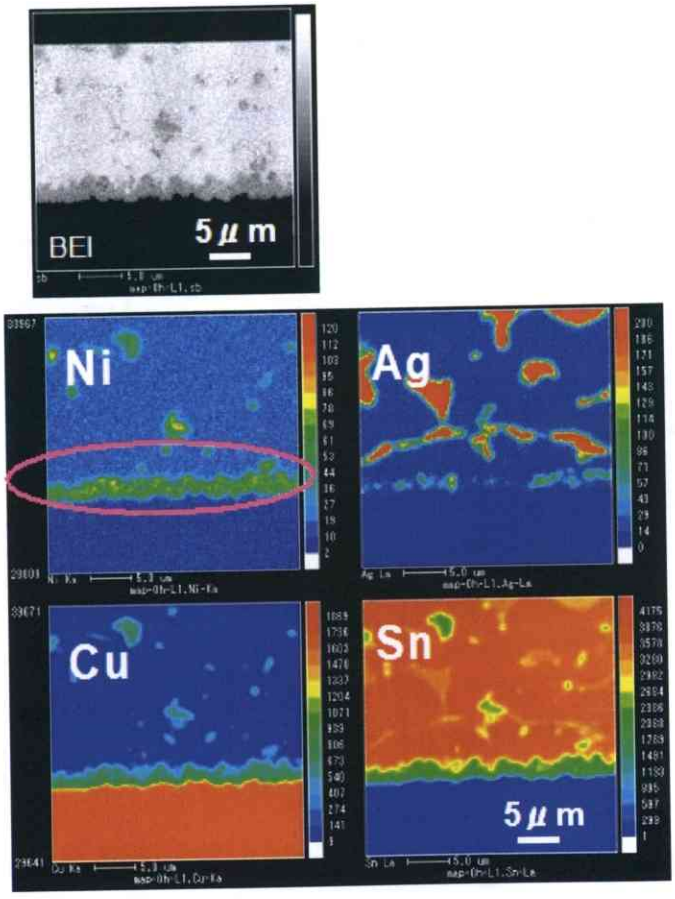

Fig.5-11 EPMA mapping analysis results of the total IMCs layers in the interfaces of the SACNG solder and Cu pad joints

Figure 5-12 shows EPMA mapping analysis results for the interfaces of the solder ball joints with the adding Ni solders and the Cu pads after heat exposure at 393K for 1000h. The similar results that the composition of Cu, Sn, and Ni were also detected in the IMCs layer, and the thickness of the total IMCs layer increased after heat exposure. Moreover, the Ni rich region that corresponded to the initial state was still observed. As the heat exposure time increased, the Ni rich region combined together to form a thin stable layer.

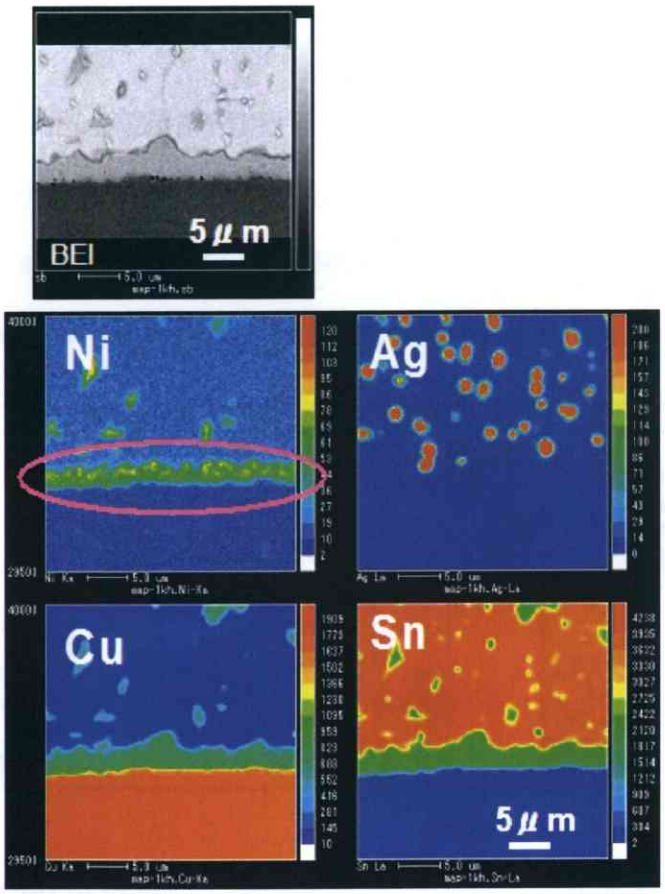

Fig.5-12 EPMA mapping analysis results of the total IMCs layers in the interfaces of the SACNG solder and Cu pad joints after heat exposure at 393K for 1000h.

As described above, the thickness growth for adding Ni solders can be modeled as schematic diagram in Fig.5-13.

In general, the ε -phase of the Cu_3Sn IMCs layer was formed by reaction of Cu with η -phase of the Cu_6Sn_5 IMCs layer at the ε / η interface[5-19-5-20]. Cu diffusion drives the growth process. The η -phase with coarsening scallop was formed by reaction of molten Sn with Cu or ε -phase at the η /Sn interface[5-19-5-20] Similar to these, the η -phase of the $(Cu, Ni)_6Sn_5$ IMCs with mop-haired shape was considered to be formed by reaction of molten (Sn,Ni) with Cu or ε -phase at the η /Sn interface.

It is considered that the Ni rich region in the IMCs layer can development to be a stable barrier layer to suppress the growth of the Cu_3Sn IMCs between Cu and η -phase.

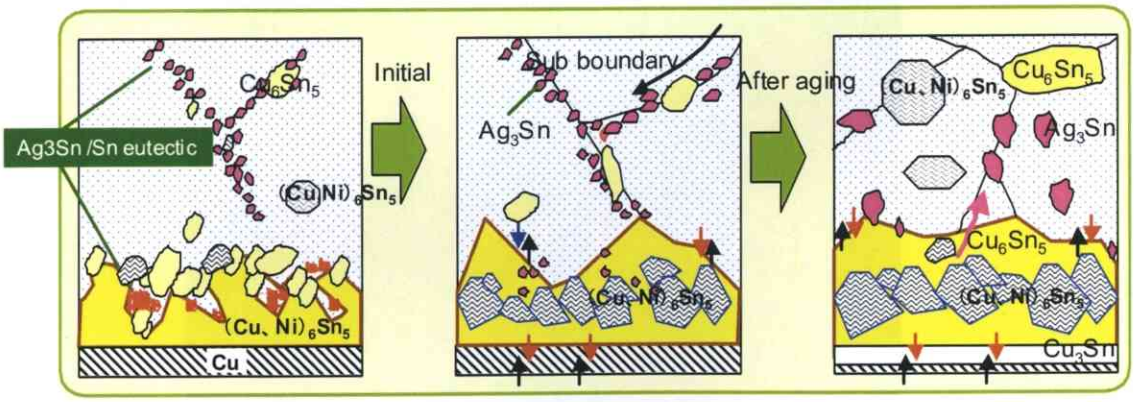

Fig.5-13 Schematic diagram of IMCs layer growth in the solders with small amounts of Ni under heat exposure.

5.4. Conclusions

The interfacial reaction layers and microstructures of various ball solders with small amounts of Ni and Cu pad joints were investigated under heat exposure and compared with those of the joints with the Sn-Ag, the Sn-Ag-Cu solders. The following conclusions are summarized.

- Adding Ni into the Sn-Ag-Cu solders has significantly effective to suppress the growth of the Cu_3Sn IMCs layer and the growth of the Cu_3Sn IMCs was scarcely sensitive for changing the amount of Ni in the range of 0.07 to 0.25 mass%.
- In the case of fixed contents of Cu, Ni in the solders, the growth rate of the Cu_3Sn IMCs layer was not affected with changing Ag content.
- A more stable $(Cu, Ni)_6Sn_5$ IMCs were formed at the interface reaction layers in the solders with small amounts of Ni. The $(Cu, Ni)_6Sn_5$ IMCs or the Ni rich region can be considered as a barrier layer to reduce the growth rate of the Cu_3Sn IMCs layer in the interface of the solder/Cu joints.

5.5. Reference

5-1. H.Nishikawa, A.Komatsu, T.Takemoto: "Microstructure of Sn-Ag-Co Solder Reacted with Cu substrate", Proc. 3rd International Conference on Lead-free Electronics, 2005,pp.231-234

5-2. A.Lalonde et al., "Quantitative Metallography of β-Sn Dentrites in Sn-3.8Ag-0.7Cu Ball Grid Array Solder Balls via Electron backscatter Fiffraction and Polarized Light Microscopy", J. Electron.Mater, 33, 2004,pp.1545-1549.

5-3. L. P. Lehman et al., "Microstructueand amage Evolution in Sn-Ag-Cu Solder", Proc. of Electronics Components and Technology Conference, 2005, pp.674-681.

5-4. T.Takemoto,Y.Kamata, H.Nishikawa, and T.Iido: "Growth Rate of Intermetallic Compounds at Sn-3.5Ag-0.5Cu/Cu Interface", Proc. of 11th Symposium on Microjoining and Assembly Technology in Electronics,2005, pp.111-114.

5-5. S.Saito, T.Ohshima, T.Narita, J.Tanaka, and T.Takashima: "Growth of Reaction Layer in Sn-Ag Based Solder/Cu-plate Interface", Proc. of 11th Symposium on Microjoining and Assembly Technology in Electronics,2005,pp.119-124.

5-6. C.W.Hwang, K.Suganuma, M.Kiso, and S.Hashimoto: "Effect of Cu Addition into Sn-Ag lead-free Solder System on Formation and Growth Mechanisms", 2003, pp.37-40.

5-7. H.Nisikawa, J.Y.Piao, T.Takemoto: "Effect of Ni Addition on Interfacial Reaction Between Sn-Cu Solder and Cu Base Metal", Proc. International Conference on Joining of Advanced and Specialty Materials VII,2004.

5-8. C.B.Lee, S.J.Suh, Y.E.Shin, C.C.Shur, and S.B.Jung:"The Growth Kinetics of Intermetallic Compound Layer at the Interface between Sn-3.5Ag Base Solder and(Cu,Electroless NiP/Cu,Immersion Au/Ni-P/Cu) Substrate",Proc. of 8th Symposium on Microjoining and Assembly Technology in Electronics, 2002,pp. 351-356.

5-9. C.M.Chuang, and K.L.Lin: "Effect of Microelements Addition on the Interfacial Reaction between Sn-Ag-Cu Solders and Cu Substrate", J. Electron. Mater.,Vol.32,No.12,2003,pp.1426-1431.

5-10. S.Terashima, and M.Tanaka: "Thermal Fatigue Properties of Sn-1.2Ag-0.5Cu-xNi Flip Chip Interconnects", Mater. Trans., Vol.45 No.03, 2004,pp.681-688.

5-11. M. N. Islam, A. Sharif, and Y. C. Chan, "Effect of Volume in Interfacial Reaction between Eutectic Sn-3.5%Ag-0.5%Cu Solder and Cu Metallization in Microelectric Packaging", J. Electron. Mater. Vol.34, 2005,pp.143-149.

5-12. R. A. Gagliano and M. E. Fine, "Thickening kinetics of interfacial Cu6Sn5 and Cu3Sn Layer duing Reacyion of Liquid Tin with Solid Copper", J. Electron. Mater. Vol.32, 2003, pp.1441-1447.

5-13. M.Ito,Y.Tanii,T.Ito,Y.Nakagawa,G.Katagira,T.Hiramori,A.Hirose,and K.F.Kobayashi: "Effect of Interfacial Nano-Structure on Joint Strength between Sn-Ag-Cu Solder Ball and Electroless NiP/Au Plating", Proc. of 10th Symposiumon Microjoining and Assembly Technology in Electronics, 2004,pp.159-164.

5-14. J.Y.TSAI: "A Study on the Reaction between Cu and Sn3.5Ag solder Doped with Small Amount of Ni", J. Electron. Meter. Vol.32, 2003, pp.1203-1208.

5-15 .Y.D. Jeon et al., "Effects of Cu Contents in Pb-Free solder Alloys on interfacial Reactions and Bump Reliability of Pb-Free solder Bumps on Electroless Ni-P Under-Bump Metallurgy", J. Electron. Mater. Vol.34, 2005, pp.80-90.

5-16. I. Shohji et al., "Reliability of solder Joint with Sn-Ag-Cu-Ni-Ge lead-Free solder Alloy under Heat Exposure Conditions", Mater. Trans. Vol.46,2005, pp.2737-2744.

5-17. H.Watanabe, and T.Suzuki: "M. Nagano, N. Hidaka, M. Shimoda, and M. Ono, J. Japan Institute of Electronics Packaging, 8, 2005,pp.495-501.

5-18. Z. Mei, A. J. Sunwoo, and J.W. Morris, Jr., "Analysis of Low-Temperature Intermetallic Growth in Copper-Tin Diffusion Couples", Metall. Mater. Trans. 23A, 1992,pp.857-864.

5-19. P.T.Vianco, J. A. Rejent ,and P.F.Hlava: "Solid-State Intermetallic Compound Layer Growth between Copper and 95.5Sn-3.9Ag-0.6Cu Solder", J. Electron.Mater.,Vol.33, 2004,pp.991-1004.

5-20. J.Oberschmidt: "Grain-boundary diffusion in some alloys", J. Appl. 53,1982, pp.5672-5677.

Chapter 6 CONCLUSION

6.1. Concluding Remarks

In chapter 1, I explained the global move toward lead-free solder alloys. Also, clarified the aim and the purpose of this research.

In chapter 2, the effect of various compositions of lead-free Sn-Ag-based solder alloys on solderability was investigated.

Based on the results of wetting evaluations performed by the eniscograph method, we found that wetting zero cross time declines as Ag content rises from 0% to 3%, due primarily to the lowering of the liquidus line temperature of the Sn-Ag alloy. The current study showed no clear consequences of adding 0.07% Ni or 0.01% Ge. With respect to wetting spreading characteristics, solder alloys with higher Ag content were found to exhibit increased spreadability.

Moreover, Cu wire rupture test was performed to examine Cu dissolution. At 300°C, rupture times were nearly half those observed at 255°C. When no Ni was added, erosion significantly reduced the diameter of the Cu wire. In these cases, we detected only extremely thin compound layers on the surface. With respect to the addition of Ag, Cu, Ni, and Ge and rupture times, adding Ni significantly extended rupture times. Ni formed a thick (Ni, Cu)-Sn compound layer on the external surface of the Cu wire. Higher concentrations of both Ni and Ag were found toward the exterior, while Ag exhibited a scattered distribution in the (Ni, Cu)-Sn compound layer and at the grain boundary.

Especially, the result of the examination was shown the viewpoint of the improvement by adding Ge. It was clarified that the amount of drossing of the S3.5ACNG (SACNG) solder was about 1/2 or less compared with S3AC solder alloy.

Moreover, the Ge has been concentrated to the surface and a very thin oxidation layer (10~30nm) of Ge was formed on the surface of S3.5ACNG solder. In addition, enriched Ge was distributed in the grain boundary region of the Sn-rich phase in the solder alloy. In the SACNG solder, the thin oxide layer (film) of Ge was very effective to prevent the oxidation of Sn.

In chapter 3, the tensile strength and low-cycle fatigue of the lead-free Sn-Ag-based solder alloys were examined as mechanical property.

It was shown that the dispersed particle in the eutectic area affects the tensile strength and elongation. The tensile strength increases with increasing content of Ag. The elongation decreases with increasing content of Ag. Also, the tensile strength of S1.0ACNG solder alloy with adding 0.07wt% Ni is better than that of S1.0AC without Ni.

However, the life of low-cycles fatigue is in same level for three kinds of S0.3AC, S1.0AC, and S1.0ACNG solder alloys between the temperature of 25℃ and 125℃. It was considered that dispersion of these particles strengthen the Sn phase which is a major part of matrix in the lead-free solder alloys. The mechanical properties of Sn-Ag-based solder alloys are determined by the microstructure of which dispersed the particles of the Ag_3Sn and Cu_6Sn_3 IMCs. Accordingly, these particles were also considered to be an important factor to contribute to the significant improvement of the creep properties and rupture strengths of the lead-free Sn-Ag-based solder alloys.

In chapter 4, creep properties as long-term mechanical property were investi -gated. Creep strength of SACNG solder alloy at 398 K was approximately three times that of the S3.0AC solder alloy. The initial microstructure of the SACNG

solder alloy was finer and more uniform than that of the S3.0AC solder alloy. Creep properties were apparently affected by IMC growth in the eutectic region. The IMCs of the $(Cu, Ni)_6Sn_5$ formed after the addition of Ni showed improved creep strength at regions of higher temperature (125℃,398 K) and lower stress (5 MPa).

Moreover, the stress exponents of the SACNG solder alloy and the S3.0AC solder alloy were 6.9 and 5.1, and their apparent activation energies at 9.8 MPa were 48 kJ/mol and 68 kJ/mol, respectively. The microstructure of the S3.0AC solder alloy appears quite sensitive to creep temperature.

Furthermore, creep strength of the bulk specimen and the TH joints sample can be plotted using LMP, a parameter of stress, temperature and rupture time. The Sn-Ag-based solder alloys can be lineup by the creep properties.

In chapter 5, the interfacial reaction layers and microstructures of various Sn-Ag-based solder alloys were investigated. Adding Ni into the Sn-Ag-Cu solders has significantly effective to suppress the growth of the Cu_3Sn IMCs layer and the growth of the Cu_3Sn IMC was scarcely sensitive for changing the amount of Ni in the range of 0.07 to 0.25 mass%. In the case of fixed contents of Cu, Ni in the solders, the growth rate of the Cu_3Sn IMCs layer was not affected with changing Ag content.

It was considered that a more stable $(Cu, Ni)_6Sn_5$ IMCs were formed at the interface reaction layers in the solders with small amounts of Ni. The $(Cu, Ni)_6Sn_5$ IMCs or the Ni rich region can be as a barrier layer to reduce the growth rate of the Cu3Sn IMCs layer in the interface of the solder/Cu joints.

6.2. Future Prospects

As the preceding chapters have illustrated, lead-free Sn-Ag-based solder alloys interconnecting reliability is an important, yet complex, subject.
A significant amount of work has been carried out over the past decade, yet more challenges still remain. Some of the most pressing issues are outlined in the following.

6.2.1. Solder Alloy Characteristics and Interfacial Interactions

As a wide range of compositions (Sn-Ag system solder alloys) are being used for the industry worldwide, it is important to determine conclusively whether or not there is any significant difference in the reliability performance of these compositions[6-1-6-3]. This is important in the effort to "standardize" the alloy composition, and if a wide range of compositions continues to be used, for determining whether or not these alloys can be used interchangeably from the perspective of the interconnect reliability, including the associated reliability models and accelerated testing methods. Work is also needed to further characterize the creep and fatigue behavior of the lead-free solder alloy.

Moreover as shown in Fig.6-1, The interfacial interactions are shown (including IMCs formation and growth, and the formation of Kirkendall voids on various PBW surface finishes) and their impact on reliability also warrant further investigation[6-4].

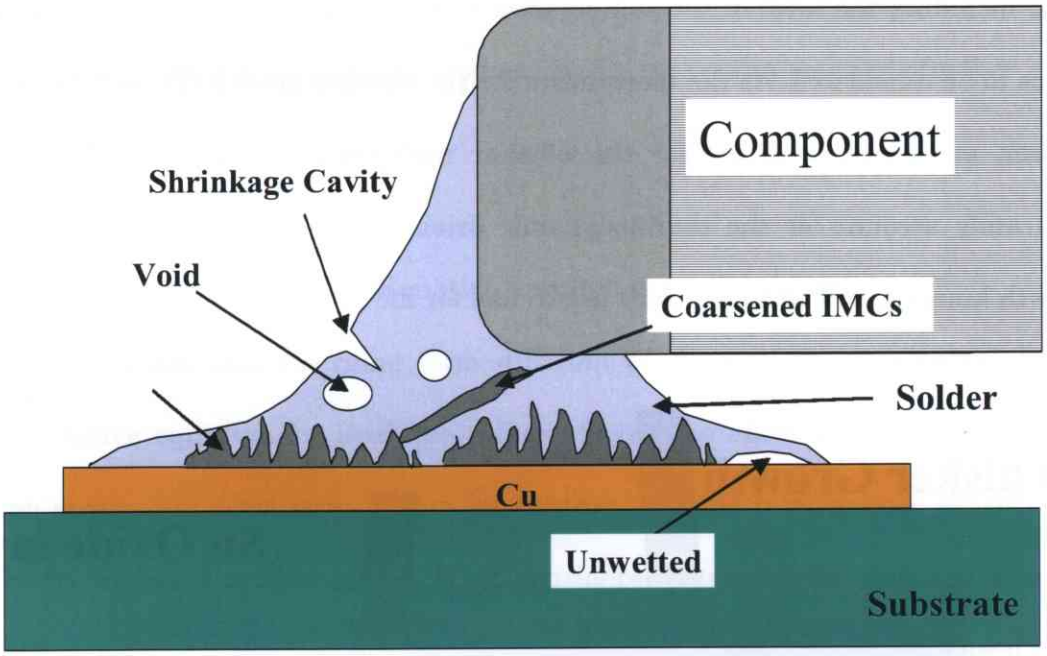

Fig. 6-1. The schematic cross-section view of the typical defects in soldering

6.2.2. Tin Whisker Growth

Many years of research points to compressive stresses as the underlying driving force for the formation and growth of tin whiskers. The compressive stress may arise form metallurgical interactions, thermomechanical factors, and/or mechanical processes. A recent nano-indetation study [6-5] suggests that tha stress field, including the level of the compressive stress, as well as the stress gradient, needs to be considered. As the mechanism for tin whisker growth (Fig.6-2) becomes clearer, predictive modeling for tin whisker nucleation and growth, which can accurately account for the thermodynamic driving force and the nucleation and growth kinetics, will become a very useful tool for life prediction and optimization.

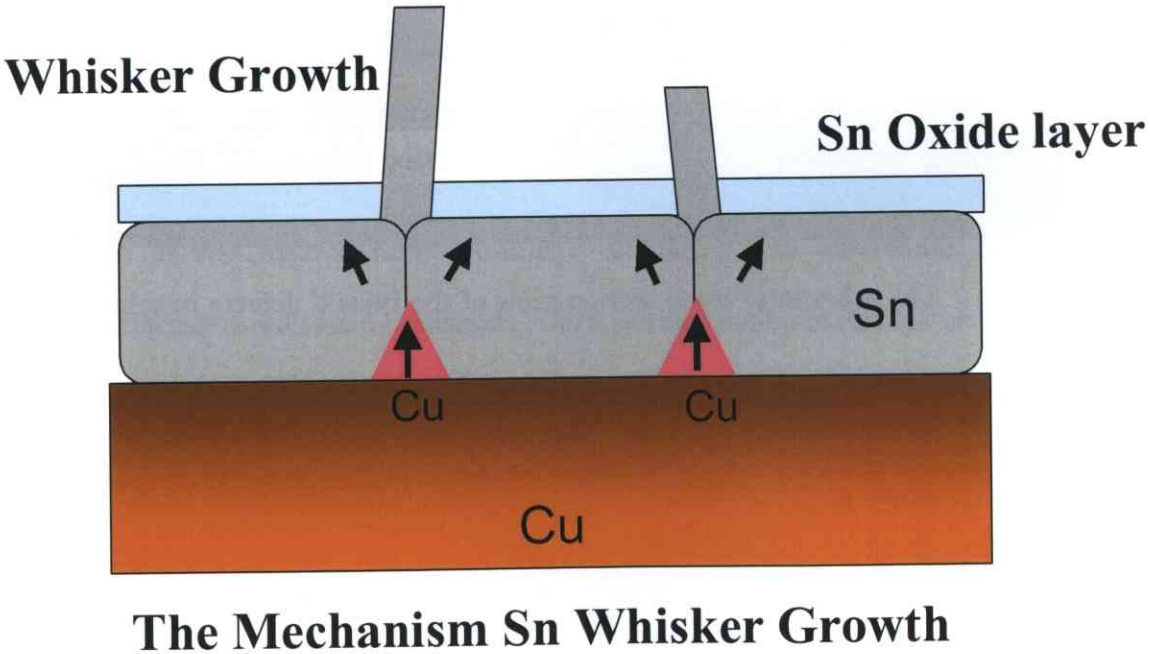

Fig. 6-2. The schematic cross-section view of the tin whisker growth

6.2.3. PWB Reliability

More work is needed to determine the critical materials parameters for the PWB (printed wiring board) to meet the reliability requirements after multiple exposures to the higher lead-free soldering temperatures (260℃ or 533K).

Board-level qualification tests also need to be developed. The work needs to be carried out for different PWB configurations. PWB reliability under mechanical shock (due to drop of a handheld product, for example) also warrants further investigation.

6.2.4. Soldering Constitutive Equation and Reliability Predction

Data are still emerging form different studies on the parameters for the constitutive equation for lead-free solder alloys. The effort is complicated by the high strain-rate sensitivity (strain hardening), and the temperature sensitivity of the Sn-Ag-based solder alloys. It is considered the complicating the situation further is the different stress dependency of the creep rates for Sn-Ag-based solder alloys, moreover, both primary creep and tertiary creeps are important for high reliability applications.

For fatigue life prediction, materials parameters need to be established to correlate the number of cycles for thermal fatigue life to the amount of damage (such as the creep strain energy density) per cycle for the solder joint.

It is important that the experimental work in this area is based on relevant mechanical and environmental loading conditions and realistic solder joint configurations (geometry and size, interfacial factors, etc.) [6-5-6-6].

6.3. Reference

6-1. JEITIA: "Japan Jisso Technology Roadmap 2009", 2009.

6-2. JEITIA: "Review for Lead-free 2009", 2009.

6-3. D.Shangguan: "Supply China Impact of Lead-free Soldering", Global SMT & Packing, 2005, pp.8.

6-4. H.R.Ghorbani, and J.K.Spelt: "An Analytical Elasto-Creep Model of Solder Joints in Leadless Chip Resistors:Part1-Devepopmant and Verification", IEEE.Trans. Adv. Packag., Vol.30,No.4,2007,pp.681-694.

6-5. D.Shangguan:"Lead-Free Solder Interconnect Reliability", ed. by D.Shangguan, ASM, 1995, pp.148-163.

6-6. H.R.Ghorbani, and J.K.Spelt: "An Analytical Elasto-Creep Model of Solder Joints in Leadless Chip Resistors:Part2-Applications in Fatigue Reliability Predictions for SnPb and Lead-free Solders", IEEE.Trans. Adv. Packag., Vol.30, No.4, 2007,pp.695-704.

6.4. Total References

1-1. D.Shangguan: "Packaging & Board Assembly Technology Trend and Impact on the Supply Chain", (Keynote) Proceedings of the 6th IEEE CPMT Conference on High Density Microsystem Design and Packaging and Component Failure Analysis (HDP'04), June 2004,pp.14-17.

1-2. W.Hofmann: "Lead and Lead Alloys" , Springer-Verlag Berlin·Heidelberg·New York 1970.

1-3. U.S. Department of Health and Human Services: "Toxicology Profile for Lead", Clement International Corporation, April 1993.

1-4. Directive 2002/95/EC of the European Parliament and of the Council of 27 January 2003 on the Restriction of the Use of Certain Hazardous Substances in Electrical and Electronic Equipment, Off. J.Eur.Union, 13,2,2003.

1-5. Japan Machiery Center for Trade and Inverstment: "WEEE Handbook V", JMC environment Update, 2003-3.

1-6. National Center for Manufacturing Sciences (NCMS): "Lead-Free Solder Project-Final report", Aug 1997.

1-7. Improved Design Life and Environmentally Aware Manufacturing of Electronics Assemblies by Lead-Free Soldering "IDEALS", BE95-1994 'IDEALS' Synthesis Report, 1999-6.

1-8. JEITA:"Lead-free Roadmap", 2002 ver.1.0, 2002.

1-9. P.Borgesen, T.Bieler, L.P.Lehman, and E.J.Cotts: "Pb-free solder: New Materials Consideration for Microelectronics Processing" Mrs Bulletin, Vol.32, 2007,pp.360-364.

1-10. D.Shangguan,G.Gao:"Lead-Free & No-Clean Soldering for Automotive Electronics", Solder. Surf. Mt. Technol., 26,1997,pp.5-8.

1-11. R.W.Johnson, J.L.Evans, P.Jacobsen, J.R.Thompson, and M.Christopher: "The Changing Automotive Environment: High-Temperature Electronics", IEEE Transactions on electronics Packaging Manufacturing, Vol.27, No.3, 2004,pp.164-175.

1-12. M.Okamoto, K.Serizawa, H.Satoh, M.Chiba, K.Omae, E.Hirao, N.Itsubo, A.Inaba, T.Takemoto, H.Nishikawa: "The Overview of IMS Project EFSOT Japan 2003", Proc. The Sixth International Conference on EcoBalance, 2004, pp.1-4.

2-1. JEITA: "Lead-free Roadmap", 2002 ver.1.0,2002.

2-2. P.Borgesen, T.Bieler, L.P.Lehman, and E.J.Cotts: "Pb-free solder: New Materials Consideration for Microelectronics Processing" Mrs Bulletin, Vol.32 ,2007, pp.360-364.

2-3. D.Shangguan, G.Gao: "Lead-Free & No-Clean Soldering for Automotive Electronics", Solder. Surf. Mt. Technol., 26,1997, pp.5-8.

2-4. R.W.Johnson, J.L.Evans, P.Jacobsen, J.R.Thompson, and M.Christopher: "The Changing Automotive Environment: High-Temperature Electronics", IEEE Transactions on electronics Packaging Manufacturing, Vol.27, No.3, 2004,pp.164-175.

2-5. JIS Z3198-4: [Test Method for Lead-free Solder, PartⅣ], 2003.

2-6. JIS Z3198-3: [Test Method for Lead-free Solder, PartⅢ], 2003.

2-7. Y.S.Lai, J.M.Song, H.C.Chang, T.T.Chiu: "Ball Impact Responses of Ni- or Ge-Doped Sn-Ag-Cu Solder Joints", J. Electron.Mater., Vol.37, No.2, 2008.

2-8. T.H.Chuang,S.F.Yen,H.M.Wu: "Intermetallic formation in Sn3Ag0.5Cu and Sn3Ag0.5Cu0.06Ni0.01Ge solder BGA Packages with immersion Ag surface finish", J. Electron. Mater., Vol.36, No.2, 2006, pp.310-318.

2-9. T.Matsumura, T. Yamamoto: "Assembly Technology Using Lead-free Solder", FUJITSU, Vol 56, No.6, 2005, pp.545-551.

2-10. T.H.Chuang, S.F.Yen, M.D.Cheng: "Intermetallic reactions in Sn3Ag0.5Cu and Sn3Ag0.5Cu0.06Ni0.01Ge solder BGA Packages with Au/Ni surface finishes",J. Electron.Mater., Vol.36, No.2, 2006, pp.302-309.

2-11. C.M.Chuang, K.L.Lin: "Effect of Microelements Addition on the Interfacial Reaction between Sn-Ag-Cu Solders and the Cu Substrate", J. Electron. Mater., Vol.32, No.12, 2003, pp.1423.

2-12. K.Habu,N.Takeda,H.Watanabe,H.Ooki,J.Abe, T.Saito,Y.Tanigachi,and K.Takayama: "Development of Highly Reliable Pb-free Solder Alloys of the Ge Doped Sn-Ag-Bi System", Proc. of 5th Symposium on Microjoining and Assembly Technology in Electronics, mate1999,1999,pp.397-402.

2-13. T.Takemoto, Y.J.Joo, T.Nishimura, S.Oki, and K.Fujimoto: "Suppression of DrossFormation in Lead-free Wave Soldeering", Proc. of 5th Symposium on Microjoining and Assembly Technology in Electronics,2001,pp.491-496.

2-14. M. Nagano, N. Hidaka, M. Shimoda and H. Watanabe: "Effect of Germanium Content on Oxidation Prevention of Sn-Ag-Cu Lead-free Solser", Proc. of New Frontiers of Process Science and Engineering in Advanced Materials, PSEA'04, 2004, pp.256-261.

2-15. O.Kubaschewski, E.Ll.Evans, and C.B.Alcock: "Metallurgical Thermo -chemistry", 1967.

2-16. K.Hauffe: "Oxidation of Metals", 1965.

3-1. D.Shangguan: "Lead-Free Solder Interconnect Reliability", ed. by D.Shangguan, ASM, 1995, pp.191-196.

3-2. T.Takemoto, M.Takahashi, R.Ninomiya, and A. Matsunawa,"Mechanical Properties and Estimation of Thermal Fatigue Properties of Lead-free Solders", Advances in Electronic Packaging, EEP-Vol.19-2, 1997, pp.1623-1628.

3-3. Y.Yoshiura, H.Chake, T.Takemoto, and Y.Kikuchi: "Improvement of Thermal Fatigue Propertis of Sn-Pb Solder by Addition of Several Elements", Proc. of 2th Symposium on Microjoining and Assembly Technology in Electronics, 1996,pp.167-172.

3-4. D.A.Spera and D.F.Mowbray: "Thermal Fatigue of Materials and Components", ASTM, 1976,pp.3-9.

3-5. JIS Z3198-2: [Tensile Test for Lead-free Solder Alloy Part Ⅱ]

3-6. T.Takahashi, S.Hioki, I.Shohji, and T.Yoshida: "Mechanical Properties of Various Lead-free Solders", Proc. of 9th Symposium on Microjoining and Assembly Technology in Electronics, 2003,pp.223-228.

3-7. Y.Kariya, T.Asai, and T.Suga: "Mechanical Properties of Lead-free Sloder Alloys Evaluated by Miniature Size Specimen", Microjoining Commission(JWS), MJ-455-2004, 2004.

3-8. Y.Kariya, T.Asai, T.Suga, and M.Otsuka: "Mechanical Properties of Lead-free Sloder Alloys Evaluated by Miniature Size Specimen", Proc. of 9th Symposium on Microjoining and Assembly Technology in Electronics, 2004,pp.61-64.

3-9. M.McCormack, and S.Jin: "Improved Mechanical Properties in New, Pb-free Solder Alloys", J. Electron. Mater., Vol.23, No.8, 1994, pp.715-720.

3-10. F.Ochoa, J.J.Williams, and N.Chawla: "Effects of Cooling Rate on the Microstructure and Tensile Behavior of a Sn-3.5 wt%Ag Solder", J. Electron. Mater., Vol.32, No.12, 2003,pp.1414-1420.

3-11. R.Ninomiya, Y.Nakahira, and T.Takemoto: "Microstructure and Mechanical Property of Sn-Ag-Bi-In Solder", Proc. of 4th Symposium on Microjoining and Assembly Technology in Electronics,1998,pp.249-252.

3-12. K.Habu, N.Sato,and H.Nagasawa: "The Effect and Stability of Composition in Pb-free Solser Alloys of the Sn-Ag-Cu-Bi System with a Small Amount of Additives", Proc. of 6th Symposium on Microjoining and Assembly Technology in Electronics, 2000,pp.287-292.

3-13. M.Nagano, N.Hidaka, M.Shimoda, and M.Ono: "Mechanical Properties and Microstructure of Sn-Ag-Cu-Ni-Ge Lead-free Solser", J.Japan. Institite of Electron. Packaging, Vol.8, No.6,2005,pp.495-501.

3-14. Y.Kariya, and W.J.Plumbridge: "Mechanical properties of Sn-3.0mass%Ag -0.5mass%Cu alloy", 7th Symposium on [Microjoining and Assembly Technology in Electronics], 2001,pp.383-388.

3-15. C.M.L.Wu, D.Q.Yu, and L.Wang: "Microstructure and Mechanical Properties of New Lead-Free Sn-Cu-RE Solder Alloys", J. Electron. Mater., Vol.31, No.8, 2002,pp.928-932.

3-16. Y.Kariya: "Mechanical Reliability of Solders in Small Volume" J.Japan. Institute of Electronics Packaging, Vol.9, No.3,2006,pp.138-142.

3-17. S.Terashima, Y.Kariya, and M.Tanaka: "Improvement on Thermal Fatigue Properties of Sn-1.2Ag-0.5Cu Flip Chip Interconnects by Nickel Addition", Mater.Trans., Vol.45, No.3, 2004,pp.673-680.

4-1. JEITA: "Lead-free Solder Technologies", published by, CORONA, 2004,pp.19-22.

4-2. R. J. Mccabe, M. E. Fine, " High Creep Resistance Tin-Based Alloys for Soldering Applications", J. Electron. Mater. Vol. 31,No.11,2002, pp.1276-1282.

4-3. V.I.Igoshev, and J.I.Kleiman: "Creep Phenomena in Lead-Free Solders", J. Electron. Mater., Vol.29, No.2, 2000, pp.244-250.

4-4. K.Wu, M.Aoyama, N.Wade, J.Cui, S.Yamada, and K.Miyahara: "Creep and Rupture Behavior of Cu Wire/Lead-Free Solder-Alloy Joint Specimen", J. Electron.Mater. Vol. 32,No.12, 2003,pp.1392-1397.

4-5. F.Garofalo: "Fundamentals of Creep and Creep Ruoture in Metals", MacMillian, 1965,pp.156-201.

4-6. K.Mariyama, and H.Nakasima: "Fundamentals of Creep in Metals and Alloys", Published by Uchida Rokakuho,2002.pp.8.

4-7. D.Shangguan: "Lead-Free Solder Interconnect Reliability", ed. by D.Shangguan, ASM, 1995, pp.88-89.

4-8. J.Askin: "Tracer Diffusion Data", Penum, 1970.

4-9. Y. Kariya, M. Otsuka, and W. J. Plumbride: "The Consititutive Creep Equation for a Eutectic Sn-Ag Alloy Using the Modified Theta-Projection Concept", J. Electron. Mater. 32, 2003, pp.1398-1402.

4-10. P.Shewmon: "Diffusion in solids", 2nd, ed., TMS, 1969,pp.189-199.

4-11. J.Christian: "The Theory of Transformations in Metals and Alloys: Part I Equilibrium and General Kinetic Theory", Pergamon,1975,pp.541-543.

4-12. J.Stephens, and D.Frear: "Time-Dependent Deformation Behavior of Near -Eutectic 60Sn-40Pb Solder", Metall.Mater.Trans.A, Vol.30A, 1999, pp.1301-1313.

4-13. T. T. Mattila, and J. K. Kivilahti, J. Electron. Mater.,Vol.34, 2005,pp.969-976.

4-14. S. Terashima, and M. Tanaka, Mater. Trans., Vol.45,2004,pp.681-688.

4-15. C. M. L. Wu and M. L. Huang: "Creep Behavior of Eutectic Sn-Cu Lead-Free Solder Alloy", J. Electron. Mater. 31, 2002,pp.442-448.

4-16. M. Kerr and N. Chawla:"Creep Deformation Behavior of Sn-3.5Ag Solder/Cu Couple at Small Length Scales", Acta.Metall., Vol. 52, 2004, pp.4527-4535.

4-17. R. J. Mccabe, M. E. Fine:"Creep of Tin, Sb-Solution-Strengthened Tin, and SbSn-Precipitate Strengthened Tin" Meta.Mate.Trans.,Vol.33A,2002, pp.1531-1538.

4-18. K. Atsumi, Y. Kariya, and M. Otsuka: "Creep Properties of Sn-3.5Ag-xBi and Sn-3.5Ag-xCu Solder Alloys", Proc. of 6th Symposium on Microjoining and Assembly Technology in Electronics, 2000,pp.281-286.

4-19. M.Nagano, N.Hidaka, M.Shimoda and H.Watanabe: "Effect of Germanium content on Oxidation Prevention of Sn-Ag-Cu Lead-Free Solder", Proc. of PSEA04, 2004, pp.256-261.

4-20. Z. Chen, Y. Shi, and Z. Xia: "Constitutive Relations on Creep for SnAgCuRE Lead-Free Solder Joints", J. Electron. Mater., Vol.33,No.9,2004,pp.964-971.

4-21. P. T. Vianco, J. A. Rejent, and A. C. Kilgo: "Creep Behavior of the Ternary 95.5Sn-3.9Ag-0.6Cu Solder-Part I: As-Cast Condition", J. Electron. Mater.,Vol.33, No.11,2004,pp.1389-1400.

4-22. Q. Xiao and W. D. Armstrong: "Tensile Creep and Microstructural Characterization of Bulk Sn3.9Ag0.6Cu Lead-Free Solder", J. Electron. Mater., Vol.34, No.7, 2005, pp.196-211.

4-23. W.J.Plumbridge, C.R.Gagg, and S.Peters: "The Creep of Lead-Free Solders at Elevated Temperatures", J. Electron. Mater., Vol.30,No.9,2001, pp.1178-1183.

4-24. T. H. Chuang, S. F. Yen, and M. D. Cheng: "Intermetallic Formation in Sn3Ag0.5Cu and Sn3Ag0.5Cu0.06Ni0.01Ge Solder BGA Packages with Immersion Ag Surface Finish", J. Electron. Mater.,Vol.35,2006,pp.302-309.

4-25. T. H. Chuang, S. F. Yen, and M. D. Cheng: "Intermetallic Reactions in Sn3Ag0.5Cu and Sn3Ag0.5Cu0.06Ni0.01Ge Solder BGA Packages with Au/Ni Surface Finish", J. Electron. Mater.,Vol.35,2006,pp.302-309.

4-26. D. Mitlin, C. H. Raeder, and R. W. Messler, Jr: "Solid Solution Creep Behavior of Sn-xBi Alloy", Metall. Mater.Trans.Vol.30A, 1999, pp.115-122.

4-27. R. Ninomaya, Y. Nakahara, and T. Takemoto,: "Microstructure and Mechanical Property of Sn-Ag-Bi-In Solder", Proc. of 9th Symposium on Microjoining and Assembly Technology in Electronics, 1998,pp.249-252.

4-28. J.J.Sundelin, S.T.Nurmi, T.K.Lepisto, and E.O.Ristolainen: "Effect of PCB surface finish on creep properties of lead-free solder joints", Soldering & Surface Mount Technology, Vol.17, No.4, 2005,pp.3-9.

4-29. Q. Xiao, L.Nguyen, and W. D. Armstrong, "Anomalously High Tensile Creep Rates from Thin Cast Sn3.9Ag0.6Cu Lead-Free Solder", J. Electron.Mater., Vol.34,No.7, 2005,pp.1065-1075.

4-30. F.Ochoa, X.Deng, and N.Chawla: "Effect of Colling Rate on Creep Behavior of a Sn-3.5Ag Alloy", J. Electron. Mater., Vol.33, No.12, 2004, pp.1596-1607.

4-31. N.Hidaka, M. Nagano, M. Shimoda, H. Watanabe, and M. Ono: "Creep Properties and Microstructure of the Sn-Ag-Cu-Ni-Ge Lead-Free Solder Alloy", Proc. ASME, InterPACK2005, 2005-73148.

5-1.H.Nishikawa, A.Komatsu, T.Takemoto: "Microstructure of Sn-Ag-Co Solder Reacted with Cu substrate", Proc. 3rd International Conference on Lead-free Electronics, 2005,pp.231-234

5-2. A.Lalonde et al., "Quantitative Metallography of β-Sn Dentrites in Sn-3.8Ag-0.7Cu Ball Grid Array Solder Balls via Electron Backscatter Diffraction and Polarized Light Microscopy", J. Electron.Mater, 33, 2004, pp.1545-1549.

5-3. L. P. Lehman et al., "Microstructueand amage Evolution in Sn-Ag-Cu Solder", Proc. of Electronics Components and Technology Conference, 2005, pp.674-681.

5-4. T.Takemoto,Y.Kamata, H.Nishikawa, and T.Iido: "Growth Rate of Intermetallic Compounds at Sn-3.5Ag-0.5Cu/Cu Interface", Proc. of 11th Symposium on Microjoining and Assembly Technology in Electronics,2005, pp.111-114.

5-5. S.Saito, T.Ohshima, T.Narita, J.Tanaka, and T.Takashima: "Growth of Reaction Layer in Sn-Ag Based Solder/Cu-plate Interface", Proc. of 11th Symposium on Microjoining and Assembly Technology in Electronics, 2005,pp.119-124.

5-6. C.W.Hwang, K.Suganuma, M.Kiso, and S.Hashimoto: "Effect of Cu Addition into Sn-Ag lead-free Solder System on Formation and Growth Mechanisms", 2003, pp.37-40.

5-7. H.Nisikawa, J.Y.Piao, T.Takemoto: "Effect of Ni Addition on Interfacial Reaction Between Sn-Cu Solder and Cu Base Metal", Proc. International Conference on Joining of Advanced and Specialty Materials VII,2004.

5-8. C.B.Lee, S.J.Suh, Y.E.Shin, C.C.Shur, and S.B.Jung:"The Growth Kinetics of Intermetallic Compound Layer at the Interface between Sn-3.5Ag Base Solder and(Cu,Electroless NiP/Cu,Immersion Au/Ni-P/Cu) Substrate",Proc. of 8th Symposium on Microjoining and Assembly Technology in Electronics, 2002,pp. 351-356.

5-9. C.M.Chuang, and K.L.Lin: "Effect of Microelements Addition on the Interfacial Reaction between Sn-Ag-Cu Solders and Cu Substrate", J.Electron. Mater.,Vol.32,No.12,2003,pp.1426-1431.

5-10. S.Terashima, and M.Tanaka: "Thermal Fatigue Properties of Sn-1.2Ag-0.5Cu-xNi Flip Chip Interconnects", Mater. Trans., Vol.45 No.03, 2004,pp.681-688.

5-11. M. N. Islam, A. Sharif, and Y. C. Chan, "Effect of Volume in Interfacial Reaction between Eutectic Sn-3.5%Ag-0.5%Cu Solder and Cu Metallization in Microelectric Packaging", J. Electron. Mater. Vol.34, 2005,pp.143-149.

5-12. R. A. Gagliano and M. E. Fine, "Thickening kinetics of interfacial Cu6Sn5 and Cu3Sn Layer duing Reacyion of Liquid Tin with Solid Copper", J. Electron. Mater.Vol.32, 2003, pp.1441-1447.

5-13. M.Ito, Y.Tanii, T.Ito, Y.Nakagawa, G.Katagira, T.Hiramori, A.Hirose, and K.F.Kobayashi: "Effect of Interfacial Nano-Structure on Joint Strength between Sn-Ag-Cu Solder Ball and Electroless NiP/Au Plating", Proc. of 10th Symposium on Microjoining and Assembly Technology in Electronics, 2004,pp.159-164.

5-14. J.Y.TSAI: "A Study on the Reaction between Cu and Sn3.5Ag solder Doped with Small Amount of Ni", J. Electron. Meter. Vol.32, 2003, pp.1203-1208.

5-15. Y.D. Jeon et al., "Effects of Cu Contents in Pb-Free solder Alloys on interfacial Reactions and Bump Reliability of Pb-Free solder Bumps on Electroless Ni-P Under-Bump Metallurgy", J. Electron. Mater. Vol.34, 2005, pp.80-90.

5-16. I. Shohji et al., "Reliability of solder Joint with Sn-Ag-Cu-Ni-Ge lead-Free solder alloy under Heat Exposure Conditions", Mater. Trans. Vol.46, 2005, pp.2737-2744.

5-17. H.Watanabe, N.Hidaka, I.Shohji, and M.Ito: "Effect of Ni and Ag on Interfaical Reaction and Microstrucure of Sn-Ag-Cu-Ni-Ge Lead-free Solder Joint", Proc. of Materials Science and Technology 2006 Conference and Exhibition (MS&T) 2006MS&T2006, pp.135-148.

5-18. Z. Mei, A. J. Sunwoo, and J.W. Morris, Jr., "Analysis of Low-Temperature Intermetallic Growth in Copper-Tin Diffusion Couples", Metall. Mater. Trans. 23A, 1992,pp.857-864.

5-19. P.T.Vianco, J. A. Rejent ,and P.F.Hlava: "Solid-State Intermetallic Compound Layer Growth between Copper and 95.5Sn-3.9Ag-0.6Cu Solder", J. Electron.Mater.,Vol.33, 2004,pp.991-1004.

5-20. J.Oberschmidt: "Grain-boundary diffusion in some alloys", J. Appl. 53,1982, pp.5672-5677.

6-1. JEITIA: "Japan Jisso Technology Roadmap 2009", 2009.

6-2. JEITIA: "Review for Lead-free 2009", 2009.

6-3. D.Shangguan: "Supply China Impact of Lead-free Soldering", Global SMT & Packing, 2005, pp.8.

6-4. H.R.Ghorbani, and J.K.Spelt: "An Analytical Elasto-Creep Model of Solder Joints in Leadless Chip Resistors:Part1-Devepopmant and Verification", IEEE.Trans. Adv. Packag., Vol.30,No.4,2007,pp.681-694.

6-5. D.Shangguan: "Lead-Free Solder Interconnect Reliability", ed. by D.Shangguan, ASM, 1995, pp.148-163.

6-6. H.R.Ghorbani, and J.K.Spelt: "An Analytical Elasto-Creep Model of Solder Joints in Leadless Chip Resistors:Part2-Applications in Fatigue Reliability Predictions for SnPb and Lead-free Solders", IEEE.Trans. Adv. Packag., Vol.30,No.4,2007,pp.695-704.

ACKNOWLEDGMENTS

First of all, I would like to thank all those who gave me the ability and wisdom to accomplish this work.

I would like to express my deepest gratitude to my academic supervisor, Professor Masayuki YOSHIBA, for his incredibly broad knowledge base and his organizational skills helped me to find out how to survive a long voyage toward Ph.D. His enthusiastic attitude towards research and everyday life and excellent sense of humor has been encouragement for me.

I would like to extend my gratitude to the other members of the thesis supervisory committee, Professor Ken-ichi MANABE, Professor Toshihisa SHIMIZU, and Professor Ming YANG. Their constructive criticisms, insightful comments and meticulous observations have contributed greatly in making this work a success.

My special regards to the peoples in Advanced Technology Laboratory Fuji electric holding Co., Ltd, especially the manager, Mr.M.Ono, whose give me the chance to start this work, and the manager Mr. K.Siokawa, the general manager K. Nakayama whose continuous support in several ways related to this work contributed a great deal in arriving at this stage. I would like to express my gratitude in particular to my colleague, Mr. H.Watanabe, Mr. M.Shimota, and Mr. T.Asai for tireless working with me. Without their help, none of this work would have been possible. My sincere gratitude also goes to Mr. S.Saito who gives me advice in many ways.

Finally, my acknowledgment goes to my family, to my son and my daughter, Sada and Mari, for their smile, which encourages me every day and night, and to my wonderful wife, Akimi, for her patience and encouragement.